Physics – Uspekhi **64** (7) 641 – 670 (2021)

REVIEWS OF TOPICAL PROBLEMS PACS numbers: **71.10. – w**, 71.10.Fd, **71.27. + a**, **74.20. – z**, 74.20.Mn, 74.25.N – , **74.72. – h**

Spin-polaron concept in the theory of normal and superconducting states of cuprates

V V Val'kov, D M Dzebisashvili, M M Korovushkin, A F Barabanov

DOI: https://doi.org/10.3367/UFNe.2020.08.038829

Contents

Abstract. The review discusses the emergence of the spin-fermion model of cuprates and the formation of the spin-polaron concept of the electronic structure of hole-doped cuprate superconductors. This concept has allowed describing the properties of cuprates in the normal phase as well as the features of superconducting pairing in the unified approach. The derivation of the spin-fermion model from the Emery model in the regime of strong electronic correlations is described, demonstrating the appearance of strong coupling between the spins of copper ions and holes on oxygen ions. Such a strong interaction against the background of the singlet state of the spin subsystem of copper ions (quantum spin liquid) leads to the formation of special Fermi quasiparticles — nonlocal spin polarons. Under doping, the spin-polaron ensemble exhibits instability with respect to superconducting d-wave pairing, whereas superconducting s-wave pairing is not implemented. At the optimal doping, the transition to the superconducting phase occurs at temperatures corresponding to experimental data. It is shown that the superconducting d-wave pairing of spin-polaron quasiparticles is not suppressed by the Coulomb repulsion of holes located on neighboring oxygen ions. It is emphasized that, when the spectral characteristics of spin-polaron quasiparticles are taken into account, the calculated temperature and doping dependences of the London penetration depth are in good agreement with experimental data.

Keywords: strongly correlated electron systems, high-temperature superconductivity, spin polarons, intersite Coulomb interaction, London penetration depth

V V Val'kov [1, a], **D M Dzebisashvili** [1, 2, b], **M M Korovushkin** [1, c], **A F Barabanov** [3, d]
[1] Kirensky Institute of Physics, Federal Research Center Krasnoyarsk Science Center of the Siberian Branch of the Russian Academy of Sciences, Akademgorodok 50/38, 660036 Krasnoyarsk, Russian Federation
[2] Reshetnev Siberian State University of Science and Technology, prosp. im. gazety Krasnoyarskii rabochii 31, 660037 Krasnoyarsk, Russian Federation
[3] Vereshchagin Institute for High Pressure Physics, Russian Academy of Sciences, Kaluzhskoe shosse 14, 108840 Troitsk, Moscow, Russian Federation
E-mail: [a] vvv@iph.krasn.ru, [b] ddm@iph.krasn.ru, [c] kmax@iph.krasn.ru, [d] abarab@bk.ru

Received 22 April 2020, revised 4 July 2020
Uspekhi Fizicheskikh Nauk **191** (7) 673 – 704 (2021)
Translated by V L Derbov

1. Introduction

Recent experimental and theoretical studies of cuprate superconductors have been aimed at clarifying the features of their electronic structure and testing the earlier-proposed mechanisms of superconducting pairing. To obtain data on the electronic properties of these materials, spectral characteristics of Fermi excitations in the normal phase of hole-doped cuprates have been actively investigated [1–3], and the behavior of quasiparticles in the pseudogap state have been analyzed [4–8]. In addition, the thermodynamic features of physical quantities under optimal doping have been discussed

[9], and the properties of cuprate superconductors in the intermediate state, induced by an external magnetic field, have been considered [10]. Studies related to the manifestation of charge fluctuations [11], structural disordering [12, 13], and charge density waves [14, 15] have been also carried out.

The accumulated results allowed a theoretical description of cuprate high-temperature superconductors (HTSCs) in the normal and superconducting phase within a unified concept. It is based on considering basic and well-established chemical and crystallographic principles of material structure. These include, in particular, data on covalence effects between the states of copper and oxygen ions, as well as on relations between the energy parameters that determine the regime of strong electronic correlation (SEC) in cuprate superconductors.

A factor of primary importance playing the main role in the formation of all physical properties of the materials mentioned above is associated with the strong spin-fermion coupling between the localized subsystem of spin moments of copper ions and holes moving over the oxygen ions that arises as a result of covalent mixing [16–19]. Such coupling is formed when SEC is taken into account and is characteristic of many superconductors with high critical temperatures. The presence of pronounced quasi-two-dimensionality in cuprate superconductors increases the role of fluctuations caused by the spin-fermion coupling. The circumstances mentioned above determine the specific features of the low-temperature properties of cuprate HTSCs in both the normal and superconducting phases [20].

Within the Emery model [22] reflecting the real structure of the CuO_2 plane of an HTSC, the authors of Ref. [21] showed that the additional hole arising in the plane under doping forms a state strongly bound with the spin moment localized on the copper ion. This circumstance gave reason to believe that the properties of cuprate HTSCs can be described within simpler effective low-energy models, such as the $t-J$ model [23]. However, the price for the relative simplicity of these models was the fact that a number of important features of the cuprate electronic structure were neglected. In particular, the real structure of the CuO_2 plane, whose unit cell includes two oxygen ions and one copper ion, was ignored, and the spatial separation of spin moments of copper and oxygen ions was not taken into account.

The above drawbacks are not inherent in the model proposed in Refs [24–30], which was later called the spin-fermion model [31]. However, in the present review, we will call this model the spin-fermion model of cuprates (SFMC) (see discussion in Section 3.3). The SFMC directly follows from the Emery model, if we consider the effects of covalent mixing of copper and oxygen orbitals using the perturbation theory with the real relations between the parameters of the initial Hamiltonian taken into account. The main advantage of the SFMC is the possibility of correctly describing strong spin-charge coupling caused by the strong exchange interaction between the spin moments of copper ions and the spins of holes on oxygen ions. This relation leads, in particular, to spin-correlated hopping accompanied by spin-flip processes. It was within the SFMC framework that the spin-polaron concept was developed [32–36] to describe the spectral properties of cuprate HTSCs in the normal phase.

From the point of view of the concept of a spin polaron, within the SFMC, the splitting of the lower band of the local polaron was investigated [37], which allowed, e.g., a description of the sharp decrease in the intensity of spectral peaks in experiments on angle-resolved photoemission spectroscopy (ARPES) upon changing the quasimomentum from $(\pi/2, \pi/2)$ to (π, π) or $(0, 0)$, as well as the possible existence of a 'shadow band' [38]. The authors of Refs [39, 40] have shown that, in the case of the SFMC considered within the spin polaron concept, it is sufficient to use only one fitting parameter, the hopping integral for holes, to describe the modification of the energy spectrum and Fermi surface of a cuprate superconductor, whereas the strong-coupling models involve a large number of doping-dependent fitting parameters.

Until recently, the spin-polaron concept success was limited to the description of cuprate properties in the normal state. The situation considerably changed when it was shown that the Cooper instability in HTSCs develops in the subsystem of spin-polaron quasiparticles rather than bare fermions [41, 42].

The efficacy of the spin-polaron approach to the HTSC problem appeared most obvious after solving the problem of neutralizing the negative influence of Coulomb repulsion of fermions, located at the nearest-neighbor lattice sites, on the implementation of the superconducting phase [43] — a long-standing problem known from the times of early theoretical papers on high-temperature superconductivity in cuprates. The point was that, at distances equal to the lattice parameter, potential screening did not work, and the real values of the Coulomb interaction were such that, e.g., in the most popular $t-J$ model, the superconductivity was completely suppressed. Taking into account the real structure of the CuO_2 plane in the ensemble of spin-polaron quasiparticles, it turned out that the Fourier transform of the intersite Coulomb interaction of holes, located on the nearest-neighbor oxygen ions, falls out from the equation for Cooper pairing of spin polarons in the d-wave channel and, therefore, does not affect the superconducting d-wave pairing [43]. In this case, a substantial role was played by considering the strong spin-fermion coupling, which resulted in a transformation of the bare interaction between the oxygen holes into interaction between the spin-polaron quasiparticles.

Further development of this direction of investigation has shown that the superconducting phase with s-wave symmetry of the order parameter is not implemented for any realistic values of the system parameters [44].

It is worth noting that the formation of a complex Fermi quasiparticle can occur not only by coupling an electron to localized spins, but also as a result of electron motion correlated with the phonon subsystem. For HTSCs this can be important, since, near the critical temperature, the lattice vibrations are significant and the number of phonons is large.

Papers on the theoretical studies of the influence of the electron–phonon interaction on the critical temperature, spectral properties of Fermi quasiparticles, and kinetic characteristics of cuprate superconductors have been written in several directions. In one of them, it was assumed that in the strongly correlated systems considered, the electron–phonon interaction is also strong. Based on this assumption, the authors of Refs [45–47] proposed variants of solving the problem of considering the above strong interactions simultaneously.

Another line of studies was based on assuming not only strong electron–phonon coupling, but also a high density of correlated fermions. In this case, it turned out that large bipolarons and delocalized carriers are formed in the system.

In this approach, it appeared possible to explain high-energy anomalies in the ARPES spectra [48], as well as charge ordering [49].

In systems with strong electron–phonon coupling, it seems relevant to develop Eliashberg's theory [50] beyond the framework of the adiabatic approximation [51].

In the present review, the effects of electron–phonon coupling are not taken into account when discussing the spin-polaron concept of electronic structure of hole-doped cuprates. The solution to the problem of a Fermi quasiparticle formed with both electron–phonon and spin-fermion interaction taken into account is an issue for the nearest future. To date, the application field for the spin-polaron approach has been extended towards the development of the theory of electromagnetic phenomena occurring in cuprates [52].

The aim of this review is to present the concept of the spin polaron and the totality of results of studying the properties of cuprate superconductors within this concept. In Section 2, we consider the basic models for describing the physical properties of cuprates (the Hubbard model, multiband p–d models, the t–J model, and the Kondo lattice model). In the course of consideration, the premises for the origin of the SFMC are revealed. Section 3 provides a detailed derivation of the SFMC from the Emery model in the SEC regime and a discussion of the general properties and fundamental differences between the SFMC and other effective models, taking into account the strong spin-fermion coupling in cuprates. Section 4 presents the concept of the spin-polaron nature of Fermi quasiparticles in cuprate superconductors. In Section 5, we consider the properties of the normal phase of spin-polaron quasiparticles, i.e., the energy structure, spectral characteristics, and Fermi surface modification under doping. Section 6 describes results on the superconducting phase of spin polarons. In particular, we analyze the stability of superconducting d-wave pairing with respect to considering the Coulomb repulsion of holes located on the neighboring oxygen ions. We also consider the problem of calculating the London penetration depth of a magnetic field into a cuprate superconductor, in which the charge carriers are spin-polaron quasiparticles. In the conclusion (Section 7), the obtained results are discussed.

2. Basic multielectron models of cuprate superconductors

2.1 Search for a theoretical model

It is well known that the microscopic theory of superconductivity, created in 1957 by Bardeen, Cooper, and Schrieffer (BCS) [53], is based on the Cooper hypothesis of the instability of the ground state of electron gas with arbitrarily weak attraction between the particles with respect to the formation of bound states (the BCS model). The attraction of electrons exceeding the Coulomb repulsion is mainly due to the interaction of electrons with crystal lattice vibrations, leading to the formation of a region of excessive positive charge surrounding the electron.

As early as 1964, Little [54] and Ginzburg [55] hypothesized the possible existence of HTSCs. Little was the first to pose the question of why the critical temperature of superconductors known at that time was not high. Little proposed a possible way to increase the critical temperature T_c of the superconducting transition to higher values by replacing the electron–phonon interaction, leading to superconductivity in the BCS model, with the interaction of conductivity electrons with bound electrons (excitons), the energy of which is much higher than that of phonons. In 1986, Bednorz and Müller [56] found superconductivity in the lanthanum–barium–copper oxide ($La_{2-x}Ba_xCuO_4$) with the critical transition temperature $T_c \approx 30$ K, record-breaking for that time.

This discovery attracted considerable attention to HTSCs, and both the intensity of research and the number of publications in the field reached unprecedented levels. The number of publications on HTSCs that appeared after 1986 substantially exceeds the total number of all earlier publications on superconductivity, starting from its discovery by Kamerlingh Onnes in 1911. Moreover, after the discovery of superconductivity in yttrium copper-oxide compounds $YBa_2Cu_3O_{6+x}$ by Wu et al. [57] with $T_c \approx 90$ K and in mercury compounds [58, 59] with $T_c \approx 135-160$ K, the HTSC problem has turned from purely scientific to practically significant because of the possibility of applying the HTSC phenomenon in technical devices.

From a theoretical point of view, it is relatively easy to explain superconductivity in doped La_2CuO_4 (LSCO) based on the usual phonon mechanism with the transition temperature $T_c \approx 30$ K. At the same time, phonon mechanisms can hardly be applied to a description of the superconducting phase in mercury and bismuth HTSCs, where the critical temperatures exceed 90 K. This fact stimulated many researchers to start looking for an alternative pairing mechanism and gave rise to a vivid discussion on the choice of an efficient theoretical model intended to describe the HTSC physical properties.

2.2 Hubbard model

The first model used to describe the properties of cuprate superconductors was the one proposed by Hubbard [60] in 1963, which is one of fundamental models of condensed matter physics. The Hubbard model is a particular case of the general model of interacting electrons, whose band structure is described within the strong coupling method [61, 62]. In the Hubbard model, it is assumed that, on each ion, only one orbitally nondegenerate energy level is relevant for the physical problem under study and taken into consideration. The existence of other quantum states is ignored based on the assumption of their energy remoteness. The quantum transitions between the ions taken into account leads to the formation of the strong-coupling band.

The Hamiltonian of the Hubbard model contains two major parameters, namely, the matrix element t of hopping between the nearest-neighbor sites and the parameter U of the Coulomb repulsion of electrons with opposite spins at one site. In the second quantization representation, the Hamiltonian is expressed as

$$\hat{H} = \sum_{f\sigma}(\varepsilon - \mu)\hat{n}_{f\sigma} + \sum_{fm\sigma} t_{fm} a^{\dagger}_{f\sigma} a_{m\sigma} + U \sum_{f} \hat{n}_{f\uparrow}\hat{n}_{f\downarrow}, \qquad (1)$$

where $a^{\dagger}_{f\sigma}(a_{f\sigma})$ is the operator of creation (annihilation) of an electron with the spin projection $\sigma = \pm 1/2$ at site f, ε is the single-site energy of the electron, μ is the chemical potential of the system, and $\hat{n}_{f\sigma} = a^{\dagger}_{f\sigma} a_{f\sigma}$ is the particle number operator at site f.

This model is characterized by one more important parameter, the concentration of electrons n (the number of electrons at a lattice site), which varies from 0 to 2. The case of

half-occupation ($n = 1$) is special since, with a certain relation between the parameters t and U, an insulator state with long-range magnetic order can arise. At large values of U, the appearance of two electrons at one lattice site becomes energy unfavorable and the initial band splits into two Hubbard subbands with a gap in the center of the band. Thus, at half-occupation, the Fermi level finds itself in the energy gap, and the ground state becomes insulator. Electrons localize at the lattice sites and behave like magnetic moments with spin $S = 1/2$; therefore, the system becomes an antiferromagnetic (AFM) insulator [63].

The Hubbard model can describe both localized ($U \gg t$) and collective ($U \ll t$) electronic states. In the intermediate case $U \approx t$, the system combines opposite tendencies of localization and delocalization of states. Electric and magnetic properties of the systems described by the Hubbard model depend on the fine balance of these competing tendencies [64]. According to Mott [65], the predominance of one tendency over the other is what determines the final result: the predominance of hopping parameter t makes the system a metal, whereas the predominance of the Coulomb repulsion parameter U, on the contrary, makes it an insulator. Therefore, a metal–insulator transition depending on the ratio t/U is called the Mott–Hubbard transition.

It is well known that, besides the metal–insulator phase transition, the Hubbard model includes paramagnetic–ferromagnetic and paramagnetic–antiferromagnetic transitions [66, 67]. In the case of large U values, the model adequately allows for SECs that can give rise not only to a magnetic order, but also to a superconducting one. In 1987, Anderson [23] hypothesized that the Hubbard model can be a key to understanding the unusual behavior of HTSC materials. In his paper, the subsystem of ionic spin moments was considered following the scenario of 'resonating valence bonds', and the ensemble of charge excitations that appears under doping was interpreted as a Fermi subsystem manifesting Cooper instability. The mechanism of superconducting phase formation arising in such an approach had an electronic nature and led to high values of T_c.

In the analysis of nonphonon mechanisms of superconductivity in the Hubbard model, the researchers used the possibility of constructing the perturbation theory in two limiting cases: (1) the Born approximation of weak coupling, $U \ll W$ ($W = 2zt$, where z is the number of nearest neighbors) and arbitrary density of charge carriers; (2) the approximation of strong coupling, $U \gg W$, and small density of carriers. One of the first papers [68] studied the conditions for implementing the Kohn–Luttinger superconducting mechanism [69] that implies the emergence of Cooper instability in systems with purely repulsive interaction [69–76] in the weak coupling limit of the two-dimensional Hubbard model at a low density of electrons. The weak coupling limit $U \ll W$ in the two-dimensional (2D) and three-dimensional (3D) Hubbard models near half-occupation was analyzed in Refs [77–82]. As a result of these studies, a phase diagram was constructed for the 2D Hubbard model at small and intermediate occupation numbers, reflecting the result of competition between different symmetry species of the order parameter. The phase diagram obtained in the first two orders of the perturbation theory showed that, in the region of small concentration of charge carriers, $0 < n < 0.52$, d_{xy}-wave superconducting pairing is implemented. For intermediate densities, $0.52 < n < 0.58$, the ground state corresponds to a superconducting phase with the p-wave symmetry of the order parameter, and at $n > 0.58$, $d_{x^2-y^2}$-wave superconductivity arises. The phase diagram for the 2D Hubbard model in the opposite limit of strong coupling, $U \gg W$, and small density of charge carriers is constructed in Refs [83, 84].

Another solution to the superconducting pairing problem with high T_c was proposed in Ref. [85], where it was shown that the ensemble of fermions described by the Hubbard model in the SEC limit regime ($U \to \infty$) in the region of low concentration of holes exhibits Cooper instability in the s-wave channel. The new scenario of superconducting pairing is based on kinematic interaction, which is initiated in an ensemble of Hubbard fermions due to quasi-Fermi anticommutation relations between the Hubbard operators [86]. The kinematic mechanism of Cooper instability also had an electronic nature and provided high critical temperatures. Considering the intersite Coulomb interaction among fermions within the Shubin–Vonsovsky model [87–89] decreased the superconducting transition temperature [90–92] (see Section 6.2 and dashed curves in Fig. 13) and led to temperatures corresponding to experimental data.

The state of theoretical studies within the Hubbard model is most thoroughly reflected in the books by Izyumov [93–95] and reviews [96–99].

In attempts to describe the physical properties of HTSCs, researchers faced a difficulty associated with the necessity of considering two sorts of ions, Cu^{2+} (configuration $3d^9$) and O^{2-} (configuration $2p^6$). Hence, the model that would adequately describe the electronic structure of cuprates must include the parameters allowing for the energies of copper d-electrons and oxygen p-electrons, the overlap of d and p wave functions of electrons at neighboring lattice sites, the energies of single-site repulsion of copper and oxygen electrons, as well as the energy of their intersite Coulomb repulsion. As a result, it became necessary to formulate a more realistic theoretical model, as opposed to the Hubbard model, to describe the physics of copper–oxygen planes.

2.3 Multiband p–d models

After analyzing the crystal structure and phase diagram of cuprates, the center of gravity of research shifted to studying model Hamiltonians describing the motion of electrons in CuO_2 planes [22]. Such a simplification was confirmed by the presence of strong copper–oxygen bonds [100–103]. It was clear that some features of the phase diagram (e.g., the existence of a finite Néel temperature) could be explained only by taking into account the coupling between the planes. However, it was expected that such details could be studied already after understanding the basic features of electronic properties related to the 2D character of fermion motion.

It was revealed that, even with such a simplification, the study of fermion ensembles for individual CuO_2 planes remains a complicated problem, since copper ions Cu^{2+} possess nine electrons on five d-orbitals, and oxygen ions O^{2-} possess three filled p-orbitals. In all HTSC structures, the degeneracy of d-orbitals due to the symmetry of isolated atoms with respect to rotations in the 3D space is lifted because of the breaking of this symmetry in the lattice. Calculations in [100, 102] have shown that the orbitals of copper and oxygen are separated in energy (Fig. 1). The maximum energy belongs to the $d_{x^2-y^2}$-orbital, and in the absence of doping it has one hole. Other orbitals with lower energies are completely occupied and can be ignored in the first approximation when constructing a Hamiltonian.

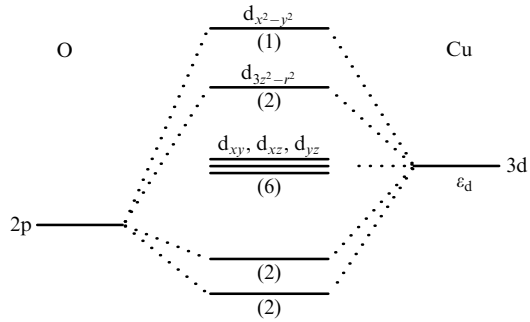

Figure 1. Relation between a Cu^{2+} ion and two O^{2-} ions. Only d-electrons of copper and p_x- and p_y-orbitals of oxygen are considered. The numbers in parentheses indicate the population of levels in an undoped structure [104].

Using these arguments, Emery proposed in 1987 a three-band model, describing a system of holes in copper–oxygen planes. At present, it is known as the p–d Emery model [22]. Based on the importance of taking into account processes with charge transfer, Varma et al. [105] formulated a similar approach. In the representation of secondary quantization operators, the Hamiltonian of the Emery model can be written as follows:

$$\hat{H} = \hat{H}_0 + \hat{H}_{\rm int}\,, \tag{2}$$

$$\hat{H}_0 = \sum_f (\varepsilon_{\rm d}\hat{n}_f^{\rm d} + U_{\rm d}\hat{n}_{f\uparrow}^{\rm d}\hat{n}_{f\downarrow}^{\rm d}) + \sum_l \varepsilon_{\rm p}\hat{n}_l^{\rm p} + \sum_{f\delta} V_{\rm pd}\hat{n}_f^{\rm d}\hat{n}_{f+\delta}^{\rm p}\,, \tag{3}$$

$$\hat{H}_{\rm int} = \hat{U}_{\rm p} + \hat{T}_{\rm pp} + \hat{V}_{\rm pp} + \hat{T}_{\rm pd}\,, \tag{4}$$

$$\hat{T}_{\rm pd} = t_{\rm pd}\sum_{f\delta\sigma}\vartheta(\delta)(d_{f\sigma}^{\dagger}p_{f+\delta,\sigma} + {\rm h.c.})\,,$$

$$\hat{T}_{\rm pp} = \sum_{l\Delta\sigma} t_{\rm pp}(\Delta)p_{l\sigma}^{\dagger}p_{l+\Delta,\sigma}\,,$$

$$\hat{U}_{\rm p} = U_{\rm p}\sum_l \hat{n}_{l\uparrow}^{\rm p}\hat{n}_{l\downarrow}^{\rm p}\,,$$

$$\hat{V}_{\rm pp} = \sum_{ll'(l\neq l')} V_{\rm pp}(l-l')\hat{n}_l^{\rm p}\hat{n}_{l'}^{\rm p}\,.$$

Here, the operator $\hat{H}_0$ describes the system of holes located on the copper and oxygen ions. $\hat{H}_0$ includes terms allowing for the Coulomb interaction between two holes, located on one copper ion. The energy of such an interaction is denoted by $U_{\rm d}$. The last term in $\hat{H}_0$ takes into account the interaction between the holes located at the nearest-neighbor copper and oxygen ions. The parameter $V_{\rm pd}$ determines the intensity of such an interaction.

The operator $\hat{H}_{\rm int}$ describes the processes of covalent mixing ($\hat{T}_{\rm pd}$), direct hopping of holes between nearest-neighbor oxygen ions ($\hat{T}_{\rm pp}$), the Hubbard repulsion of two holes on one oxygen ion ($\hat{U}_{\rm p}$), as well as intersite Coulomb repulsion of holes located on oxygen ions ($\hat{V}_{\rm pp}$).

In expression (2), $d_{f\sigma}^{\dagger}(d_{f\sigma})$ and $p_{l\sigma}^{\dagger}(p_{l\sigma})$ are creation (annihilation) operators of d- and p-holes with the spin projection $\sigma = \pm 1/2$ on a copper ion, whose position is numbered by subscript f, and an oxygen ion, located at the lattice site l, respectively. By δ we denote the magnitude of one of four vectors, connecting the copper ion number f and the oxygen ion number $l = f + \delta$ in the CuO_2 plane:

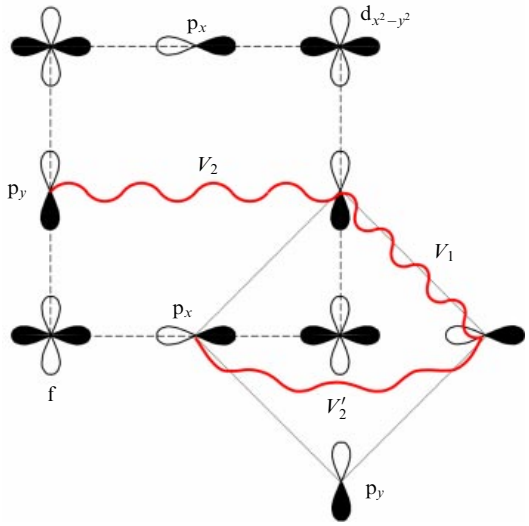

Figure 2. Structure of the CuO_2 plane. V_1 is the Coulomb interaction of holes located on the nearest-neighbor oxygen ions, V_2 and V_2' are the Coulomb repulsions of holes located on the next-nearest-neighbor oxygen ions. Black (white) areas correspond to the positive (negative) sign of the orbital lobe.

$\delta = \{\pm x/2, \pm y/2\}$, where $x = (a, 0)$ and $y = (0, a)$, a being the unit cell parameter (Fig. 2). The operators of the particle number on copper and oxygen ions are defined by the expressions $\hat{n}_f^{\rm d} = \sum_\sigma \hat{n}_{f\sigma}^{\rm d} = \sum_\sigma d_{f\sigma}^{\dagger}d_{f\sigma}$ and $\hat{n}_l^{\rm p} = \sum_\sigma \hat{n}_{l\sigma}^{\rm p} = \sum_\sigma p_{l\sigma}^{\dagger}p_{l\sigma}$, respectively, and $\varepsilon_{\rm d}$ and $\varepsilon_{\rm p}$ are the bare single-site energies of holes on copper and oxygen ions. Parameters $U_{\rm p}$ and $V_{\rm pp}$ correspond to the energies of Coulomb repulsion of holes on one oxygen ion and on different oxygen ions, respectively; $t_{\rm pd}$ is the integral of hole hopping from an oxygen ion to a copper one. The function $\vartheta(\delta)$ allows for the influence of phases of copper and oxygen orbitals on the hybridization processes. For orbital profiles shown in Fig. 2, the function $\vartheta(\delta)$ takes the following values upon varying δ: $\vartheta(\delta) = \mp 1$ for $\delta = \pm x/2$ or $\delta = \pm y/2$. The integral of hole hopping between the nearest oxygen orbitals is determined as $t_{\rm pp}(\Delta) = t\rho(\Delta)$. Its sign is determined by the function $\rho(\Delta)$, where Δ is the magnitude of the vector connecting the nearest-neighbor oxygen ions. For the chosen sequence of phases of oxygen orbitals, $\rho(\Delta) = 1$ for $\Delta = \pm(x + y)/2$ and $\rho(\Delta) = -1$ for $\Delta = \pm(x - y)/2$.

The Emery Hamiltonian is a Hamiltonian of the multi-band theory of metals in the strong-coupling representation. At large values of the Hubbard repulsion parameters, it describes a system with SEC. Hence, the Emery model is sometimes referred to as a three-band or extended Hubbard model.

An important parameter of the model is the difference between the energies of holes on the copper and oxygen ions, $\Delta_{\rm pd} = \varepsilon_{\rm p} - \varepsilon_{\rm d}$. If $\Delta_{\rm pd} > 0$, then, in the nondoped case, when a single hole corresponds to each cell, the d-orbital of a copper ion at $t_{\rm pd} = 0$ is occupied, while the p-orbitals of oxygen ions are empty. Upon doping, new holes will occupy the oxygen orbitals, if $U_{\rm d} > \Delta_{\rm pd}$. This completely agrees with the experimental results of the electron energy loss spectroscopy (EELS) [106].

The values of the Emery model energy parameters were extracted from band structure calculations by several teams [107–109]. At present, the following values of the parameters

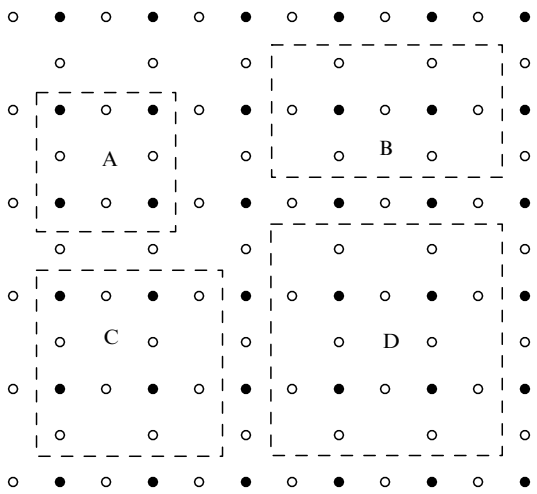

Figure 3. Clusters used for exact diagonalization of the Emery Hamiltonian. The number of atoms is $N_a = 8, 9, 12, 16$ for clusters A, B, C, and D, respectively. Dark dots — Cu atoms, circles — O atoms [114].

are most frequently used [107, 110] (in [eV]):

$$\Delta_{pd} = 3.6\,, \quad t_{pd} = 1.3\,, \quad t_{pp} = 0.65\,, \qquad U_d = 10.5\,, \quad U_p = 4\,, \quad V_{pd} = 1.2\,. \tag{5}$$

Because of Coulomb interactions, the Emery model is difficult for theoretical analysis. The presence of four bare vertices significantly limits the possibilities of applying various forms of perturbation theory to considering the model in the general case. The absence of exact solutions of the Emery model and the difficulties arising when trying to reasonably simplify it stimulated the use of computer analysis methods. Numerical calculations were mainly carried out using the Monte Carlo method and the method of exact diagonalization of finite clusters. The Monte Carlo method [111, 112] allowed studying relatively large clusters of $N_a = 50-100$ atoms [113], but the precision of calculations sharply fell with a decrease in temperature. Therefore, the most interesting case of $T \leqslant T_c \approx 100$ K turned out to be beyond consideration [114]. The method of exact diagonalization of finite clusters [115, 116] is free of this drawback and allows studying both the ground ($T = 0$) and the excited states of the system. A disadvantage of this method is the cluster size limitation, imposed by computer memory and operating speed. Nevertheless, this method is quite acceptable for qualitatively understanding the properties of systems with SEC. Figure 3 shows copper–oxygen clusters, whose ground states were studied in a number of papers for various values of the Emery Hamiltonian parameters: A [115, 117], B, D [116], C [118, 119], A, B, C, D [120]. Among these four clusters, only one (C) with $N_a = 12$ possesses the symmetry of the CuO_2 plane and allows periodic boundary conditions. The cluster of maximal size for which the exact diagonalization of the three-band p–d model has been carried out is Cu_4O_{12} (cluster D).

Later, as a result of considering the electronic structure of copper oxides, with the specific features of their chemical bond and SEC taken into account [121–123], it was noted that, besides the $3d_{x^2-y^2}$-orbitals of copper and $2p_x$- and $2p_y$-orbitals of oxygen, which are considered in the three-band p–d model, it is also necessary to allow for other copper orbitals (see Fig. 1). A considerable (10–15%) population of the $3d_{3z^2-r^2}$-orbitals of copper in all p-wave HTSCs was revealed by EELS experiments [124, 125] and experiments using polarized X-ray absorption spectroscopy (XAS) [126, 127].

The authors of Ref. [108] theoretically demonstrated the importance of the $3d_{3z^2-r^2}$-orbitals of copper. Having estimated the values of the p–d model parameters, they calculated the states of a CuO_4 cluster, considering all 12 p-orbitals and 5 d-orbitals, and compared the results with experimental data. It was found that the orbitals $3d_{3z^2-r^2}$, $3d_{xy}$, $3d_{xz}$, and $3d_{yz}$ noticeably contribute to the formation of electronic states. The authors of Ref. [108] noted that the $3d_{3z^2-r^2}$-orbitals are the most important, because they are stabilized by bonds with apical oxygen atoms [128].

A number of superconductivity mechanisms have been proposed in which the $3d_{3z^2-r^2}$-orbital plays an essential role. In Refs [129, 130], an electronic mechanism of pairing is formulated — the Gaididei–Loktev–Weber exciton mechanism [64]. Paper [131] shows that the combined effect of Hund pairing and superexchange interaction between holes in the $3d_{x^2-y^2}$-orbital leads to efficient attraction between quasiparticles that appear in the $3d_{3z^2-r^2}$-orbital upon doping.

Later on, experimental evidence appeared that apical oxygen plays an important role in the electronic structure of cuprates and can affect their superconducting properties. For example, in some structures, a significant isotopic effect for the apical oxygen was found [132, 133], as was an obvious correlation between the maximum temperature T_c of various cuprates and their Cu–O_z bond [134]. This fact led some researchers to the conclusion that, for an even more realistic description of the electronic structure, it is also necessary to consider the $2p_z$-orbital of the apical oxygen. As a result, a conclusion was made that the minimal model of copper–oxygen planes is the five-band p–d model [129, 135] that includes two d-orbitals, $3d_{x^2-y^2}$ and $3d_{3z^2-r^2}$, as well as $2p_x$- and $2p_y$-orbitals on each oxygen ion, and the $2p_z$-orbital on the apical oxygen [61].

2.4 $t-J$ model

Since multiband p–d models include several parameters, which complicates their theoretical analysis, attempts have been made to reduce them to simpler models. Zhang and Rice [21] were the first to succeed in this regard, following the considerations presented below.

Consider a copper ion surrounded by four oxygen ions (a CuO_4 cluster). The hole added upon doping appears on the oxygen ion in a symmetric or antisymmetric state with respect to the central hole on copper. Thus, the hole on oxygen can form a strong bond with the hole on copper and form a singlet or a triplet spin state. The authors of Ref. [21] showed that near the atomic limit in the second order of perturbation theory the spin singlet has a lower (by 3–4 eV) energy than the rest possible double-hole states. When doped, holes fall into this singlet state (Zhang–Rice singlet), and it would seem that one can work in the singlet subspace without violating the physics of the problem. As a result, the hole moves over the square lattice of copper ions, whereas oxygen ions are no longer present in the effective model explicitly. Zhang and Rice in [21] concluded that an effective Hamiltonian describing the physics of the three-band model is the Hamiltonian of the so-called $t-J$ model [63], which is an effective low-energy version of the Hubbard model in the limit $t/U \ll 1$ [136, 137]. The Hamiltonian of this model without three-center terms (see below) in the secondary quantization representation is

expressed as

$$\hat{H} = \sum_{f}(\varepsilon - \mu)\hat{n}_f + \sum_{fm\sigma} t_{fm}(1 - \hat{n}_{f\bar{\sigma}})a^{\dagger}_{f\sigma}a_{m\sigma}(1 - \hat{n}_{m\bar{\sigma}}) + \sum_{fm} J_{fm}\left(\mathbf{S}_f\mathbf{S}_m - \frac{\hat{n}_f\hat{n}_m}{4}\right), \quad (6)$$

where $\hat{n}_f = \sum_\sigma \hat{n}_{f\sigma}$ is the operator of the number of electrons with spin $\sigma = \pm 1/2$ on site f, t_{fm} is the hopping matrix element, $a^{\dagger}_{f\sigma}(a_{f\sigma})$ is the creation (annihilation) operator for an electron with spin σ at site f, $J_{fm} = 2t^2_{fm}/U$ is the effective exchange integral, U is the parameter of the Hubbard repulsion of electrons, and $\mathbf{S}_f$ is the operator of spin $S = 1/2$ at site f. The factors $1 - \hat{n}_{f\bar{\sigma}}$ forbids an electron with spin σ to be located at site f already containing an electron with spin $\bar{\sigma} \equiv -\sigma$. Thus, the $t-J$ model describes the motion of electrons over the nonoccupied lattice sites. The elimination of states with a pair of electrons on a site is equivalent to the appearance of an effective exchange interaction of electrons at neighboring sites with the exchange integral of the AFM sign.

It should be noted that, in the derivation of the $t-J$ model Hamiltonian (6) from the Hubbard model (1) in the SEC regime, in addition to exchange terms, so-called three-center terms arise [41, 138–144] with the same order of smallness as the exchange terms and describing spin-correlated hopping. With these terms taken into account, the corresponding model is referred to as the $t-J^*$ model. The three-center terms play an essential role in the description of the superconducting d-wave phase in cuprates [41, 140–144]. It should also be noted that the $t-J$ model can be generalized at the expense of both single-site and intersite Coulomb interactions within the $t-J-U$ and $t-J-U-V$ models, respectively [145–148].

The $t-J$ model acquired exclusive popularity after the appearance of Anderson's idea [23] that the electronic properties of HTSCs can be described by Hamiltonian (6). A review of theoretical studies of normal and superconducting properties of cuprates within the $t-J$ model is presented in Refs [7, 63, 67, 110]. The issue of complete and consistent derivation of an effective single-band model from a three-band model and multiband p–d models was thoroughly considered in Refs [149–158] using the cluster form of perturbation theory.

2.5 Kondo lattice model

As one more variant of an effective low-energy Hamiltonian of a three-band p–d model in studies of cuprate superconducting properties, the Kondo lattice Hamiltonian, or s–d(f) exchange model [94, 95, 161–163], is often used [32–36, 41, 159, 160]:

$$\hat{H}_{\mathrm{K}} = \sum_{fm\alpha} t_{fm}c^{\dagger}_{f\alpha}c_{m\alpha} + J\sum_{f\alpha\beta} c^{\dagger}_{f\alpha}\boldsymbol{\sigma}_{\alpha\beta}c_{f\beta}\mathbf{S}_f + \frac{1}{2}\sum_{fm} I_{fm}\mathbf{S}_f\mathbf{S}_m\,. \quad (7)$$

It takes into account not only the exchange interaction J between fermions and localized spins, but also the Heisenberg AFM interaction between localized spins with the exchange constant I_{fm}. In Hamiltonian (7), $c^{\dagger}_{f\alpha}(c_{f\alpha})$ are the creation (annihilation) operators of a quasiparticle at site f with the spin projection α, t_{fm} is the integral of fermion hopping from site f to site m, $\mathbf{S}_f$ is the operator of localized spin $S = 1/2$ at site f, and $\boldsymbol{\sigma} = (\sigma_x, \sigma_y, \sigma_z)$ is a vector composed of Pauli matrices.

The limit cases of the Kondo lattice model correspond to other theoretical models, frequently used in the physics of systems with SEC [164]. In the absence of doping, the Kondo lattice model is reduced to the Heisenberg AFM model with spin $S = 1/2$ (sometimes in the literature, the Kondo lattice model is referred to as the Kondo–Heisenberg lattice model), which is capable of describing the physics of undoped cuprates [165–170]. For large J, the formation of Zhang–Rice singlets takes place (see Section 2.3), and the low-energy dynamics of the generalized Kondo lattice model can be reflected by the $t-J$ model [21]. In the presence of oxygen–oxygen hopping, the Kondo lattice model can be reduced to the generalized $t-J$ model, including the hopping of fermions to the second and third coordination spheres of a square lattice, as well as the hopping accompanied by a spin flip [171]. For Heisenberg interaction close to zero, the Kondo lattice model is equivalent to the common Kondo model [172].

In Section 3, it is shown that the Hamiltonian of the Kondo lattice model (7) can be consistently derived from the Emery model Hamiltonian [173]. However, for this purpose, it is necessary to ignore the effective spin-correlated hopping, playing an important role in the formation of a spin-fermion quasiparticle, meaning that, to describe the properties of hole-doped cuprate superconductors adequately, Hamiltonian (7) should be substantially extended.

3. Spin-fermion model of cuprates

3.1 Drawbacks of single-band models

In spite of the considerable success achieved in the description of the physical properties of cuprate superconductors within the Hubbard model and $t-J$ model [7, 63, 67, 110], the justification of reducing the Emery model to them remained an open and controversial question. Emery and Reiter [174] showed that, in a three-band model, the Zhang–Rice singlet overlaps with a triplet at the boundaries of the Brillouin zone. This gives rise to elementary excitations possessing charge and spin, in contrast to singlets formed in the effective single-band $t-J$ model. The authors of Ref. [174] presented arguments in favor of the important role played by oxygen ions in the formation of the hole ensemble properties in CuO_2 planes, due to which they should not be excluded from explicit consideration. The result by Emery and Reiter was based on an analysis of the exact solution against the background of ferromagnetic interaction, and the conclusion was that the $t-J$ model does not fully reflect the physics of the three-band p–d model. Zhang and Rice [175] and Emery and Reiter [176] continued the exchange of ideas on this issue, but never reached an agreement, although further cluster calculations [177] within the three-band p–d model seemed to confirm that the Zhang–Rice singlet is well separated in energy from the remaining higher-energy two-hole states.

The authors of Ref. [178] have shown that the charge degrees of freedom give rise to new physical effects, when the Coulomb interaction between holes on copper and oxygen ions is comparable in magnitude with the energy of hybridization and the energy difference between copper and oxygen levels Δ_{pd}. In this case, the presence of two sorts of ions is a key factor; therefore, the three-band model cannot be reduced to an effective single-band one. In Ref. [178], it was noted that one of the main features of the three-band model is the

existence of collective excitations (resonances of charge transfer) and intra-unit-cell instabilities that can determine the HTSC mechanism.

Actually, having rigorously demonstrated in Ref. [21] a significant advantage in the bonding orbital energy, Zhang and Rice further substantiated the equivalence of the $t-J$ and p–d models only by means of qualitative considerations. The papers cited above [149–158], claiming to be rigorous in the proof of this statement, actually use a number of approximations related to either ignoring long-range interactions or disregarding a considerable part of unit-cell states. However, it is worth noting that in the rigorous derivation of the Emery model Hamiltonian in the SEC regime, the constant of spin-fermion coupling and spin-correlated hopping turns out to be the largest parameter of the effective model. Due to this fact, further interpretation of these interactions within the common perturbative approaches used by the authors of Refs [149–158] seems unfounded.

The spin polaron concept [32–36], on the contrary, is based on the fact that the strong spin-fermion coupling arising in the Emery model effective Hamiltonian should be considered exactly. Section 3.2 is devoted to a detailed derivation of the Emery model effective Hamiltonian — the spin-fermion model of cuprates (SFMC) — and analysis of spin-fermion interactions arising in the second order with respect to the p–d hybridization parameter.

3.2 Effective Hamiltonian of the Emery model in the strong correlation regime

As already mentioned, in the undoped case at low temperatures, cuprates are AFM insulators. This phase corresponds to the ground state of the Emery Hamiltonian (2) if the energy parameters satisfy the condition

$$\Delta_{\mathrm{pd}} > 0\,, \quad \frac{\left|t_{\mathrm{pd}}(\delta)\right|}{\Delta_{\mathrm{pd}}} \ll 1\,, \quad \frac{\left|t_{\mathrm{pd}}(\delta)\right|}{U_{\mathrm{d}} - \Delta_{\mathrm{pd}} - 2V_{\mathrm{pd}}} \ll 1\,. \tag{8}$$

The positive value of the gap with charge transfer $\Delta_{\mathrm{pd}} = \varepsilon_{\mathrm{p}} - \varepsilon_{\mathrm{d}}$ provides the localization of holes presumably on copper ions implementing the states with spin $S = 1/2$. The second inequality establishes a weak intensity of the processes of covalent mixing of d-states on copper ions and p-states on oxygen ions.

If the third inequality in (8) is valid, the SEC regime is implemented, in which the localization of two holes at one copper ion becomes energy unfavorable. Therefore, in the absence of doping, the insulator Mott–Hubbard phase is formed, and upon doping an additional hole appears at the p-orbital of an oxygen ion. However, due to hybridization of this orbital with the d-orbital of the nearest copper ion, virtual transitions of the additional hole to high-energy states of copper ions with two holes occur. Such transitions give rise to the effective interaction of an oxygen hole with the spins localized on copper ions, which destroys the long-range magnetic order. These processes can be correctly taken into account by constructing an effective Hamiltonian.

Inequalities (8) allow considering the processes of covalent mixing of p-orbitals of oxygen ions and d-orbitals of copper ions within the perturbation theory. A regular way to implement this procedure consists in constructing an effective Hamiltonian $\hat{H}_{\mathrm{eff}}$ with further development of the theory of cuprate superconductors on this basis. The feasibility of introducing $\hat{H}_{\mathrm{eff}}$ is related to the fact that in this Hamiltonian the abovementioned processes of p–d hybridization accompanied by transitions of copper ions to two-hole states, as well as to states of these ions without holes, manifest themselves via the appearance of effective interactions. In this case, it is important that for the subsystem of copper ions the Hamiltonian $\hat{H}_{\mathrm{eff}}$ act only on the class of homeopolar states identified by the values of spin projection. Such a reduction of the Hilbert space allows not only simplifying subsequent calculations but also a clear understanding of the key features of the low-energy spectrum of elementary excitations based on the physical interpretation of arising effective interactions.

To find $\hat{H}_{\mathrm{eff}}$, the Schrieffer–Wolff method of unitary transformations [179] or the operator form of perturbation theory is used [180, 181]. When using the second approach, the calculations are relatively simple in the atomic representation. For this purpose, let us introduce four basis states of a copper ion at site f: $|f;0\rangle$, the state without a hole, $|f;\alpha\rangle = d^{\dagger}_{f\alpha}|f;0\rangle$, the state with one hole having the spin projection α, and $|f;2\rangle = d^{\dagger}_{f\uparrow}d^{\dagger}_{f\downarrow}|f;0\rangle$, the state with two holes.

The Hubbard operators in the basis of these states are defined as usual:

$$X_f^{pq} = |f;p\rangle\langle q;f|\,, \tag{9}$$

where p and q are the indices of single-ion states. Applying the well-known representation of the second quantization operators in terms of the Hubbard operators

$$d_{f\alpha} = X_f^{0\alpha} + 2\alpha X_f^{\bar{\alpha}2}\,, \quad \alpha = \pm\frac{1}{2}\,, \quad \bar{\alpha} \equiv -\alpha\,, \tag{10}$$

we present the Emery Hamiltonian (2) in a form convenient for using the operator form of the perturbation theory. In the atomic representation, the operator $\hat{H}_0$ (3) is expressed as

$$\hat{H}_0 = \sum_{f\alpha}\varepsilon_{\mathrm{d}}X_f^{\alpha\alpha} + \sum_f(2\varepsilon_{\mathrm{d}} + U_{\mathrm{d}})X_f^{22} + \sum_f\varepsilon_{\mathrm{p}}(\hat{n}^{\mathrm{p}}_{f+x/2} + \hat{n}^{\mathrm{p}}_{f+y/2}) + V_{\mathrm{pd}}\sum_{f\delta}\left(\sum_{\alpha}X_f^{\alpha\alpha} + 2X_f^{22}\right)\hat{n}^{p}_{f+\delta}\,. \tag{11}$$

In the interaction operator (4), only the term $\hat{T}_{\mathrm{pd}}$ will change form:

$$\hat{T}_{\mathrm{pd}} = \sum_{f\delta\alpha}t_{\mathrm{pd}}\vartheta(\delta)(X_f^{\alpha 0} + 2\alpha X_f^{2\bar{\alpha}})\,p_{f+\delta,\alpha} + \mathrm{h.c.} \tag{12}$$

Using conditions (8) and applying the operator form of perturbation theory, we arrive at a formal representation of the effective Hamiltonian in the form of a power series in the parameter t_{pd}:

$$\hat{H}_{\mathrm{eff}} = P\hat{H}P + \hat{H}^{(2)} + \hat{H}^{(3)} + \hat{H}^{(4)} + \ldots\,, \tag{13}$$

where the projection operator

$$P = \prod_f(X_f^{\uparrow\uparrow} + X_f^{\downarrow\downarrow}) \tag{14}$$

is defined through the diagonal Hubbard operators $X_f^{\alpha\alpha} = |f;\alpha\rangle\langle\alpha;f|$ possessing the projective property $(X_f^{\alpha\alpha})^2 = X_f^{\alpha\alpha}$. Operator P is seen to implement projection on the subspace, from which the states with two holes or no holes on copper ions are excluded.

The term of zero order in $t_{\mathrm{pd}}(\delta)$ describes the system of oxygen holes, which in this approximation is isolated from the

subsystem of holes on copper ions,

$$P\hat{H}P = N\varepsilon_{\rm d} + \sum_{l\alpha}\tilde{\varepsilon}_{\rm p}\hat{n}_{l\alpha} + \hat{U}_{\rm p} + \hat{V}_{\rm pp} + \hat{T}_{\rm pp}\,. \tag{15}$$

The term $N\varepsilon_{\rm d}$ appears due to the fact that the operator $\hat{n}_f$ becomes a unit operator in the class of homeopolar states of copper ions. Here, N denotes the number of unit cells in the CuO_2 plane. The energy renormalization for an oxygen hole, $\tilde{\varepsilon}_{\rm p} = \varepsilon_{\rm p} + 2V_{\rm pd}$, occurs because of the interaction of this hole located on an oxygen ion with two holes that form homeopolar states of the two nearest-neighbor copper ions.

The operator $\hat{H}^{(2)}$ containing only terms quadratic in $t_{\rm pd}(\delta)$ is determined by the expression

$$\hat{H}^{(2)} = -P\hat{T}_{\rm pd}(\hat{H}_0 - E_0)^{-1}\hat{T}_{\rm pd}P\,. \tag{16}$$

Using the algebra of Hubbard operators $X_f^{nm}X_f^{pq} = \delta_{mp}X_f^{nq}$, after simple calculations, we get an explicit form of $\hat{H}^{(2)}$ in the tight-binding representation:

$$\hat{H}^{(2)} = -\frac{4Nt_{\rm pd}^2}{\Delta_{\rm pd} + V_{\rm pd}} + \hat{\tau} + \hat{J}\,. \tag{17}$$

The first term on the right-hand side of Eqn (17) determines the contribution of covalent effects to the binding energy of an undoped system. The second term,

$$\hat{\tau} = \frac{\tau}{2}\sum_{f\delta\delta'\alpha}\vartheta(\delta)\vartheta(\delta')\,p^{+}_{f+\delta,\alpha}\,p_{f+\delta',\alpha}\,, \tag{18}$$

describes the motion of holes leading to the broadening of the energy levels of the oxygen orbitals. In this case, the width of the arising band is given by

$$\tau = \frac{t_{\rm pd}^2}{\Delta_{\rm pd}}\left(1 - \frac{\Delta_{\rm pd}}{U_{\rm d} - \Delta_{\rm pd} - 2V_{\rm pd}}\right). \tag{19}$$

The third term in Eqn (17) is responsible for the exchange coupling between the subsystem of localized spins and oxygen holes,

$$\hat{J} = \frac{J}{4}\sum_{f\delta\delta'\alpha\beta}\vartheta(\delta)\vartheta(\delta')\,p^{\dagger}_{f+\delta,\alpha}\mathbf{S}_f\boldsymbol{\sigma}_{\alpha\beta}\,p_{f+\delta',\beta}\,, \tag{20}$$

where the exchange operator is

$$J = \frac{4t_{\rm pd}^2}{\Delta_{\rm pd}}\left(1 + \frac{\Delta_{\rm pd}}{U_{\rm d} - \Delta_{\rm pd} - 2V_{\rm pd}}\right). \tag{21}$$

The operator $\hat{J}$ describes both the spin-correlated hopping of holes between oxygen ions and the exchange interaction of a hole located on an oxygen ion with spins on the nearest-neighbor copper ions. Here, $\mathbf{S}_f$ is the vector spin operator localized at site f, and the vector operator $\boldsymbol{\sigma}$ is composed of Pauli matrices, $\boldsymbol{\sigma} = (\sigma^x, \sigma^y, \sigma^z)$.

The third-order perturbation theory terms in the effective Hamiltonian are usually not taken into account, since they possess additional smallness with respect to both the concentration of oxygen holes and the parameter of covalent mixing. Therefore, in the low-doping region, the contribution of such terms can be disregarded.

Among the contributions of the fourth order, of major importance are the terms of zeroth power with respect to the concentration of oxygen carriers. These contributions are known to give rise to the formation of AFM-type exchange interaction in the subsystem of localized spins. Simple calculations yield an operator describing the Heisenberg exchange interaction,

$$\hat{I} = \frac{I}{2}\sum_{f\delta}\mathbf{S}_f\mathbf{S}_{f+2\delta}\,, \tag{22}$$

in which the exchange integral is expressed as

$$I = \frac{4t_{\rm pd}^4}{(\Delta_{\rm pd} + V_{\rm pd})^2}\left(\frac{1}{U_{\rm d}} + \frac{1}{\Delta_{\rm pd}}\right). \tag{23}$$

To obtain a physically simpler form of operators $\hat{\tau}$ and $\hat{J}$, we move to the quasimomentum representation. Taking into account that there are two orbitals (p_x and p_y) per unit cell of the CuO_2 plane, we write down the Fourier transform as

$$\begin{aligned} p_{f\pm x/2,\alpha} &\equiv a_{f\pm x/2,\alpha} = \frac{1}{\sqrt{N}}\sum_k \exp\left[{\rm i}k\left(f \pm \frac{x}{2}\right)\right]a_{k\alpha}\,,\\ p_{f\pm y/2,\alpha} &\equiv b_{f\pm y/2,\alpha} = \frac{1}{\sqrt{N}}\sum_k \exp\left[{\rm i}k\left(f \pm \frac{y}{2}\right)\right]b_{k\alpha}\,. \end{aligned} \tag{24}$$

Then, the combination of second quantization operators entering the definition of operators $\hat{\tau}$ and $\hat{J}$ takes the form

$$\begin{aligned} \sum_\delta \vartheta(\delta)p_{f+\delta,\alpha} &= a_{f+x/2,\alpha} + b_{f+y/2} - a_{f-x/2,\alpha} - b_{f-y/2,\alpha}\\ &= \frac{1}{\sqrt{N}}\sum_k \exp({\rm i}kf)2{\rm i}\left(a_{k\alpha}\sin\frac{k_x}{2} + b_{k\alpha}\sin\frac{k_y}{2}\right). \end{aligned} \tag{25}$$

Collecting the terms (13) together, we arrive at the SFMC Hamiltonian [24–31]:

$$\hat{H} = \hat{H}_{\rm h} + \hat{J} + \hat{I} + \hat{U}_{\rm p} + \hat{V}_{\rm pp}\,, \tag{26}$$

$$\hat{H}_{\rm h} = \sum_{k\alpha}\left[\xi_{k_x}a^{\dagger}_{k\alpha}a_{k\alpha} + \xi_{k_y}b^{\dagger}_{k\alpha}b_{k\alpha} + t_k(a^{\dagger}_{k\alpha}b_{k\alpha} + b^{\dagger}_{k\alpha}a_{k\alpha})\right],$$

$$\hat{J} = \frac{J}{N}\sum_{fkq\alpha\beta}\exp\left[{\rm i}f(q-k)\right]u^{\dagger}_{k\alpha}\mathbf{S}_f\boldsymbol{\sigma}_{\alpha\beta}\,u_{q\beta}\,,$$

$$\hat{I} = \frac{I}{2}\sum_{f\delta}\mathbf{S}_f\mathbf{S}_{f+2\delta}\,,$$

$$\hat{U}_{\rm p} = \frac{U_{\rm p}}{N}\sum_{pkq}(a^{\dagger}_{p+q\uparrow}a^{\dagger}_{k-q\downarrow}a_{k\downarrow}a_{p\uparrow} + b^{\dagger}_{p+q\uparrow}b^{\dagger}_{k-q\downarrow}b_{k\downarrow}b_{p\uparrow})\,,$$

$$\hat{V}_{\rm pp} = \frac{4V_1}{N}\sum_{\substack{pkq\\ \alpha\beta}}\cos\frac{q_x}{2}\cos\frac{q_y}{2}\,a^{\dagger}_{p+q,\alpha}b^{\dagger}_{k-q,\beta}b_{k\beta}a_{q\alpha}$$

$$+\frac{1}{N}\sum_{\substack{p,k,q\\ \alpha\beta}}\Big\{\left[V_2'\exp({\rm i}q_x) + V_2\exp(-{\rm i}q_y)\right]a^{\dagger}_{p-q,\alpha}a^{\dagger}_{k+q,\beta}a_{k\beta}a_{q\alpha}$$

$$+\left[V_2'\exp({\rm i}q_y) + V_2\exp(-{\rm i}q_x)\right]b^{\dagger}_{p+q,\alpha}b^{\dagger}_{k-q,\beta}b_{k\beta}b_{q\alpha}\Big\}.$$

In Hamiltonian (26), the operator $\hat{H}_{\rm h}$ in the chemical potential representation describes free holes on oxygen ions, the operator $\hat{J}$ allows for the interaction of these holes with spins of copper ions, the operator $\hat{I}$ corresponds to the exchange interaction between the localized spins of copper

ions. In these expressions, the following functions are used:

$$\xi_{k_{x(y)}} = \varepsilon_{\rm p} + 2V_{\rm pd} + \tau(1 - \cos k_{x(y)}) - \mu\,, \tag{27}$$

$$t_k = (2\tau - 4t)\sin\frac{k_x}{2}\sin\frac{k_y}{2}\,, \tag{28}$$

where μ is the chemical potential of the system. The function t_k describes both the hybridization processes in the second-order perturbation theory (parameter τ) and the direct hopping of holes between oxygen ions (here, the parameter $t_{\rm pp}$ in the initial Emery model (2) is denoted by t for brevity).

We emphasize that in the SFMC the coupling between the subsystem of localized spins and the subsystem of holes on oxygen is described by the operator $\hat{J}$ with the real structure of the CuO_2 plane taken into account. This means that orbitals p_x and p_y are taken into account in each unit cell. Formally, this circumstance is reflected by the fact that the operators $u_{k\alpha}$ entering $\hat{J}$ are written as superpositions

$$u_{k\alpha} = a_{k\alpha}\sin\frac{k_x}{2} + b_{k\alpha}\sin\frac{k_y}{2}\,. \tag{29}$$

Operator $\hat{U}_{\rm p}$ describes the Hubbard repulsion of holes on oxygen ions. The last term of the SFMC Hamiltonian corresponds to the intersite Coulomb interaction. Here, the term with the parameter V_1 describes the repulsion of holes located on the nearest-neighbor oxygen ions. Because of the specific structure of the CuO_2 plane, the interaction of a hole located at site number l with another hole located at next-nearest-neighbor site number l' depends on both the position of site l and the direction of vector $\mathbf{r}_{ll'}$ (see Fig. 2). The presence of two parameters, V_2 and V_2', in the operator $\hat{V}_{\rm pp}$ is due to this fact.

A characteristic feature of Hamiltonian (26) is the SU(2)-invariant form of the operator of spin-fermion interaction $\hat{J}$. It is in this form that the operator $\hat{J}$ was written in one of the seminal papers by Emery and Reiter [174]. The SFMC Hamiltonian in the momentum representation had been considered earlier in Ref. [182] when studying the spectrum of Fermi quasiparticles in $Sr_2CuO_2Cl_2$ within the self-consistent Born approximation. In the cited papers, however, the operators of Coulomb interaction $\hat{U}_{\rm p}$ and $\hat{V}_{\rm pp}$ were not taken into account.

3.3 General properties and fundamental distinctions of the spin-fermion model of cuprates and other effective models

As mentioned in Section 3.2, the SFMC was formulated almost immediately after the discovery of cuprate HTSCs and has found wide application in the description of their physical properties [24–30]. Note that at that time this model had no special name; however, in 1998, in Ref. [31], the model with Hamiltonian (26) was first called spin-fermion.

On the other hand, in the early 1990s, in Refs [183–185], a semiphenomenological approach was developed, which allowed an explanation of the high values of the critical temperature of d-wave superconductivity based on the spin-fluctuation mechanism of Cooper pairing. This mechanism was discussed in detail in Ref. [186] based on the model with the Hamiltonian

$$\hat{H} = \sum_{k\sigma}\varepsilon_k\varphi^{\dagger}_{k\sigma}\varphi_{k\sigma} + \frac{1}{2N}\sum_{kq\alpha\beta} g(q)\varphi^{\dagger}_{k+q,\,\alpha}\mathbf{S}_{-q}\boldsymbol{\sigma}_{\alpha\beta}\varphi_{k\beta}\,. \tag{30}$$

When analyzing the properties of the system within Hamiltonian (30), it was assumed that the statistical properties of the spin-fluctuating operator $\mathbf{S}$ are specified by the spin-spin correlation function (the tensor of dynamic susceptibility $\chi_{ij}(q,\omega)$) [184].

The model with Hamiltonian (30) was called a spin-fermion model (SFM) in 1996 in Ref. [187]. During further development of the theory within this model [188–196], the effective Hamiltonian allowing for the low-energy excitations and exchange interaction between spin moments was used:

$$\hat{H} = \sum_{k\alpha} v_{\rm F}(k - k_{\rm F})c^{\dagger}_{k\alpha}c_{k\alpha} + \sum_q \chi_0^{-1}(q)\mathbf{S}_q\mathbf{S}_{-q} + \frac{g}{\sqrt{N}}\sum_{kq\alpha\beta} c^{\dagger}_{k+q,\,\alpha}\boldsymbol{\sigma}_{\alpha\beta}c_{k\beta}\mathbf{S}_{-q}\,. \tag{31}$$

This model describes fermions in the so-called hot points, arising at the intersection of the Fermi surface with the boundary of the AFM Brillouin zone and interacting via the exchange magnetic fluctuations that have a maximum at the point $\mathrm{Q} = (\pi, \pi)$.

Thus, at the end of the 20th century, in the theory of strongly correlated systems, a situation arose, in which at least two models were independently referred to as spin-fermion models. For this reason, in the present review, we will refer to the model with Hamiltonian (26) as the SFMC, and use the abbreviation SFM for model (31). In the present section, we consider the general properties of these models and indicate their fundamental differences.

As noted by the authors of Refs [188–192, 194–196], one of the ways to derive the SFM is based on using the Stratonovich–Hubbard transformation in order to transform the four-fermion interaction in a Hubbard-type Hamiltonian. The spin-fermion coupling arising as a result of such a procedure leads to an effective interaction between fermions in the second order with respect to the coupling constant.

To formulate the model, the authors of Refs [188–192, 194–196] relied on the experimental fact that the AFM instability in a system of interacting fermions is mainly caused by fermions whose energy is comparable to the width of the fermion band W. On the other hand, the Cooper pairing is induced by fermions from the vicinity of the Fermi surface, if the temperature of Cooper instability $T_{\rm ins} \ll W$. This separation of scales allows studying the Cooper instability within the effective low-energy model, in which high-energy Fermi degrees of freedom (responsible for antiferromagnetism) are already integrated.

Thus, the parameters of model (31) are the Fermi velocity $v_{\rm F}$, the spin-fermion coupling constant g (which at half-filling is of the order of the Hubbard parameter U), as well as the spin correlation length ξ defined by the static spin susceptibility $\chi_0(\mathbf{q}) = \chi_0\xi^2/[1 + (\mathbf{q} - \mathbf{Q})^2\xi^2]$ that has a peak at point Q of the Brillouin zone (the dynamic part of spin susceptibility is assumed to be due to the interaction with low-energy fermions and, therefore, is not included in the model).

From the above, it follows that in both the SFMC and SFM an ensemble of fermions on a 2D lattice is considered, which interact with the spin subsystem. This is a common property of both models. However, in the rest the difference between them is significant.

Since the key role in the difference between the two models is played by the operators $\hat{H}_{\rm h}$ and $\hat{J}$, let us consider them in more detail. For this purpose, let us write down the SFM exchange coupling operator in the Wannier representation:

$$\hat{J}_{\rm sf} = g\sum_{f\alpha\beta} c^{\dagger}_{f\alpha}\mathbf{S}_f\,\boldsymbol{\sigma}_{\alpha\beta}c_{f\beta}\,. \tag{32}$$

It is seen that in the SFM the exchange coupling between the subsystem of localized spins and collective fermions is taken into account only if the spin and the hole are in the same cell. In fact, this is the interaction that determines the well-known s – d(f) exchange Vonsovsky model.

To simplify further a comparison of the SFMC and SFM, we exclude direct hopping of holes between oxygen ions from the former. In addition, let us begin by ignoring the Coulomb interaction in the subsystem of oxygen holes. The effective Hamiltonian of the Emery model in the form not taking into account the Coulomb interactions $\hat{V}_{\rm pd}$, $\hat{U}_{\rm p}$, and $\hat{V}_{\rm pp}$ was used in the study of properties of the cuprate superconductors in Refs [26, 27, 159, 160].

Performing the canonical transformation

$$\begin{aligned} \varphi_{k\alpha} &= v_{k_x} a_{k\alpha} + v_{k_y} b_{k\alpha}\,, \\ \psi_{k\alpha} &= -v_{k_y} a_{k\alpha} + v_{k_x} b_{k\alpha}\,, \end{aligned} \tag{33}$$

in which

$$\begin{aligned} v_{k_x} &= \frac{\sin(k_x/2)}{v_k}\,, \quad v_{k_y} = \frac{\sin(k_y/2)}{v_k}\,, \\ v_k &= \sqrt{1 - \frac{\cos k_x + \cos k_y}{2}}, \end{aligned} \tag{34}$$

we arrive at the diagonal form of the operator:

$$\hat{H}_{\rm h} = \sum_{k\alpha} \varepsilon_{\rm p} \psi^{\dagger}_{k\alpha} \psi_{k\alpha} + \sum_{k\alpha} \tau_k \varphi^{\dagger}_{k\alpha} \varphi_{k\alpha}\,. \tag{35}$$

It is seen that the mixing of the initial hole states gives rise to two types of fermions. For one of them, the energy spectrum remains free of dispersion, and for the other, it is given by the expression

$$\tau_k = \tau(2 - \cos k_x - \cos k_y)\,. \tag{36}$$

Operator $\hat{J}$ in the new representation takes the form of exchange coupling between localized spins and only that subsystem of collective fermions which is described by the states $\varphi^{\dagger}_{k\alpha}|0\rangle$ (φ-states),

$$\hat{J}_{\varphi} = \frac{J}{N} \sum_{fkq\alpha\beta} \exp\left[{\rm i}f(q-k)\right] v_k v_q \varphi^{\dagger}_{k\alpha} \mathbf{S}_f \boldsymbol{\sigma}_{\alpha\beta} \varphi_{q\beta}\,. \tag{37}$$

Moving to the Wannier representation for bonding $\varphi_{k\alpha}$-orbitals and nonbonding $\psi_{k\alpha}$-orbitals,

$$\begin{aligned} \varphi_{k\alpha} &= \frac{1}{\sqrt{N}} \sum_f \exp(-{\rm i}kf) \varphi_{f\alpha}\,, \\ \psi_{k\alpha} &= \frac{1}{\sqrt{N}} \sum_f \exp(-{\rm i}kf) \psi_{f\alpha}\,, \end{aligned} \tag{38}$$

we obtain the following structure of the operator $\hat{J}_{\varphi}$:

$$\begin{aligned} \hat{J}_{\varphi} &= 2Jv^2(0) \sum_f \mathbf{S}_f \mathbf{s}_f + 2J \sum_{f \neq f'} v^2_{ff'} \mathbf{S}_f \mathbf{s}_{f'} \\ &+ Jv(0) \sum_{f \neq f'} v_{ff'} \left(\varphi^{\dagger}_{f\alpha} \mathbf{S}_f \boldsymbol{\sigma}_{\alpha\beta} \varphi_{f'\beta} + {\rm h.c.}\right) \\ &+ J \sum_{f \neq f_1 \neq f_2} v_{ff_1} v_{ff_2} \varphi^{\dagger}_{f_1\alpha} \mathbf{S}_f \boldsymbol{\sigma}_{\alpha\beta} \varphi_{f_2\beta}\,. \end{aligned} \tag{39}$$

The form of the first term on the right-hand side of Eqn (39) coincides with the SFM interaction (32). However, in the SFMC this interaction is strong and requires an approach in which single-site correlations should be rigorously taken into account. To demonstrate this circumstance, let us calculate the energy of exchange splitting between the triplet and singlet states, formed when, in a cell with number f, there is a fermion in the state $\varphi^{\dagger}_{f\alpha}|0\rangle$.

From the expression for $\hat{J}_{\varphi}$, it follows that the exchange coupling within one unit-cell is defined as

$$\hat{J}_{\varphi}(0) = 2Jv^2(0) \mathbf{S}\mathbf{s}\,, \tag{40}$$

where $\mathbf{S}$ is the vector operator of localized spin $S = 1/2$, $\mathbf{s}$ is the vector operator of hole spin, and $v(0)$ is the value of unit-cell renormalization

$$v(0) = \frac{1}{N} \sum_k v_k = 0.96\,. \tag{41}$$

Using the values of parameters of the Emery model (5), we get

$$\Delta E_J = 2Jv^2(0) = 5.38 \text{ eV}\,. \tag{42}$$

Such a large value of exchange splitting testifies to the presence of strong spin-fermion coupling, which is one of the distinctive features of the SFMC. Therefore, when using the SFMC, a problem of primary importance is how to take this coupling into account correctly. The solution to this problem is implemented by a transition to quasiparticles, in which the spin-fermion correlations of spins with the nearest environment of oxygen holes is considered exactly. This leads to the formation of spin-polaron quasiparticles, which determine the properties of the normal phase of cuprates (see Section 5) and also substantially affect the mechanism of Cooper instability and the symmetry properties of the superconducting state (see Section 6).

The second term on the right-hand side of Eqn (39) takes into account the exchange interaction of localized spins and spins of holes located in different unit cells.

Worth special attention is the third term of Eqn (39), reflecting the processes of hole transfer from site f' to site f, in which this hole strongly correlates with the localized spin described by the operator $\mathbf{S}_f$. As a result, so-called spin-correlated hopping occurs [159, 173, 197–199], in the course of which the spin of the transferred hole either changes or does not change its projection, in rigorous correspondence with the change or lack of change of the localized spin projection. Importantly, the matrix element of the spin-correlated hopping between the nearest sites is not small and has a value of ~ 0.2 eV. It is because of this fact that the spin-correlated hopping plays a substantial role in the formation of a correct spectrum dependence of Fermi excitations.

The last term in Eqn (39) describes such spin-correlated hopping, for which all three operators correspond to different cells.

In the expression presented, the rate of decrease in the intensity of effective interactions is determined by the dependence of the function $v_{ff'} = (1/N) \sum_k \exp[{\rm i}k(f-f')] v_k$ on the distance between the cells f and f'. In this connection, note that, although the value $v_0 = 0.96$ is substantially greater than $v_{\rm a} = -0.14$, this fact by no means indicates a fast decrease in parameters v_R upon increasing R. In fact, after a rapid decrease in v_R at the first step, a deceleration of the rate

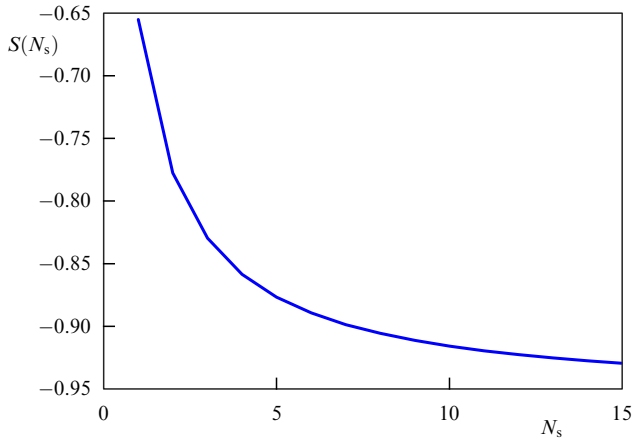

Figure 4. Dependences $S(N_s)$ on the number of the coordination sphere, up to which the summation of coefficients $v(R)$ is performed.

of decrease begins to manifest itself. Since with increasing number of the coordination sphere the number of its sites also increases, the justification for deliberately ignoring the hopping between sites from distant coordination spheres is not obvious. This can be verified by using the exact 'sum rule'

$$\sum_R v_R = v_0 + \sum_{R\neq 0} v_R = 0\,. \tag{43}$$

Let us introduce the quantity

$$S(N_s) = \sum_{R\neq 0}^{R_{N_s}} v_R\,, \tag{44}$$

which denotes a sum of coefficients v_R for coordination spheres, starting from the first one to the coordination sphere with the number N_s inclusive. From definition (44) and sum rule (43), it follows that, at $N_s \to \infty$, the sum $S(N_s) \to -v_0 = -0.96$.

Figure 4 illustrates the behavior of the function $S(N_s)$ upon varying the number of coordination sphere from $N_s = 1$ to $N_s = 15$. It is seen that, after the sum initially quickly tends to its asymptotic value, a transition to its slow decrease occurs. Hence, with the increase in R, the contribution of distant coordination spheres remains noticeable.

Thus, direct calculations confirm that proceeding to the single-band description is achieved at the expense of using a Hamiltonian, in which it is necessary to take into account the spin-correlated hopping between the sites located at large interatomic distances. As a result of comparing the two models, the following conclusions can be drawn.

First, in the SFMC, the exchange interaction between the spins of copper ions and holes on oxygen ions is strong. Therefore, correctly considering this strong coupling becomes a question of primary importance. The solution to this problem is found by moving to quasiparticles, in which the spin-fermion correlations of spins with the nearest-neighbor holes on oxygen ions is taken into account rigorously. This gives rise to the formation of spin-polaron quasiparticles, for which the Cooper pairing is then considered. The energy spectrum characteristics are determined in terms of the initial parameters of the Emery model. On the contrary, in the SFM, the spin-fermion interaction is considered in the weak coupling regime, and the Fermi spectrum is modeled based on a comparison with experimental data.

Second, a substantial difference between the two models is related to the fact that in the SFMC the terms that describe spin-correlated hopping are present. It is established in [159, 173, 197–199] that the spin-correlated hopping has a long-range character and just taking these processes into account plays an important role in the description of the experimentally observed minimum at the point $(\pi/2, \pi/2)$ of the Brillouin zone for the quasimomentum dependence of the spectrum of Fermi excitations in the normal phase. In this case, the correct energy spectrum is obtained as a result of using the same parameters of the initial Emery model, rather than introducing additional model parameters affecting the spectrum form.

Third, the difference between the models becomes even more substantial if the direct hopping of holes between the oxygen ions and the Coulomb interaction are taken into account. In this case, the transition to a single-band description becomes problematic because, when direct hopping is taken into account, the Fermi degrees of freedom in the second band come into play. However, an even stronger argument in favor of the inadequacy of the single-band description is related to the Coulomb interaction of holes located at the nearest-neighbor oxygen sites. The fact is that, as shown in Section 6.2, when using the SFMC to describe the superconducting phase, an important effect arises, manifesting itself in the fact that the above Coulomb interaction does not suppress the superconducting d-wave pairing. It turns out that this effect is of a symmetry nature; therefore, it is important to take into account the real structure of the CuO_2 plane, with two oxygen ions and one copper ion in a unit cell. When trying to proceed to a single-band description, the real structure of the lattice does not work, which results in a distortion of the effective Coulomb interaction. Therefore, the important effect of the neutralization of the negative influence of Coulomb interaction is missing, and superconductivity becomes suppressed.

Thus, in spite of the formal resemblance between the SFMC and SFM, there are substantial differences between them. This discrepancy arises because the SFMC takes specific features of the crystallographic structure of CuO_2 planes into account and the arising effective interactions are rigorously derived based on the small parameters in the SEC regime with the major interactions of the original Emery model taken into account.

3.4 Reduced forms of the spin-fermion model of cuprates

From the form (39) of the operator $\hat{J}_\varphi$ in the tight-binding representation, it follows that the SFMC can be considered a generalization of the Kondo lattice model with the Hamiltonian $\hat{H}_K$ (7). The extension of the Kondo lattice model is specified by taking into account the spin-fermion interactions with distant coordination spheres (in $\hat{H}_K$, this interaction is local), as well as spin-correlated hopping.

Although the Kondo lattice model includes the spin-fermion coupling in an extremely simple form, in a number of papers [164, 185, 200–205], the Kondo lattice was also referred to as a spin-fermion model. Many studies using the notion of the spin polaron as a 'correct' quasiparticle (including the case of cuprate HTSCs) rely just on the model with Hamiltonian (7) [32–36, 41].

We emphasize again that the Kondo lattice, as well as the $t-J$ model, turns out to be insufficient for an adequate description of the low-temperature properties of hole-doped cuprate superconductors. The main difference from the

SFMC arises due to the unjustified omitting of the long-range spin-correlated hopping in the Hamiltonian $\hat{H}_{\mathrm{K}}$ (7). Another essential difference is due to the absence of Coulomb interactions in $\hat{H}_{\mathrm{K}}$: considering these interactions in the derivation of the SFMC in the tight-binding representation gives rise to additional long-range terms [155, 206]. The addition of the Coulomb interaction operator to the Hamiltonian of the Kondo lattice model (7) is associated with this circumstance [41].

4. Spin polaron concept

4.1 Spin-polaron nature of Fermi quasiparticles in cuprates

It seems impossible to ascertain the mechanism of Cooper instability without understanding the structure of quasiparticles and the nature of their interactions in the normal phase. Important information about the properties of quasiparticles is obtained by studying the topology and evolution of the Fermi surface upon doping HTSCs [20, 39]. The ARPES data unambiguously indicate the rigid-band model inapplicability to the description of the observed modification of the Fermi surface with an increase in the concentration of holes in the system [1, 207–210]. The differences between the energy spectra of optimally doped cuprates and the spectra of undoped compounds lead to a conclusion that a description of Fermi excitation dynamics in HTSCs cannot be considered adequate, if it allows no correct reflection of the evolution of the spectral density of quasiparticles $A(\mathbf{k}, \omega)$, observed upon doping.

To date, the results of ARPES studies of undoped materials [1, 211–215] have indicated the realization of an isotropic bottom of the band in the vicinity of the point $\mathrm{N} = (\pi/2, \pi/2)$ in the quasimomentum space. In optimally doped cuprates, a flat band region having the shape of a saddle prolate in the direction $(0, \pi/2) \to (0, \pi)$ of the Brillouin zone was found [207, 216–221] (at low and intermediate doping, the flat band region is also observed in the direction $(0, \pi) \to (\pi/2, \pi)$), as were a large Fermi surface centered at $\mathrm{M} = (\pi, \pi)$ and the so-called 'shadow band' [38] (shadow Fermi surface, resembling the main Fermi surface, but displaced by the AFM vector $\mathbf{Q} = (\pi, \pi)$). Moreover, under intermediate doping, a pseudogap behavior is observed near the points $\mathrm{X} = \{(\pi, 0), (0, \pi)\}$ with an energy of ~ 0.1 eV [212, 222–224].

In Ref. [39], it is shown that many ARPES results in a wide doping interval can be naturally explained within the spin polaron concept [32].

The initial idea of this concept is that an elementary excitation in a doped 2D antiferromagnet can be presented as a 'bare' particle (an electron or a hole) surrounded by a certain deformation of the spin insulator substrate [33]. Dressing a fermion in a 'coat' of spin excitations — paramagnons — occurs due to the interaction of spin and charge degrees of freedom: the exchange interaction of fermions with a separate spin subsystem, as in the Kondo lattice model and SFMC, or between the spins of fermions from the same subsystem, e.g., in the $t-J$ model. Depending on the magnitude of the spin-fermion interaction, two regimes of spin-polaron quasiparticle formation can be specified: the strong coupling regime and the weak coupling one. Let us dwell on these regimes in more detail.

4.2 Spin polaron in the weak coupling regime

Early papers on spin-polaron theory were based on the $t-J$ model and s–d(f) model described above, as well as their modifications. The main difference between them is that the $t-J$ model is single-band, i.e., the same particles possess both Fermi and spin degrees of freedom. The s–d(f) model consists of two subsystems: the conduction electrons induce the Fermi dynamics, whereas the localized electrons determine the magnetic properties. In both models, the main parameters are the hopping integral t, determining the band width W, and the exchange integral J. The weak coupling regime is characterized by a small magnitude of the exchange interaction, as compared to the kinetic energy of a quasiparticle: $J \ll t$. Correspondingly, in the weak coupling regime, the exchange interaction is considered a perturbation, and the corrections to the self-energy of a spin-polaron quasiparticle are constructed by powers of J.

The simplest implementation of the spin polaron concept in the considered weak coupling regime is proposed in Refs [26, 160] within the Kondo lattice model with Hamiltonian (7). The approach is based on the Holstein–Primakoff representation for spin operators with subsequent diagonalization by the Bogoliubov transformation method. The Néel state was considered a ground state of the system in Refs [26, 160], and the properties of the resulting effective Hamiltonian were investigated using standard field theory methods.

In recent paper [225], a similar idea, associated with introducing magnon Bose operators within the Kondo lattice model, is implemented based on a diagram analysis of effective electron–electron interactions via spin fluctuations (with a maximum at vector $\mathbf{Q} = (\pi, \pi)$). Since in the second order these interactions have a standard form arising in the description of coupling of a charge carrier with Bose-type excitations, the effective Hamiltonian of the Kondo lattice model in [225] was written in the form

$$\hat{H} = \sum_{k\alpha} \xi_k c^{\dagger}_{k\alpha} c_{k\alpha} + g \sum_{k,q} \left(b^{\dagger}_q + b_{-q}\right) c^{\dagger}_{k,\alpha} c_{k+q+Q,\alpha} + \Omega \sum_q b^{\dagger}_q b_q \,, \tag{45}$$

where ξ_k is the Fourier transform of the hopping integral t_{fm}, g is a certain effective coupling constant, Ω is the resonance frequency of spin wave excitations in the vicinity of the wave vector $\mathbf{Q}$, and $b^{\dagger}_q(b_q)$ are the creation (annihilation) operators of spin wave excitations with the wave vector $\mathbf{q}$. Based on Hamiltonian (45) in the momentum average approximation [226], in Ref. [225], the pseudogap behavior and transition from a large-radius to a small-radius polaron were analyzed.

A specific feature of the description of spin-polaron quasiparticles within the $t-J$ model, as noted in Section 2, is due to the fact that, in this model, the same fermions cause both charge and spin degrees of freedom. For this reason, the exchange interaction in the $t-J$ model describes the coupling directly between the charge carriers (electrons or holes). In addition, of great importance in the $t-J$ model is the kinematic interaction, determined by the SEC [62, 85, 92, 227, 228].

The general idea of theoretical approaches being developed to describe the spectral properties of cuprates within the $t-J$ model is based on representing the Hubbard operators $X^{\alpha 0}_m = a^{\dagger}_{m\alpha}(1 - \hat{n}_{m\bar{\alpha}})$ obeying complicated commutation relations as a product of two usual Fermi and Bose second-quantization operators. In this case, the spin index relates to only one of these operators, and just this operator describes the spin degrees of freedom. The second 'spinless' operator, corresponding to slave particles, describes the charge degrees of freedom. If the spinless operator is a Bose one, then the

representation is called slave-boson, and if it is a Fermi operator, it is called slave-fermion.

The slave-boson representation was used to study the spectral properties within the $t-J$ model in Refs [229–234], and the slave-fermion one in Refs [63, 235–239].

The class of slave-fermion representations also includes the representation in which, instead of the Bose operator, a spin operator is used [240–243]. The spin-fermion representation explicitly implements the idea of spin-charge separation in systems with SEC. In review [63], the method of slave particles is thoroughly described, and some results obtained by applying this method to the $t-J$ model are discussed.

The formalism of slave particles used in the above papers to describe spectral properties of cuprate superconductors with the magnetoactive ion spin $S = 1/2$ can be generalized over a system with a more complex structure of the Hamiltonian. Thus, in the recent study [224] of the photoemission spectrum features in Ca_2RuO_4 within the spin-polaron approach, the spin-fermion representation was applied to the Hamiltonian of the $t-J$ model with strong anisotropic interaction between the ruthenium spins $S = 1$.

A considerable difficulty in using the slave particle method is related to the necessity of considering the so-called constraint, i.e., the condition that eliminates nonphysical states, which inevitably arise in this approach. The constraint is used to limit the basis of the Hilbert space of states at each lattice site. However, practically, it is considered only on average over the entire crystal, which seems a rather rough approximation.

It should be noted that, in an overwhelming majority of papers on the spin-polaron topic, carried out within the slave particle method, the state with long-range AFM order is chosen as the ground state. This is fully justified, especially for systems which in the degree of doping are close to the AFM region of the phase $T-x$ diagram, where the AFM fluctuations are strong enough. At a significant doping degree, the magnetic subsystem is in the quantum spin liquid state, and against the background of just this strongly correlated state one should construct the Fermi spin-polaron excitations.

4.3 Spin polaron in the strong coupling regime

The strong coupling regime corresponds to the relation $J \gg t$ between the exchange integral and the hopping parameter. For systems described within the s–d(f) exchange model or the Kondo lattice model, this means that the local exchange coupling between current carriers and localized spins should be described rigorously, and the hopping of carriers should be considered as a perturbation. Such an approach to the formation of the local magnetic polaron is well known in the theory of magnetic semiconductors [245], although the idea as such was developed much earlier in Ref. [246].

In application to cuprate HTSCs, the concept of the spin polaron based on the strong spin-fermion coupling was developed within both the Kondo lattice model [32–36, 41] and the SFMC [39, 40, 42–44, 52, 197]. In these papers, it was assumed that the magnetic subsystem of the spin moments of copper ions in the CuO_2 plane can be described based on the 2D AFM-frustrated Heisenberg model with $S = 1/2$. From experiments on Raman [247–251] and neutron [252] scattering, it is known that the AFM interaction between the nearest-neighbor spins of copper ions in the LSCO equals $I \approx 0.13$ eV, which considerably exceeds the magnitude of interlayer exchange. However, even at relatively weak hole doping, the long-range AFM order vanishes in the entire range of temperatures. Such a behavior is modeled well enough by introducing the frustration [253]. The cluster calculations indicate the presence of a sufficiently large frustration parameter, even for an undoped LSCO [254]. The quantitative consideration of the spin subsystem in Refs [39, 197] was performed within the spherically symmetric self-consistent approach [255–257]. It is necessary to note that at any finite temperature and sufficient frustration in the spin subsystem, it is the spherically symmetric (SU(2) invariant) state that is most realistic.

In principle, the characteristics of a local spin polaron can be determined by solving the cluster problem [34, 35]. After choosing the lowest-energy states of a small cluster, it is possible to describe the motion of the local spin polaron against the background of AFM ordering.

However, a more efficient approach to the description of spectral characteristics of spin-polaron quasiparticles, proposed in Refs [39, 197], is based on the Zwanzig–Mori projection technique [19, 258–262]. The strong spin-charge correlations within this approach are taken into account by extending the basis set of Fermi operators into which, in addition to the initial operators of hole creation and annihilation in the $p_{x(y)}$-orbitals of oxygen ions (see Eqn (26)), the multiplicative operators are included, defined as the product of spin and Fermi operators related to neighboring sites. Constructing the equations of motion for the introduced set of basis operators with subsequent application of the projection technique allows a rigorous consideration of short-range spin-fermion correlations, since for the basis multiplicative operators no uncoupling procedure is used. As a result, the spectrum of Fermi excitations becomes dependent on the spin-fermion correlations, which substantially affect the concentration dependence of the Fermi contour.

At zero temperature, the motion of a local spin polaron must depend on the presence or absence of long-range order in the spin subsystem. This means that the next important step in the development of the considered concept is taking into account the interaction of a local spin polaron with spin waves having the quasimomentum $\mathbf{Q} = (\pi, \pi)$. Therefore, it becomes necessary to introduce the so-called composite spin polaron [33]. The composite spin polaron is a local polaron moving against the background of AFM ordering, surrounded by a cloud of spin fluctuations with a quasimomentum close to $\mathbf{Q}$ [36]. The structure of the low-lying spectrum of a composite spin polaron is determined by the splitting of the lower band of the local polaron.

The correctness of the projection method for a Green's function used in the spin-polaron concept can be demonstrated by comparing the results at zero temperature [263] with the spectral function of a bare hole $A_h(\mathbf{k}, \omega)$, obtained within the self-consistent Born approximation for a local spin polaron [31]. It can be seen that the lower band of the composite polaron in the projection method approximation successfully reproduces the quasiparticle peak and its intensity obtained within this approximation. As to the upper bands, corresponding to the excited states, they effectively describe the incoherent part of $A_h(\mathbf{k}, \omega)$.

To finalize the section, note that the spin polaron concept can also be implemented in the framework of the diagram technique with strong coupling [264], based on cumulant decomposition of the Green's functions. Based on this approach, spin-polaron excitations were studied in the single-band Hubbard model [265], the $t-t'-t''-U$ model [266], and the Emery model (at $t_{pp} = 0$) [267]. Moreover,

recently, one more version of the diagram technique has been proposed [268] to describe spin-polaron quasiparticles within the SFMC, referred to as the 'bundle' technique by the authors.

5. Spin-polaron quasiparticles in the normal phase of cuprate high-temperature superconductors

Investigating the Fermi state arising under the hole doping of cuprates is one of the main problems in HTSC physics. These properties determine the normal phase features and affect the mechanism of high-temperature superconductivity.

In Sections 5.1 and 5.2, we discuss the nature of the formation of spin-polaron states in hole-doped cuprates and the modification of the Fermi surface in the ensemble of spin-polaron quasiparticles upon an increase in the concentration of holes. The solution to the spin polaron problem and the study of the statistical properties of the ensemble of such quasiparticles is performed within the SFMC (26).

5.1 Fermionic states in the strong coupling regime

To justify the spin-polaron nature of Fermi quasiparticles arising in the CuO_2 plane under weak doping, in Ref. [42], the solution to the Schrödinger equation for a single hole was considered, based on the variation method. According to the Mermin–Wagner theorem [269], in the absence of doping, the 2D subsystem of localized spin moments at arbitrarily low temperature is in the ground state $|G\rangle$ without long-range magnetic order. For an AFM-type exchange interaction, this state is characterized by the properties [270]

$$\mathbf{S}_{\rm tot}^2|G\rangle = 0|G\rangle\,, \quad \langle G|S_f^{x,y,z}|G\rangle = 0\,, \quad \mathbf{S}_{\rm tot} = \sum_f \mathbf{S}_f\,. \quad (46)$$

The assumption of the singlet state character of the considered 2D system at a finite temperature is related to the result of Ref. [271]. In this paper, it was shown with mathematical rigor that the ground state of a system of an arbitrarily large but finite number of localized spins, located at square lattice sites and AFM-interacting with each other, is a singlet (Marshall's theorem).

Keeping in mind the Hamiltonian symmetry properties, we conclude that, for each irreducible representation k of the group of translations, the single-hole state $|\psi_{k\alpha}\rangle$ with the spin projection α can be expressed in the form

$$|\psi_{k\alpha}\rangle = \sum_j \varkappa_{jk} A_{jk\alpha}^{\dagger}|G\rangle\,, \quad (47)$$

where $A_{jk\alpha}^{\dagger}$ denotes both the usual operators of hole creation in the subsystem of oxygen ions and combinations of products of hole creation operators and operators related to the localized subsystem (see below).

From the condition of the energy functional stationarity under the additional condition $\langle\psi_{k\alpha}|\psi_{k\alpha}\rangle = 1$, using the Lagrange method, it is shown in [42] that the energies of excitations $\varepsilon_k = E_k - E_G$ (here, E_k and E_G are the energies of the states $|\psi_{k\alpha}\rangle$ and $|G\rangle$, respectively) and the coefficients $\varkappa_{jk}$ are determined by the homogeneous system of linear equations

$$\sum_j \left[D_{ij}(k) - \varepsilon_k K_{ij}(k)\right]\varkappa_{jk} = 0\,, \quad (48)$$

where

$$D_{ij}(k) = \langle G|\{[A_{ik\alpha}, \hat{H}], A_{jk\alpha}^{\dagger}\}|G\rangle\,, \quad (49)$$

$$K_{ij}(k) = \langle G|\{A_{ik\alpha}, A_{jk\alpha}^{\dagger}\}|G\rangle\,. \quad (50)$$

Because of the strong spin-fermion coupling, a hole that appears in the CuO_2 plane is significantly affected by the subsystem of localized spins. This circumstance requires a correct description of spin-fermion correlations and leads to the extension of the set of basis operators that adequately describe spin-polaron quasiparticles. Numerical calculations [42] have shown that a description of the states of the single hole sector, optimal from the point of view of reaching the minimum energy with a minimal set of basis operators, can be achieved restricting the set to three operators:

$$A_{1k\alpha} \equiv a_{k\alpha}\,, \qquad A_{2k\alpha} \equiv b_{k\alpha}\,,$$

$$A_{3k\alpha} \equiv L_{k\alpha} = \frac{1}{N}\sum_{fq\beta} \exp\left[\mathrm{i}f(q-k)\right]\mathbf{S}_f\boldsymbol{\sigma}_{\alpha\beta}\,u_{q\beta}\,. \quad (51)$$

As shown below, the main role in basis (51) is played by the third operator, which couples the spin and Fermi subsystems.

Operators (51) for each k and α determine three states $A_{jk\alpha}^{\dagger}|G\rangle$ $(j = 1, 2, 3)$. The orthogonality of these states is easy to prove, taking into account conditions (46): $\langle G|A_{ik\alpha}A_{jq\alpha'}^{\dagger}|G\rangle = \delta_{ij}\delta_{kq}\delta_{\alpha\alpha'}K_{jj}(k)$.

Having calculated matrix elements (49) and (50), let us define via their ratio the following functions ($K_{ij} = \delta_{ij}K_{ii}$):

$$\xi_{x(y)} = \frac{D_{11}(k)}{K_{11}(k)} = \frac{D_{22}(k)}{K_{22}(k)} = \xi_{k_{x(y)}}\,,$$

$$t_k = D_{12}(k) = D_{21}(k) = (2\tau - 4t)\sin\frac{k_x}{2}\sin\frac{k_y}{2}\,,$$

$$J_{x(y)} = \frac{D_{1(2),3}(k)}{K_{33}(k)} = J\sin\frac{k_{x(y)}}{2}\,,$$

$$\xi_L(k) = \frac{D_{33}(k)}{K_{33}(k)} = \tilde{\varepsilon}_{\rm p} - \mu - 2t + \frac{5\tau}{2} - J + \left[(\tau - 2t)(-C_1\gamma_{1k} + C_2\gamma_{2k}) + \frac{\tau(-C_1\gamma_{1k} + C_3\gamma_{3k})}{2} + \frac{JC_1(1 + 4\gamma_{1k})}{4} - IC_1(\gamma_{1k} + 4)\right]K_k^{-1}\,, \quad (52)$$

$$K_{11}(k) = K_{22}(k) = 1\,, \quad K_k = K_{33}(k) = \frac{3}{4} - C_1\gamma_{1k}\,,$$

where γ_{jk} are the square lattice invariants,

$$\gamma_{1k} = \frac{\cos k_x + \cos k_y}{2}\,, \qquad \gamma_{2k} = \cos k_x \cos k_y\,,$$

$$\gamma_{3k} = \frac{\cos 2k_x + \cos 2k_y}{2}\,.$$

When calculating matrix elements (49) and (50), it was taken into account that the subsystem of spins localized on copper ions is in the state of a quantum spin liquid, which possesses a spherical symmetry in the spin space [255–257]. In this case, the spin correlation functions $C_j = \langle S_0 S_{r_j}\rangle$ that appear in Eqn (52) satisfy the relations

$$C_j = 3\langle S_0^x S_{r_j}^x\rangle = 3\langle S_0^y S_{r_j}^y\rangle = 3\langle S_0^z S_{r_j}^z\rangle\,, \quad (53)$$

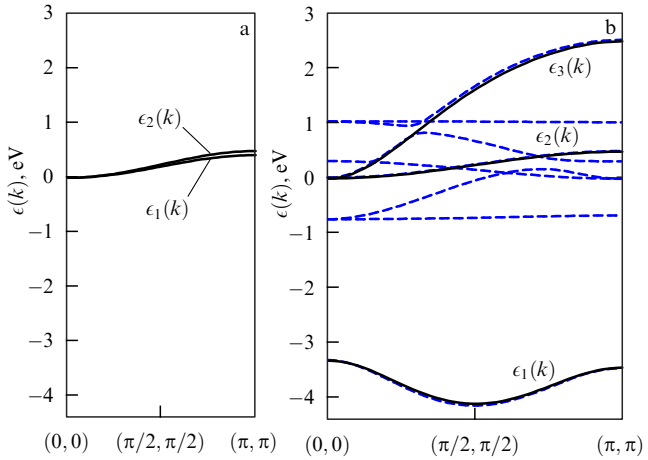

Figure 5. Dependences of the energies of single-hole states on the quasi-momentum along the main diagonal of the Brillouin zone for the set of parameters $\tau = 0.11$, $J = 2.86$, $t = 0.1$, $I = 0.02$ (all in [eV]) and the values of spin correlators $C_1 = -0.255$, $C_2 = 0.075$, $C_3 = 0.064$. (a) Energy spectrum $\epsilon_j(k)$ obtained considering two operators: $a_{k\alpha}$ and $b_{k\alpha}$. (b) Energies of single-hole states ϵ_{jk} calculated in the basis of three operators (51) (solid curves) and in the basis of eight operators (54) (dashed curves). The lower branches of the spectrum, coincident for both bases, (51) and (54), correspond to spin-polaron states [42].

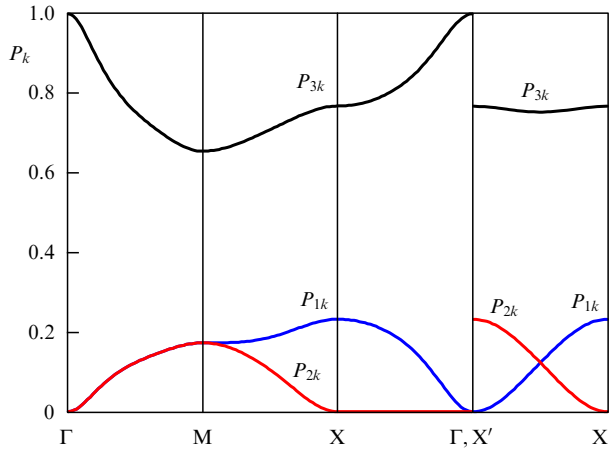

Figure 6. Partial contributions of basis states to the single-hole state, corresponding to the lower branch of the spectrum in Fig. 5b. The values of the model parameters are the same as in Fig. 5. Here, the Brillouin zone points are $\Gamma = (0,0)$, $\mathrm{M} = (\pi,\pi)$, $\mathrm{X} = (0,\pi)$, $\mathrm{X}' = (\pi,0)$ [42].

where r_j is the coordinate of a copper ion in the coordination sphere with the number j. In this case, $\langle S_f^x \rangle = \langle S_f^y \rangle = \langle S_f^z \rangle = 0$. The dependences of the correlators C_j on the doping level were found together within the spherically symmetric self-consistent approach for a frustrated antiferromagnet [270]. The choice of values for correlators C_j is discussed in Section 5.2 in more detail.

The calculation results presented in Figs 5 and 6 demonstrate the importance of considering the interaction between the spin and charge degrees of freedom, as well as the spin-polaron character of the lower branch of the spectrum of single-hole states. Figure 5a shows the quasimomentum dependence (along the principal axis of the Brillouin zone) of the energy spectrum of single-hole states, arising when using only two operators, $a_{k\alpha}$ and $b_{k\alpha}$. In fact, these branches describe the spectrum of holes that do not interact with the subsystem of spin moments of copper ions.

Adding the third operator, $L_{k\alpha}$, to the variation procedure leads to important qualitative changes, the main one being related to the appearance of a split branch with the minimum at a point close to $(\pi/2, \pi/2)$. This is seen from the spectrum of single-hole states, obtained in the basis of three operators and shown in Fig. 5b by solid curves. The decrease in the energy of such single-hole states is due to the term $\sim J$ in the Hamiltonian, describing both the exchange interaction between a hole and the nearest copper ion and spin-correlated hopping. It is including the operators explicitly allowing for this strong spin-fermion correlation into the basis that provides the significant gain in energy. In this case, the renormalization of two bare branches of the spectrum also occurs.

The physical reason for the origin of spin-polaron states is similar to the appearance of the states of a spin polaron in the exactly solvable problem of a single electron with a flipped spin in a ferromagnetic matrix with the AFM type of s–d exchange coupling between the electron spin and the localized spin moment [272].

When the quasimomentum varies in other directions of the Brillouin zone, the above qualitative modifications of the spectrum of single-hole states are preserved. It is important to note that the effect of lower spin-polaron band splitting is preserved when increasing the number of basis operators. To demonstrate this fact, Fig. 5b presents the results of the variation calculation of the Fermi spectrum within a basis consisting of eight operators,

$$\tilde{A}_{jk} = \frac{1}{\sqrt{N}} \sum_f \exp(-\mathrm{i}kf) \tilde{A}_{jf}, \quad j = 1, \ldots, 8, \tag{54}$$

where

$$\tilde{A}_{1(2)f} = c_{f+g_{x(y)}/2}, \quad \tilde{A}_{3(4)f} = \tilde{S}_f c_{f+g_{x(y)}/2},$$
$$\tilde{A}_{5(6)f} = \tilde{S}_f c_{f-g_{x(y)}/2}, \quad \tilde{A}_{7(8)f} = \mathbf{S}_f \mathbf{S}_{f+g_{x(y)}} c_{f+g_{x(y)}/2}.$$

The first two operators of this basis coincide with the corresponding operators of basis (51). Each of the four operators $\tilde{A}_{jk}$ with $j = 3, \ldots, 6$ describes the correlation of a localized spin with a hole, localized on one of four oxygen ions, nearest to this spin. The last two operators, $\tilde{A}_{7k}$ and $\tilde{A}_{8k}$, describe the correlation of a hole on an oxygen ion with two spins at once on the nearest-neighbor copper ions. The calculated eight branches of the Fermi spectrum are presented in Fig. 5b by dashed lines. It is essential that the dispersion dependence for the lower branch of the spin-polaron spectrum be virtually unchanged. Thus, the basis of three operators (51) is sufficient to describe the low-energy part of the spectrum of Fermi quasiparticles with high accuracy. This spectrum is determined by the solutions of the dispersion equation

$$\det_k(\omega) = (\omega - \xi_x)(\omega - \xi_y)(\omega - \xi_L) - 2J_x J_y t_k K_k$$
$$- (\omega - \xi_y) J_x^2 K_k - (\omega - \xi_x) J_y^2 K_k - (\omega - \xi_L) t_k^2 = 0. \tag{55}$$

The lower branch ϵ_{1k} is significantly separated from the two upper bands ϵ_{2k} and ϵ_{3k}; therefore, at low doping levels x, the dynamics of holes on oxygen ions is determined exclusively by the band ϵ_{1k}.

With the characteristic values of SFMC energy parameters, it is possible to obtain an approximate analytical

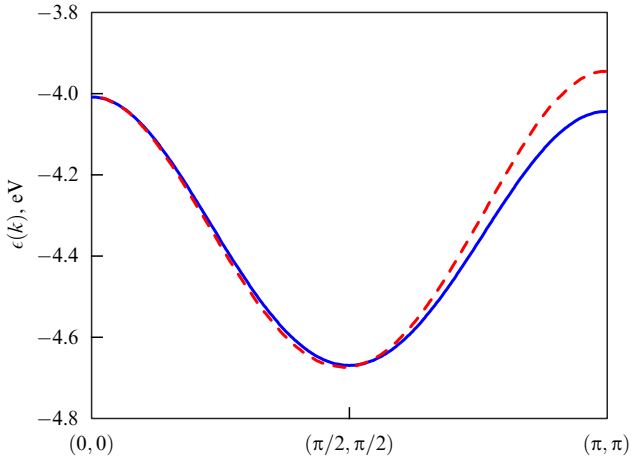

Figure 7. Dependences of spin polaron energies on the quasimomentum ϵ_{1k} and $\epsilon_{sp}(k)$ along the main diagonal of the Brillouin zone, obtained as a result of the exact solution of dispersion equation (55) (solid curve) and a result of using Eqn (56) (dashed curve). The parameter values are the same as in Fig. 5.

expression for the spectrum of a spin-polaron quasiparticle:

$$\epsilon_{sp}(k) = \frac{\tau_k + \Lambda_k/K_k}{2} - \sqrt{\frac{(\tau_k - \Lambda_k/K_k)^2}{4} + 16J^2K_kv_k^2}\,, \quad (56)$$

in which the energy and renormalization functions of quasimomentum are defined by expressions (34) and (36), as well as

$$\Lambda_k = J(-3 + C_1 + 8C_1\gamma_{1k}) + \tau W_k - IC_1(4 + \gamma_{1k}) + t\left(-\frac{3}{2} + 4C_1\gamma_{1k} - 2C_2\gamma_{2k}\right),$$
$$W_k = \frac{15}{8} - 4C_1\gamma_{1k} + C_2\gamma_{2k} + \frac{1}{2}\,C_3\gamma_{3k}\,. \quad (57)$$

Figure 7 shows the quasimomentum dependences of the spin-polaron spectrum ϵ_{1k}, found from dispersion equation (55), and $\epsilon_{sp}(k)$, determined by expression (56). The dependences are seen to coincide with good accuracy.

The weight contributions P_{1k} and P_{2k} of the bare hole states $a^\dagger_{k\alpha}|G\rangle$ and $b^\dagger_{k\alpha}|G\rangle$ are defined by the expressions $P_{1k} = |\varkappa_{1k}|^2$, $P_{2k} = |\varkappa_{2k}|^2$. For the weight contribution P_{3k} of the spin-polaron basis state we obtain $P_{3k} = K_k|\varkappa_{3k}|^2$. Figure 6 shows the results of calculations [42] for the values of the introduced partial contributions for quasimomenta in four directions of the Brillouin zone. It is seen that the values of P_{3k} exceed those of P_{1k} and P_{2k} by several times. This proves the spin-polaron nature of the single-hole state, corresponding to the lower split branch of the energy spectrum.

5.2 Modification of Fermi surfaces in LSCO under hole doping

In Ref. [40], based on the SFMC, the efficiency of the spin-polaron approach is demonstrated by an example of describing the ARPES results and Fermi surface modification upon doping in the LSCO [210]. In particular, the authors of Ref. [40] investigated the region of concentrations from $x = 0.03$, at which the LSCO is an undoped insulator, to $x = 0.3$, at which the LSCO becomes a normal metal. It was shown in [40] that the spin-polaron concept allows reproducing fine peculiarities of the LSCO Fermi surface evolution in the nodal direction upon varying the doping level x. In this case, the key role was played by the spin-correlated hopping of carriers and the change in the inverse magnetic correlation length with doping.

The fitting of strong-coupling models to the experimental data is known to require many fitting parameters. For example, to achieve satisfactory agreement between the Fermi surface calculated in the mean field approximation and the one reconstructed from experimental data, the authors of Ref. [210] for each concentration of holes had to choose its own set of four parameters, namely, three hopping integrals, t_1, t_2, t_3, and the energy shift value ε_0. Refs [40, 197] show that, within the concept of the spin polaron in the SFMC, the modification of the energy spectrum and Fermi surface is determined only by the strong correlation between the subsystem of localized spins on copper ions, being in the state of a quantum spin liquid, and the subsystem of oxygen holes, as well as by the change in the correlation characteristics of this liquid upon doping. In particular, in Ref. [40] only one fitting parameter was used, the hole hopping integral t, which was chosen based on a comparison with the LSCO experiment data [210].

In Ref. [42], taking into account the strong coupling between the subsystem of localized spins of copper ions and the spin of an oxygen hole, the Fermi quasiparticle spectrum is constructed based on the variation method. In fact, only one hole was considered. In the case of a finite number of holes, it is convenient to calculate the spectrum of Fermi excitations using the Zwanzig–Mori projection technique [19, 258–262], which, in combination with the formalism of retarded Green's functions, allows calculating the necessary thermodynamic averages, as well as describing superconducting pairing in the ensemble of spin polarons, as shown in Section 6.

Within the projection technique, the minimal basis of operators A_{jf} $(j = 1, \ldots, n)$ is chosen, which is assumed to be sufficient for an adequate description of quasiparticle excitation in the system. Then, the two-time retarded Green's functions are introduced:

$$G_{ij}(k,t) = \langle\langle A_{ik}(t)|A^\dagger_{jk}(0)\rangle\rangle = -\mathrm{i}\theta(t)\langle[A_{ik}(t), A^\dagger_{jk}(0)]\rangle\,,$$
$$i, j = 1, \ldots, n\,, \quad (58)$$

where the operator A_{jk} is a Fourier transform of the operator A_{jf}. The equations of motion for the Fourier transforms of the introduced Green's functions have the form

$$\omega\langle\langle A_{ik}|A^\dagger_{jk}\rangle\rangle_\omega = K_{ij}(k) + \langle\langle \Phi_{ik}|A^\dagger_{jk}\rangle\rangle_\omega\,, \quad (59)$$

where $\Phi_{ik} = [A_{ik}, \hat{H}]$, $K_{ij}(k) = \langle\{A_{ik}, A^\dagger_{jk}\}\rangle$. Then, each term on the right-hand side of Eqns (59) should be projected on the subspace, which is a linear shell, formed by the set of basis operators. In other words, the process of decomposing the operator Φ_{ik} is reduced to calculating the projection component according to the following algorithm:

$$\Phi_{ik} \to \sum_l \frac{\langle\{\Phi_{ik}, A^\dagger_{lk}\}\rangle}{\langle\{A_{ik}, A^\dagger_{lk}\}\rangle}\,A_{lk}\,. \quad (60)$$

As shown in Section 5.1, to take into account the strong spin-charge coupling in the system correctly, it is a matter of principle to introduce into the basis set the operator $L_{k\alpha}$

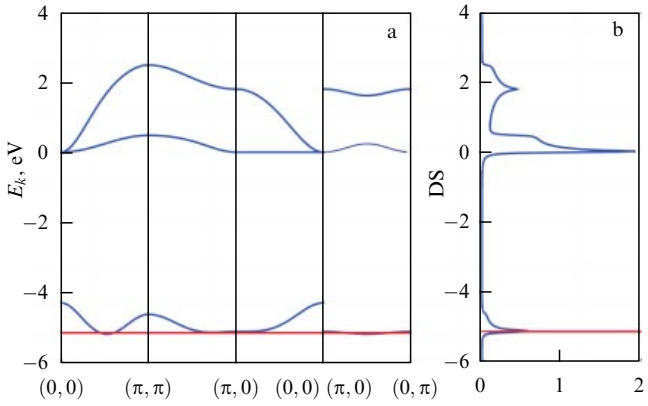

Figure 8. (Color online.) Energy structure (a) and density of states (DS) (b) of the spin-fermion model in the normal phase, calculated for the set of parameters $t_{pd} = 1.3$, $\Delta_{pd} = 3.6$, $U_d = 10.5$, $V_{pd} = 1.2$, $U_p = V_1 = V_2 = 0$, $t = 0.12$ (all parameters in [eV]) and the doping level $x = 0.12$. The lower branch $\epsilon_{1\mathbf{k}}$ corresponds to spin-polaron excitations. The red line shows the position of chemical potential μ.

alongside operators $a_{k\alpha}$ and $b_{k\alpha}$. After introducing Fourier transforms of the Green's functions G_{ij} $(j = 1, 2, 3)$,

$$G_{11} = \langle\langle a_{k\uparrow} | a^{\dagger}_{k\uparrow}\rangle\rangle_{\omega}\,, \quad G_{21} = \langle\langle b_{k\uparrow} | a^{\dagger}_{k\uparrow}\rangle\rangle_{\omega}\,, \quad G_{31} = \langle\langle L_{k\uparrow} | a^{\dagger}_{k\uparrow}\rangle\rangle_{\omega}\,, \tag{61}$$

the closed system of equations, obtained within the projection technique, can be written in the form

$$\begin{aligned}
(\omega - \xi_x) G_{1j} &= \delta_{1j} + t_k G_{2j} + J_x G_{3j}\,,\\
(\omega - \xi_y) G_{2j} &= \delta_{2j} + t_k G_{1j} + J_y G_{3j}\,,\\
(\omega - \xi_L) G_{3j} &= \delta_{3j} K_k + (J_x G_{1j} + J_y G_{2j}) K_k\,.
\end{aligned} \tag{62}$$

The Green's functions G_{i2} and G_{i3} $(i = 1, 2, 3)$ are defined similarly, with the only difference being that $a^{\dagger}_{k\uparrow}$ is replaced with operators $b^{\dagger}_{k\uparrow}$ and $L^{\dagger}_{k\uparrow}$, respectively.

When writing down system of equations (62), the functions (52) are used. Note that in expressions (59) and (60) the angle brackets denote thermodynamic averaging over the Gibbs ensemble, whereas in definitions (49) and (50) of similar matrices, the averaging is carried out over the ground state $|G\rangle$ of the system. Nevertheless, it turns out that in the low-density regime the results of calculations using both methods coincide and are given by expressions (52).

The energy spectrum of quasiparticles determined by the poles of the Green's function

$$G_{ij}(k, \omega) = \sum_{n=1}^{3} \frac{z^{n}_{(i,j)}(k)}{\omega - \epsilon_{nk}}\,, \quad i, j = 1, 2, 3\,, \tag{63}$$

where $z^{n}_{(i,j)}(k)$ are the residues of the Green's function, and can be calculated from the dispersion equation (55), is presented in Fig. 8. As noted in Section 5.1, for cuprate HTSCs only the lower polaron band with the dispersion ϵ_{1k} is relevant, because the chemical potential μ lies in this band, and the two other bands with ϵ_{2k} and ϵ_{3k} are separated from ϵ_{1k} by a considerable energy gap.

Studies of density modification of Fermi states [273] caused by a change in the value of the hopping integral for holes on oxygen ions have shown that a decrease in t gives rise to a shift of the van Hove singularity of the spin-polaron band, presented in Fig. 8. This, in particular, causes a shift of the maximum of the concentration dependence of the superconducting critical temperature towards a smaller density of holes (see Section 6).

Table. Values of doping level x and the corresponding values of frustration parameter p and spin correlation functions [40, 270].

x	p	C_1	C_2	C_3
0.03	0.15	−0.287	0.124	0.0950
0.07	0.21	−0.255	0.075	0.0640
0.15	0.25	−0.231	0.036	0.0510
0.22	0.275	−0.214	0.009	0.0450
0.30	0.30	−0.194	−0.0222	0.0457

An essential feature of the approach used is that the correlation functions C_1, C_2, and C_3 that enter the functions (52), as well as the gap $\Delta_Q(p)$ in the spectrum of magnetic excitations in the vicinity of point $Q = (\pi, \pi)$ of the Brillouin zone, are found together within the spherically symmetric self-consistent approach for a frustrated antiferromagnet [255–257, 270]. In this case, Δ_Q is linearly related to the inverse magnetic correlation length ξ^{-1}. On the other hand, according to data on neutron scattering and nuclear magnetic resonance (see, e.g., [274, 275]), the quantity ξ^{-1} is determined by the doping level x and for the LSCO increases several-fold with x increasing in the interval $x = 0.03-0.3$. Accordingly, the accepted values of frustration (see table) correspond to the case when the spin gap increases 2.5-fold with the growth of the frustration parameter from $p = 0.15$ to $p = 0.3$. The table also presents spin correlators calculated by the above technique for five values of the parameter p, which correlate with five values of the doping level x.

For the LSCO, the Fermi energy can be determined from the equality of the number of bare holes n_h and the doping level x. The number n_h at small values of x, which is interesting for us, equals the spectral density integrated over the Brillouin zone and summed over the spin α: $n_{h,\alpha}(k) = z^{1}_{(1,1)}(k) + z^{1}_{(2,2)}(k)$.

Figure 9 presents the spectral density distribution over the Brillouin zone. At the point $\Gamma = (0, 0)$, $n_{h,\alpha}(k) = 0$, but, as we move off this point, the spectral weight rapidly increases, and when approaching the antinodal X−X line, becomes saturated.

To demonstrate the formation of the flat band region in the vicinity of X-points of the k-space, Fig. 10 presents a contour plot $\epsilon_{1k} = \text{const}$ of the lower spin-polaron band, calculated at $x = 0.15$. The existence of a flat band in this region has been established in many papers [207, 216–221], in particular, in Ref. [210] at $x \leqslant 0.15$. The results of calculations presented in Fig. 10 allow estimating the effective mass of spin-polaron quasiparticles, which, as seen from the figure, is highly anisotropic. Thus, in the nodal direction (Γ−M), the calculations yield the mass value of $m_{\Gamma-M} = 1.25 m_e$, where m_e is the mass of a free electron. In the antinodal (X−X) direction, the effective mass is $m_{X-X} = 9.4 m_e$.

The contours $n_{h,\sigma}(k) = \text{const}$ and $\epsilon_{1k} = \text{const}$ presented in Figs 9 and 10 were calculated at the value of the direct oxygen–oxygen hopping parameter of $t = 0.094$ eV. This single fitting parameter was chosen based on the requirement of agreement between the Fermi surface topology and the ARPES data [210]. It is important to note that the same value of t was used to describe the Fermi surface at all five levels of doping x presented in the table. The Fermi surfaces calculated

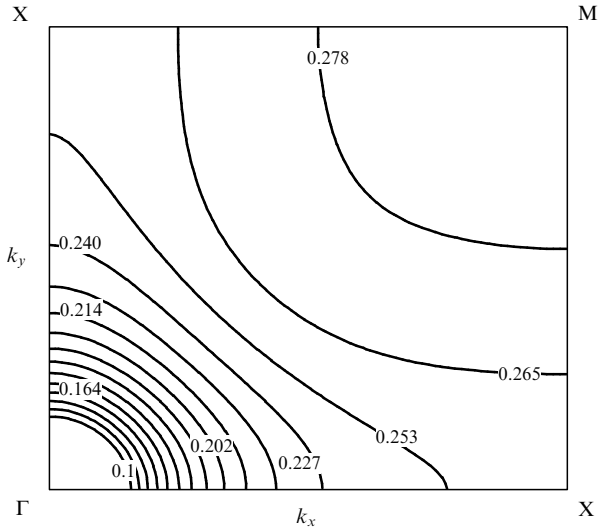

Figure 9. Bare-hole constant spectral density lines $n_{h,\sigma}(k)$ for the lower polaron band in the first quadrant of the quasimomentum space at the doping level $x = 0.15$. Numbers indicate the values of $n_{h,\sigma}(k)$ [40].

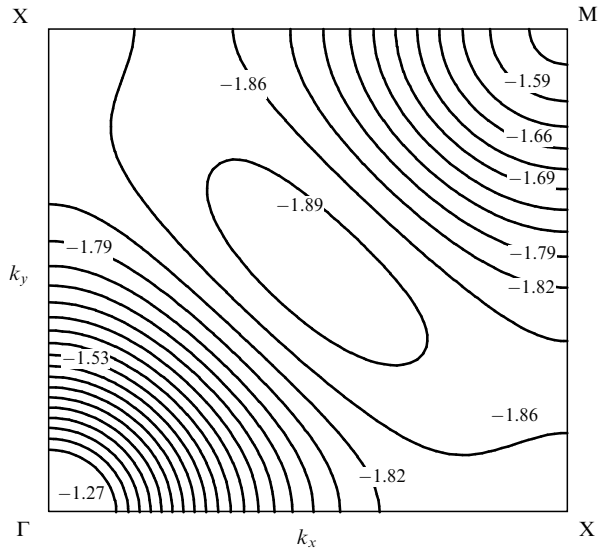

Figure 10. Constant energy lines in the lower polaron band $\epsilon_1(k) = \text{const}$ in the first quadrant of k-space at the doping level $x = 0.15$. The numbers indicate the values of $\epsilon_1(k)$ in [eV] [40].

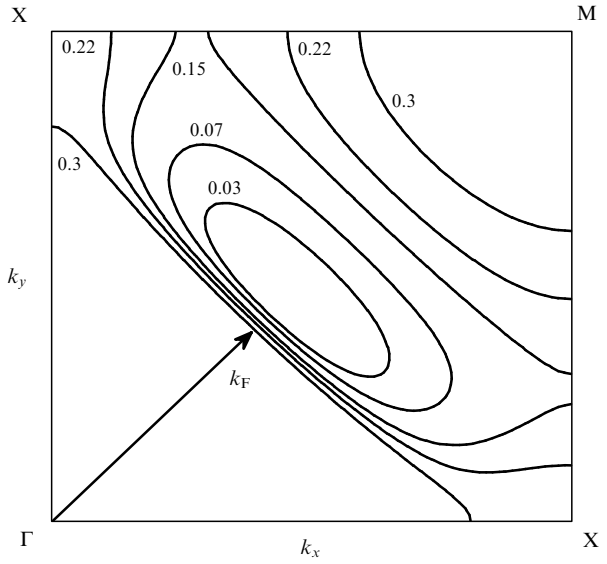

Figure 11. Fermi surfaces in the first quadrant of the Brillouin zone for five values of doping level x, indicated on the corresponding Fermi contours [40].

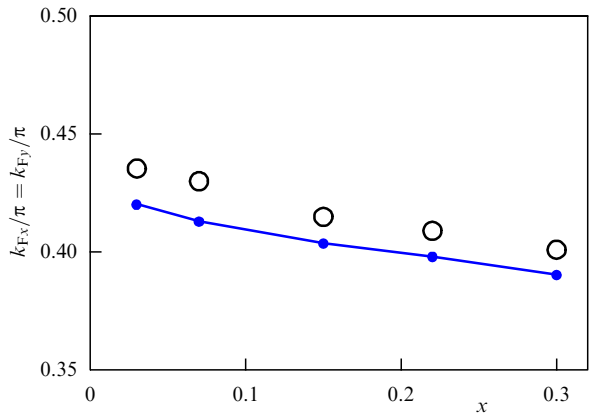

Figure 12. Fermi momentum k_F versus doping level x. The solid line connects the values of k_F calculated within the spin-polaron approach. Circles denote the experimental values of k_F [40] presented in [210].

together with spin correlators for the above five values of x are presented in Fig. 11. It is seen that, at a doping level of $x \approx 0.16$, the electron type of the Brillouin zone topology becomes changed for the hole type, which agrees with the experimental data [210]. To characterize the Fermi surface, the authors of Ref. [210] introduced the Fermi momentum k_F, equal to the distance from the point $\Gamma = (0, 0)$ of the Brillouin zone to the point of intersection of the Fermi surface with the nodal line. They determined the dependence of k_F on the doping level and demonstrated a transformation of the Fermi surface electronic topology into the hole one upon a transition over the critical value of the doping level.

A comparison of the concentration dependences of k_F, theoretically calculated and measured in Ref. [210], is presented in Fig. 12. It is seen that the weak experimental dependence $k_F(x)$ is well reproduced within the spin-polaron approach: the maximum discrepancy between the experimental and theoretical values of k_F does not exceed 4%.

6. Superconducting phase of spin-polaron quasiparticles

6.1 Cooper instability of spin polarons

Success in applying the spin polaron concept to the description of properties of the normal state of cuprates made it urgent to answer the question of implementing the superconducting phase under conditions where the Cooper instability develops in the subsystem of spin polarons, rather than for bare fermions [276]. Ref. [41] has shown that the ensemble of spin-polaron quasiparticles arising in the simplest model of cuprate superconductors — the 2D Kondo lattice in the SEC regime — possesses Cooper instability with the $d_{x^2-y^2}$-wave symmetry of the order parameter. The role of the Cooper pairing constant was played by the integral of exchange interaction between the localized spins. It was shown that three-center interactions in the spin-polaron ensemble in the spin liquid phase of the subsystem of localized spins, in contrast to interactions in the $t-J^*$ model [140, 141], facilitate Cooper pairing and provide

the realization of the superconducting phase with high critical temperatures.

Later, in Ref. [42], the theory of superconductivity in an ensemble of spin polarons was developed in SFMC, which was an important stage in the progress of the spin polaron concept. To analyze the superconducting phase, the basis set of three operators (51) was completed with three more operators ($\bar{\alpha} = -\alpha$):

$$a^{\dagger}_{-k\bar{\alpha}}, \quad b^{\dagger}_{-k\bar{\alpha}}, \quad L^{\dagger}_{-k\bar{\alpha}}. \tag{64}$$

Consideration of these three operators allowed us to introduce anomalous thermodynamic averages. It was demonstrated that a strong spin-fermion coupling arising due to hybridization mixing of the states of copper and oxygen ions in the original Emery model not only affects the formation of spin-polaron quasiparticles but also provides an effective attraction between them through the exchange interaction. This induces the Cooper instability with d-wave pairing in the system of spin polarons. Within such an approach, the phase $T-x$ diagram was constructed [42], correlating well with the experimental data on cuprate superconductors (see curve *1* in Fig. 15 of Section 6.2).

It is necessary to note that in Ref. [42] the superconductivity theory was constructed without considering the influence of intersite Coulomb interactions of fermions. The problem of allowing for these interactions, having primary importance for a realistic description of superconducting pairing in cuprate superconductors, is considered within the spin-polaron concept in Section 6.2.

6.2 Problem of intersite Coulomb interaction

Alongside the necessity to correctly describe the strong spin-charge coupling in cuprates, an even more important problem has manifested itself, related to considering the intersite Coulomb repulsion of holes on oxygen. The fact is that the Cooper instability, considered in the Hubbard model [85], $t-J$ model [19, 63, 186], or $t-J^*$ model [139–141], experiences strong suppression as soon as one takes into account the intersite Coulomb repulsion between particles located at the nearest-neighbor sites of a square lattice.

For the superconducting phase with s-wave symmetry of the order parameter, induced by the relatively strong Zaitsev kinematic mechanism [85, 90–92], Cooper pairing is preserved even upon switching on a sufficiently large V, as shown in Fig. 13. The self-consistency equation that determines the superconducting transition temperature in this case has the form

$$1 + V\frac{1}{N}\sum_{\mathbf{q}}(\cos q_x + \cos q_y)^2\Phi_q = 4t_1\frac{1}{N}\sum_{\mathbf{q}}(\cos q_x + \cos q_y)\Phi_q, \tag{65}$$

where $\Phi_q = [1/(2E_q)]\tanh[E_q/(2T_c)]$. However, the superconducting s-wave pairing in cuprates is not observed experimentally.

For the superconducting phase with d-wave symmetry of the order parameter, which is actually realized in cuprates [279–282], with the intersite repulsion of fermions taken into account, the situation is even more dramatic. Since the parameter V of Coulomb repulsion additively enters the coupling constant in the equation for T_c,

$$1 = \frac{J-V}{N}\sum_{q}(\cos q_x - \cos q_y)^2\Phi_q, \tag{66}$$

for complete suppression of superconductivity, as seen from Fig. 14, a relatively weak V is sufficient. As a result, to compensate the strong repulsive contribution caused by the intersite interaction of holes, it was necessary to additionally allow for the contributions related to electron–phonon, spin-fluctuation, and charge-fluctuation processes [228, 283–285]. Note that, in the above papers, the magnitude of Coulomb interaction between holes in different cells is $V = 0.2$ eV, which is much smaller than the magnitude of spin-fluctuation coupling at the expense of kinematic interaction $g_{sf} = 1.5$ eV, and only because of this fact the superconducting d-wave phase was preserved.

Thus, the superconducting d-wave phase, necessary for explaining the experiment, was significantly suppressed by the Coulomb repulsion of holes located at the nearest-

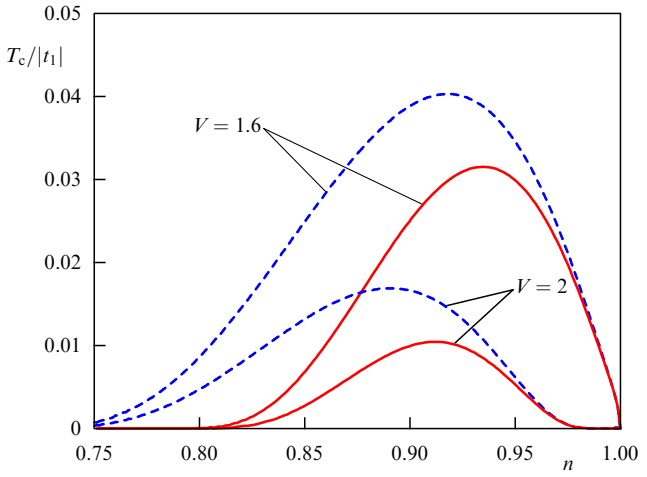

Figure 13. (Color online.) Dependences of the temperature of a transition to the superconducting s-wave phase on the concentration of electrons n in the $t-V$ model, obtained for two values of V taking into account (red solid curves) and not taking into account (blue dashed curves) the effects of inducing the band of fluctuation states [277], caused by the effect of strong intersite Coulomb correlations [278].

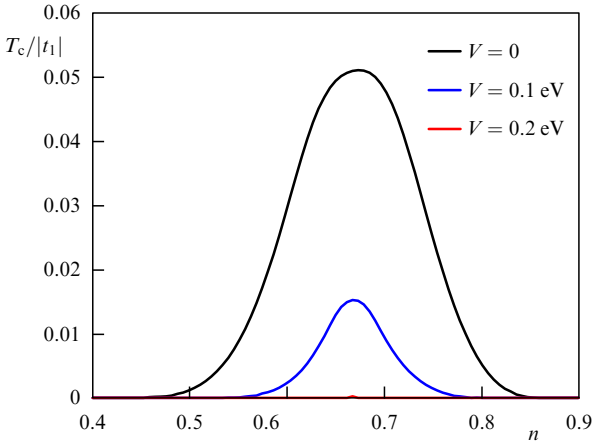

Figure 14. (Color online.) Dependences of the superconducting phase transition temperature on the concentration of electrons in the $t-J$ model at $J = 2|t_1|/U = 0.24$, obtained for three values of V.

neighbor sites. We should note that the sometimes-used argumentation, related to screening of the Coulomb interaction, in this case seems unconvincing, since it was about the repulsion of holes, located at nearest distances [286]. The low efficiency of screening in HTSCs was noted also in Ref. [105] and was associated with the low concentration of holes on oxygen ions.

The problem of neutralization of the Coulomb repulsion of holes on oxygen requires a revision of the theory of Cooper instability in HTSCs. In this connection, note that a similar problem in its time existed in the theory of classical superconductors. Its solution became possible after it was shown in [287, 288] that the electron–phonon interaction in a certain domain of the momentum space initiates effective attraction between fermions that can compensate the bare repulsion.

An important result obtained in the course of developing the superconductivity theory within the spin-polaron concept [42] was just the solution of the problem of intersite Coulomb interaction V_1 of holes on the nearest-neighbor oxygen ions. In Ref. [42], it was shown that in cuprate HTSCs the neutralization of the negative influence of the intersite Coulomb interaction of holes on the Cooper instability in the d-wave channel occurs due to the effect of two factors. The first of them is related to considering the real crystallographic structure of the CuO_2 plane, for which the Fourier transform of the intersite interaction has the form $V_q = 4V_1 \cos(q_x/2) \times \cos(q_y/2)$ and corresponds to the symmetry of the oxygen sublattice [186]. The second factor is due to the strong coupling between localized spins of copper ions and holes on oxygen ions. As noted in Section 6.1, this factor leads to the development of Cooper instability in the ensemble of spin-polaron quasiparticles [42]. In this case, the Coulomb repulsion between bare holes with the Fourier transform V_q is renormalized into the interaction between spin-polaron quasiparticles in such a way that the momentum dependence of this effective interaction comes to correspond to the structure of the sublattice of copper ions rather than oxygen ions. As a result, a situation arises in which the effective repulsion between spin polarons is eliminated from the kernel of the integral equation for the superconducting order parameter with the $d_{x^2-y^2}$-wave symmetry.

In Ref. [43] and its advanced version [289], when calculating the energy structure and analyzing the conditions for the development of Cooper instability in SFMC, the well-established values of parameters (5) of the Emery model [107, 110] were used. Using this set, for the magnitude of the exchange coupling between the localized spins of copper and spins of holes on oxygen ions, the relation $J = 3.38\ \text{eV} \gg \tau \approx 0.10\ \text{eV}$ was achieved. For the integral of hole hopping between oxygen ions, the value $t = 0.12$ eV was used, and the constant of exchange interaction between the spins of copper ions was chosen to be $I = 0.136$ eV, which agrees with the experimental data on cuprate superconductors. The parameters of Coulomb repulsion of holes located on the nearest-neighbor and next-nearest-neighbor oxygen ions were chosen to be $V_1 = 1-2$ eV [290] and $V_2 = V_2' = 0.5-1$ eV [289, 291], respectively.

The closed system of equations for normal, G_{ij} (61), and anomalous, F_{ij}, Green's functions ($j = 1, 2, 3$)

$$
\begin{aligned}
F_{11} &= \langle\langle a^{\dagger}_{-k\downarrow} | a^{\dagger}_{k\uparrow}\rangle\rangle_{\omega}\,, \\
F_{21} &= \langle\langle b^{\dagger}_{-k\downarrow} | a^{\dagger}_{k\uparrow}\rangle\rangle_{\omega}\,, \\
F_{31} &= \langle\langle L^{\dagger}_{-k\downarrow} | a^{\dagger}_{k\uparrow}\rangle\rangle_{\omega}\,,
\end{aligned}
\tag{67}
$$

obtained within the projection method, has the form [289]

$$
\begin{aligned}
(\omega - \xi_x) G_{1j} &= \delta_{1j} + t_k G_{2j} + J_x G_{3j} + \Delta_{1k} F_{1j} + \Delta_{2k} F_{2j}\,, \\
(\omega - \xi_y) G_{2j} &= \delta_{2j} + t_k G_{1j} + J_y G_{3j} + \Delta_{3k} F_{1j} + \Delta_{4k} F_{1j}\,, \\
(\omega - \xi_L) G_{3j} &= \delta_{3j} K_k + (J_x G_{1j} + J_y G_{2j}) K_k + \frac{\Delta_{5k}}{K_k} F_{3j}\,, \\
(\omega + \xi_x) F_{1j} &= \Delta^{*}_{1k} G_{1j} + \Delta^{*}_{3k} G_{2j} - t_k F_{2j} + J_x F_{3j}\,, \\
(\omega + \xi_y) F_{2j} &= \Delta^{*}_{2k} G_{1j} + \Delta^{*}_{4k} G_{2j} - t_k F_{1j} + J_y F_{3j}\,, \\
(\omega + \xi_L) F_{3j} &= \frac{\Delta^{*}_{5k}}{K_k} G_{3j} + (J_x F_{1j} + J_y F_{2j}) K_k\,.
\end{aligned}
\tag{68}
$$

For F_{i2} and F_{i3} ($i = 1, 2, 3$), the same second-index notations are taken as for normal Green's functions (61). In the formulation of the system of Eqns (68), functions (52) were used.

The components of the superconducting order parameter are related to the anomalous averages as follows:

$$
\begin{aligned}
\Delta_{1k} &= -\frac{2}{N}\sum_q \left[\frac{U_{\text{p}}}{2} + V_2 \cos(k_y - q_y) + V_2' \cos(k_x - q_x)\right] \\
&\quad \times \langle a_{q\uparrow} a_{-q\downarrow}\rangle\,, \\
\Delta_{2k} &= -\frac{4V_1}{N}\sum_q \phi_{k-q} \langle a_{q\uparrow} b_{-q\downarrow}\rangle\,, \\
\Delta_{3k} &= -\frac{4V_1}{N}\sum_q \phi_{k-q} \langle b_{q\uparrow} a_{-q\downarrow}\rangle\,, \\
\Delta_{4k} &= -\frac{2}{N}\sum_q \left[\frac{U_{\text{p}}}{2} + V_2 \cos(k_x - q_x) + V_2' \cos(k_y - q_y)\right] \\
&\quad \times \langle b_{q\uparrow} b_{-q\downarrow}\rangle\,, \\
\Delta_{5k} &= \frac{1}{N}\sum_q \Big[I_{k-q}\big(\langle L_{q\uparrow} L_{-q\downarrow}\rangle - C_1 \langle u_{q\uparrow} u_{-q\downarrow}\rangle\big) + 8IC_1 \langle u_{q\uparrow} u_{-q\downarrow}\rangle\Big] \\
&\quad + \frac{J}{N}\sum_q \left[-2\gamma_{1q}\langle L_{q\uparrow} L_{-q\downarrow}\rangle + \left(\frac{3}{2} - 4C_1\gamma_{1k}\right)\langle u_{q\uparrow} u_{-q\downarrow}\rangle\right] \\
&\quad + \frac{2}{N}\sum_q \big(\xi(q_x) s_{q,x} + t_q s_{q,y}\big)\langle a_{q\uparrow} L_{-q\downarrow}\rangle \\
&\quad + \frac{2}{N}\sum_q \big(\xi(q_y) s_{q,y} + t_q s_{q,x}\big)\langle b_{q\uparrow} L_{-q\downarrow}\rangle \\
&\quad - \frac{U_{\text{p}}}{N}\sum_q \left[\left(\frac{3}{8} - \frac{C_1}{2}\cos k_x\right)\langle a_{q\uparrow} a_{-q\downarrow}\rangle\right. \\
&\quad \left. + \left(\frac{3}{8} - \frac{C_1}{2}\cos k_y\right)\langle b_{q\uparrow} b_{-q\downarrow}\rangle\right] \\
&\quad - \frac{V_1}{N}\sum_q \left[\left(\frac{3}{4} - 2C_1\gamma_{1k} + C_2\gamma_{2k}\right) s_{q,x}\, s_{q,y}\right. \\
&\quad \left. + C_2 \sin k_x \sin(k_y)\phi_q\right]\big(\langle a_{q\uparrow} b_{-q\downarrow}\rangle + \langle b_{q\uparrow} a_{-q\downarrow}\rangle\big) \\
&\quad - \frac{1}{N}\sum_q \Big\{ V_2(C_1 \cos k_y - C_2\gamma_{2k}) \cos q_y \\
&\quad + V_2'\left[-\frac{3}{8} + C_1 \cos k_x - \frac{C_3}{2}\cos(2k_x)\right]\cos q_x \Big\}\langle a_{q\uparrow} a_{-q\downarrow}\rangle
\end{aligned}
$$

$$-\frac{1}{N}\sum_q\Big\{V_2(C_1\cos k_x - C_2\gamma_{2k})\cos q_x + V_2'\Big[-\frac{3}{8}+C_1\cos k_y-\frac{C_3}{2}\cos(2k_y)\Big]\cos q_y\Big\}\langle b_{q\uparrow}b_{-q\downarrow}\rangle\,. \tag{69}$$

Here, $I_k = 4I\gamma_{1k}$ and the functions $s_{k,x} = \sin(k_x/2)$, $s_{k,y} = \sin(k_y/2)$, $\phi_k = \cos(k_x/2)\cos(k_y/2)$ are introduced.

Since it is the regime of weak doping that is relevant for cuprates, the contributions to expressions (69) resulting from the decoupling of averages and proportional to density-density correlators are not considered here.

To analyze the conditions for Cooper instability, in Ref. [289] the necessary anomalous Green's functions were expressed in terms of the parameters Δ_{lk}^{*} $(l = 1, \ldots, 5)$. Then, using the spectral theorem [292], expressions were found for the anomalous averages, and a closed system of homogeneous integral equations for the components of the superconducting order parameter was found. This system of equations was used to find the critical temperature of the transition of an ensemble of spin polarons to the superconducting state with given symmetry of the order parameter. From the system, it followed that the kernels of the integral equations have a split form and its solution should be sought in the form

$$\begin{aligned}
\Delta_{1k} &= B_{11} + B_{12}\cos k_x + B_{13}\cos k_y\,,\\
\Delta_{2k} &= B_{21}\phi_k + B_{22}s_{k,x}s_{k,y}\,,\\
\Delta_{3k} &= B_{31}\phi_k + B_{32}s_{k,x}s_{k,y}\,,\\
\Delta_{4k} &= B_{41} + B_{42}\cos k_x + B_{43}\cos k_y\,,\\
\Delta_{5k} &= B_{51} + B_{52}\cos k_x + B_{53}\cos k_y\\
&\quad + B_{54}\cos k_x\cos k_y + B_{55}\sin k_x\sin k_y\\
&\quad + B_{56}\cos(2k_x) + B_{57}\cos(2k_y)\,,
\end{aligned} \tag{70}$$

where 17 B amplitudes determine the contribution of the corresponding basis functions to the decomposition of the order parameter components. After substituting Eqn (70) into the system of equations for the components of the superconducting order parameter and equating the coefficients at the corresponding trigonometric functions, a system of 17 algebraic equations for the B amplitudes was obtained [289]. Solving this system together with the equation for the chemical potential μ yielded the dependence of the temperature T_c on the doping level x for various symmetries of the order parameter. The results of the numerical solution are presented in Fig. 15. Curve *1* shows the dependence of the critical temperature of superconducting $d_{x^2-y^2}$-wave pairing on the doping level at $U_p = V_1 = V_2 = 0$. This curve, obtained earlier in Ref. [42], agrees well with the experimental data both in the absolute value of T_c and in the doping interval in which the Cooper instability develops.

An important aspect of the developed approach is that, as mentioned above, allowing for the Coulomb interaction V_1 of fermions located on the nearest oxygen ions does not affect the dependence $T_c(x)$ for the superconducting $d_{x^2-y^2}$-wave pairing: curve *1* in Fig. 15 does not change [43]. In the doping region, where this type of pairing is realized at $T \lesssim T_c$, the solutions to the algebraic system for amplitudes B showed that only four of them, B_{52}, B_{53}, B_{22}, B_{32}, are nonzero; in this case, $B_{52} = -B_{53}$, $B_{22} = -B_{32}$, and $|B_{52}|/|B_{22}| \sim 10^3$. This means that the quasimomentum dependence of the superconducting gap is mainly determined by the fifth component

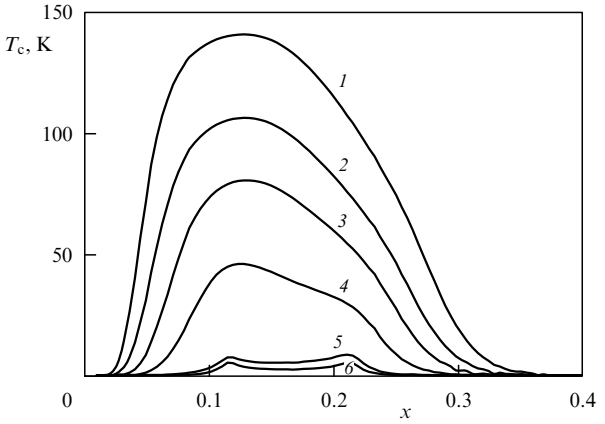

Figure 15. Dependences of the critical temperature of a transition to the superconducting phase for $d_{x^2-y^2}$-wave pairing on the doping level x, obtained for the model parameters $J = 3.38$, $\tau = 0.10$, $t = 0.12$, $I = 0.136$ at $U_p = V_2 = 0$ (curve *1*), $U_p = 0$, $V_2 = 0.2$ (curve *2*), $U_p = 3$, $V_2 = 0$ (curve *3*), $U_p = 3$, $V_2 = 0.2$ (curve *4*), $U_p = 0$, $V_2 = 0.8$ (curve *5*), and $U_p = 3$, $V_2 = 0.5$ (curve *6*) (all parameters in [eV]) [295].

of the order parameter Δ_{5k}, which has the form

$$\Delta_{5k}^{(d)} = B_{52}(\cos k_x - \cos k_y)\,. \tag{71}$$

For the superconducting $d_{x^2-y^2}$-wave pairing at $U_p = V_2 = 0$, the amplitudes B_{52} and B_{53} in the equation for Δ_{5k} are determined exclusively by the exchange constant I, rather than the parameter V_1. Therefore, the intersite Coulomb repulsion of holes on the nearest-neighbor oxygen ions does not suppress the Cooper instability in the d-wave channel [43].

For $U_p = V_2 = 0$, instead of 17 equations, only one equation can be derived and solved for T_c (as in Refs [42, 273, 279]), which has the form

$$1 = \frac{I}{N}\sum_q(\cos q_x - \cos q_y)^2\big(M_{33}(q,\epsilon_{1q}) - C_1 M_{uu}(q,\epsilon_{1q})\big)\,, \tag{72}$$

where the functions

$$\begin{aligned}
M_{uu}(q) &= -s_{q,x}^2 M_{11}(q) - s_{q,y}^2 M_{22}(q)\\
&\quad - s_{q,x}s_{q,y}\big(M_{21}(q) + M_{12}(q)\big)\,,\\
M_{nm}(q) &= \frac{S_{nm}(q,E_{1q}) + S_{nm}(q,-E_{1q})}{4E_{1q}(E_{1q}^2 - E_{2q}^2)(E_{1q}^2 - E_{3q}^2)}\tanh\left(\frac{E_{1q}}{2T}\right),\\
S_{11}(k,\omega) &= -Q_y(k,-\omega)Q_y(k,\omega)\,,\\
S_{12}(k,\omega) &= -Q_y(k,-\omega)Q_x(k,\omega)\,,\\
S_{21}(k,\omega) &= S_{12}(k,-\omega)\,,\\
S_{22}(k,\omega) &= -Q_x(k,-\omega)Q_x(k,\omega)\,,\\
S_{33}(k,\omega) &= Q_{xy}(k,-\omega)Q_{xy}(k,\omega)\,,\\
Q_{x(y)}(k,\omega) &= (\omega - \xi_{x(y)})J_{y(x)} + t_k J_{x(y)}\,,\\
Q_{xy}(k,\omega) &= (\omega - \xi_x)(\omega - \xi_y) - t_k^2
\end{aligned} \tag{73}$$

are introduced.

From Eqn (72), in particular, it follows that the mechanism giving rise to superconducting pairing is the exchange interaction between the spin moments of copper ions, which, as mentioned above, transforms into the effective attraction as a result of strong spin-charge coupling. The results of

solving Eqn (72) and the system of 17 equations for B amplitudes for d-wave pairing at $U_p = V_2 = 0$ apparently coincide and correspond to curve *1* in Fig. 15.

In contrast to the intersite interaction of holes on the nearest-neighbor oxygen ions, considering the Coulomb interaction U_p of two holes on one oxygen ion leads to a suppression of the superconducting d-wave phase [44]. However, as follows from a comparison of curve *3* ($U_p = 3$ eV and $V_2 = 0$) and curve *1* ($U_p = V_2 = 0$) in Fig. 15, this suppression is not essential for the realization of HTSC, since in the region of optimal doping, $x \simeq 0.16$, the temperature T_c remains high.

References [289, 291] consider the influence of the Coulomb repulsion V_2 of holes on next-nearest-neighbor oxygen ions in the CuO_2 plane on superconducting pairing. Curve *2* in Fig. 15 corresponds to the dependence $T_c(x)$ obtained for $U_p = 0$, $V_2 = 0.2$ eV, and curve *5*, to the dependence $T_c(x)$ for $U_p = 0$, $V_2 = 0.8$ eV. It is seen that, in contrast to V_1, considering V_2 leads to a suppression of the superconducting $d_{x^2-y^2}$-wave pairing. This suppression increases if $U_p \neq 0$ (curves *3*, *4*, and *6*). But even with simultaneously taking into account the above Coulomb interactions, $d_{x^2-y^2}$-wave pairing is preserved and can be suppressed only at unrealistically high values of $V_2 > 0.5$ eV [289, 291].

Figure 16 presents a modification of the gap in the spectrum of elementary excitations of spin-polaron quasiparticles at the Fermi contour in the superconducting phase upon varying the magnitude of Coulomb interactions U_p and V_2, calculated in Ref. [294]. From the figure, it is seen that the quasimomentum dependence of the gap in the first Brillouin zone is characterized by $d_{x^2-y^2}$-wave symmetry of the order parameter. Since the Coulomb interaction V_1 of holes on the neighboring ions of oxygen does not affect the superconducting d-wave pairing, the behavior of the superconducting gap is determined by only three components of the order parameter, Δ_{1k}, Δ_{4k}, and Δ_{5k}, from system (69). The self-consistent solution to the system of three equations for these components together with the equation for chemical potential (now without using the linear approximation in Δ_{jk} when finding necessary anomalous Green's functions) yields the dependences $\Delta(k)$, presented in Fig. 16.

It can be shown [52, 295] that these dependences can be described analytically due to the low density of current carriers, as well as the high value of $\sim J$ of the energy gap between the lower spin-polaron band and the energy level of holes in p-orbitals of oxygen (see Fig. 2). In this case, the expression for E_k can be presented in the classical form,

$$E_k = \sqrt{\epsilon_{1k}^2 + \Delta_k^2}\,, \tag{74}$$

where the gap function Δ_k^2 is expressed in terms of the order parameter components Δ_{jk} ($j = 1, \ldots, 5$) in an additive way:

$$\Delta_k^2 = |\Delta_{1k}|^2 + |\Delta_{2k}|^2 + |\Delta_{3k}|^2 + |\Delta_{4k}|^2 + \frac{|\Delta_{5k}|^2}{K_k^2}\,. \tag{75}$$

An important consequence of Eqn (75) for the superconducting gap is that the function Δ_k for d-wave pairing cannot be written as a simple difference of cosines, $\cos k_x - \cos k_y$. The presence of the function K_k in the denominator of Eqn (75) will lead to the fact that the quasimomentum dependence of the gap will always slightly decline from the function $\cos k_x - \cos k_y$. A detailed discussion of the issue related to the dispersion of the superconducting gap in cuprate HTSCs can be found in Refs [296, 297] and references therein.

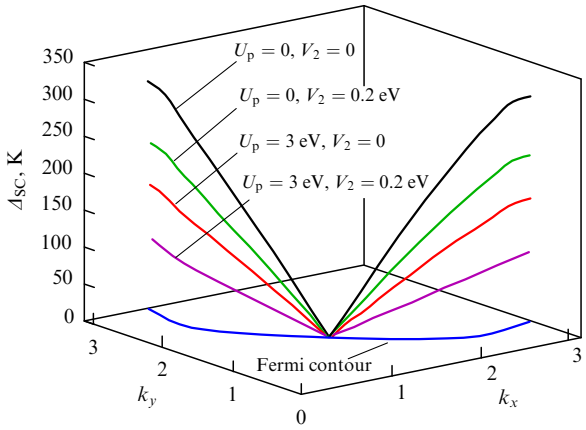

Figure 16. Quasimomentum dependence of the superconducting gap Δ_{SC} on the Fermi contour at $x = 0.125$, $I = 0.136$ eV, $T = 0$, and various magnitudes of Coulomb interaction [294].

The issue of implementing s-wave pairing in an ensemble of spin polarons was considered in Ref. [44], for simplicity, without considering the long-range Coulomb interaction, $V_2 = 0$. In this case, from the system of integral equations for the components of the superconducting order parameter it follows that the solution corresponding to s-wave pairing should have the form

$$\begin{aligned} \Delta_{1k}^{(s)} &= \Delta_{4k}^{(s)} = B_{11}\,, \\ \Delta_{2k}^{(s)} &= \Delta_{3k}^{(s)} = 0\,, \\ \Delta_{5k}^{(s)} &= B_{51} + 2B_{52}\gamma_{1k} + B_{54}\gamma_{2k}\,. \end{aligned} \tag{76}$$

Calculations show that at all realistic parameters of the model the system has no nontrivial solution, corresponding to the superconducting s-wave pairing [44]. Therefore, in the SFMC, correctly considering the strong coupling of holes on oxygen ions with the spin moments of copper ions, the superconducting phase with s-wave symmetry of the order parameter is not realized.

6.3 London penetration depth

The spin-polaron approach, which has proven successful in describing the equilibrium properties of hole-doped cuprates both in the normal and in the superconducting phase, can be applied to the investigation of the system response to an electromagnetic perturbation, as well. In particular, it is highly interesting to study the penetration depth λ of magnetic field into a superconductor, since this characteristic allows clarifying a number of experimentally observed features of the temperature dependence of the superconducting current density. A comparison with experimental data yields important information, not only about the critical current, but also, e.g., about the mechanism of pseudogap phase formation in cuprates [298, 299].

A characteristic feature of the temperature dependence of λ^{-2} in cuprates is a linear slanted region of the function $\lambda^{-2}(T)$ at low temperatures. Such a behavior, according to Ref. [300], is due to the presence of nodal points at the gap on the normal-phase Fermi surface. The appearance of nodal points in cuprates, as is known, is associated with the

realization of d-wave symmetry of the superconducting order parameter. In s-wave superconductors, the nodal points are absent, and the gap reduction in the low-temperature region is described by an exponential function.

One more important feature of the London depth temperature dependence in cuprate HTSCs is due to the presence in a number of compounds of so-called inflection points (i.e., points where the curvature changes sign) of the function $\lambda^{-2}(T)$, observed at certain doping levels in $La_{1.83}Sr_{0.17}CuO_4$ [301, 302], $YBa_2Cu_3O_{7-\delta}$ [303, 304], and $Bi_{2.15}Sr_{1.85}CaCu_2O_{8+\delta}$ [305].

To explain why an inflection point appears, the authors of Ref. [301] hypothesize that in $La_{1.83}Sr_{0.17}CuO_4$ there are two superconducting gaps, with d-wave and s-wave symmetry of the order parameter existing simultaneously. However, as demonstrated in Ref. [52], the above feature in the temperature dependence of the magnetic field penetration depth in a cuprate superconductor can be obtained without using artificial hypotheses. For this purpose, the spin-polaron concept was invoked, the key feature of which is that the charge carriers in these compounds are spin-polaron quasiparticles.

In the local approximation, the relation between the density of the superconducting current **j** and the magnetic field vector potential **A** is determined by the London equation

$$\mathbf{j} = -\frac{c}{4\pi\lambda^2}\,\mathbf{A}\,, \tag{77}$$

where c is the speed of light. To calculate the density of superconducting current **j**, the SFMC Hamiltonian (26) is written in the Wannier representation. Then, using the Peierls substitution, a term describing the magnetic field is added to this Hamiltonian. The Peierls substitution leads to renormalization of all hopping integrals by the phase factor

$$\exp\left(\frac{ie}{c\hbar}\,R^x_{mn}A^x_{q=0}\right), \tag{78}$$

where $R_{mn} = R_m - R_n$ is the difference between radius vectors for sites with the indices m and n, $\hbar$ is the Planck constant, e is the electron charge, and $A^x_{q=0}$ is a Fourier component of the vector potential considered in the long-wave limit (see, e.g., [306]). For simplicity, the vector potential A is chosen directed along the x-axis.

The standard procedure of calculating the paramagnetic and diamagnetic parts of the current consists in extracting from the Hamiltonian corrections linear and quadratic in the vector potential $A^x_{q=0}$ with subsequent variation of these corrections with respect to $A^x_{q=0}$ [306–309]. When using the spin polaron concept, it is appropriate to modify the approach by abandoning the expansion of the phase factors (78) in powers of $A^x_{q=0}$, i.e., leaving these factors in their initial form. Then, after moving to the quasimomentum representation, the only change (due to switching on the magnetic field) in the operators $\hat{H}_{\rm h}$ and $\hat{J}$ (26) of the Hamiltonian will be the appearance of an additional phase α_x in the argument of the trigonometric function $s_{k,x}$ [52]:

$$s_{k,x} \to s_{k,x} = \sin\left(\frac{k_x}{2} - \alpha_x\right), \tag{79}$$

where

$$\alpha_x = \frac{eg_x}{2c\hbar}\,A^x_{q=0}\,, \tag{80}$$

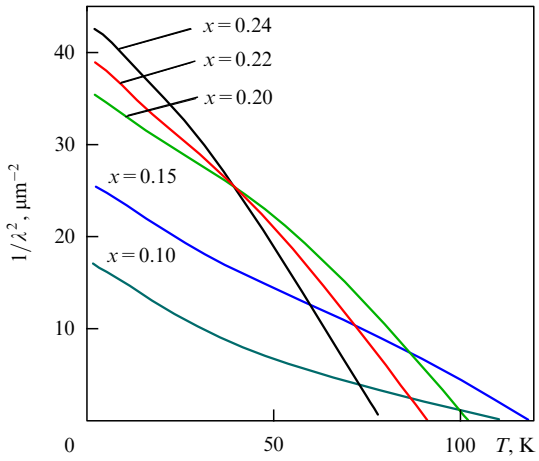

Figure 17. (Color online.) Temperature dependence of the inverse London penetration depth λ, calculated for various values of the doping level x with the set of model parameters $\tau = 0.225$, $J = 2.86$, $I = 0.118$, $t = 0.12$, $U_{\rm p} = V_2 = V_2' = 0$ (all parameters in [eV]) [52].

with g_x being the lattice constant along the x-axis. The function $s_{k,y}$ remains unchanged, since in the considered case $A^y_{q=0} = 0$.

Note that the appearance of the quantity α_x as a phase in the argument of the function $s_{k,x}$ is not unexpected, since the renormalization (79) corresponds to the known replacement of the quasimomentum $\hbar k_x$ upon switching on the magnetic field:

$$\hbar k_x \to \hbar k_x - \frac{e}{c}\,A^x_{q=0}\,.$$

The variation in the expressions of the operators $\hat{H}_{\rm h}$ and $\hat{J}$ with respect to the vector potential leads to the following expression for the superconducting current density:

$$j_x = \frac{eg_x}{\hbar}\sum_{k\alpha}\cos\left(\frac{k_x}{2} - \alpha_x\right)\left[2\tau s_{k,x}\langle a^\dagger_{k\alpha}a_{k\alpha}\rangle + (2\tau - 4t)s_{k,y}\langle a^\dagger_{k\alpha}b_{k\alpha}\rangle + J\langle a^\dagger_{k\alpha}L_{k\alpha}\rangle\right]. \tag{81}$$

The dependence of j_x on the vector potential in the region of small $A^x_{q=0}$ must be linear, and the coefficient that determines this linear dependence, according to the London equation, is directly expressed in terms of λ^{-2}. This coefficient is calculated numerically [52] based on Eqn (81), and the results of calculations of the temperature dependence of the magnetic field penetration depth in an ensemble of spin polarons at different doping levels are presented in Fig. 17.

Although the model parameters were chosen equal to those used in the previous papers (see Section 3), rather than found by a fitting procedure, the curves presented in Fig. 17 demonstrate good enough quantitative agreement with the experimental data [300–305, 310–312]. At low temperatures, all curves demonstrate a linear behavior up to the lowest of the considered temperatures $T = 2$ K. Such behavior, as mentioned above, is a consequence of d-wave symmetry of the superconducting order parameter.

An important feature of the obtained temperature dependences of λ^{-2} is the existence of inflection points, which, as mentioned above, are observed in some cuprate HTSCs. Figure 18 presents the dependence $\lambda^{-2}(T)$ at $x = 0.17$. The inflection point position of this dependence is marked by a vertical dashed-dotted straight line. The authors

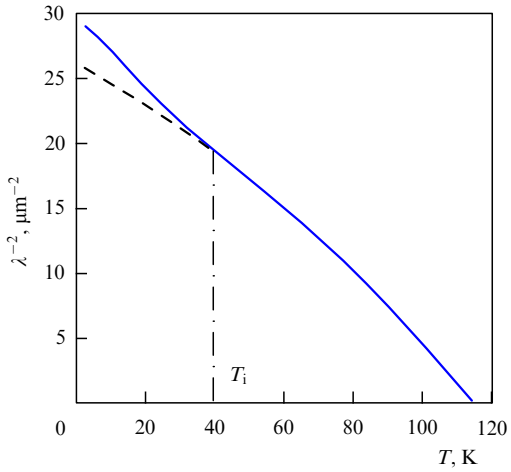

Figure 18. Temperature dependence of λ^{-2} at $x = 0.17$. The model parameters $J = 2.86$ eV and $I = 0.118$ eV are chosen such that the boundary values of the curve correspond to the experimental data [301, 302, 312]. The remaining parameters are chosen just as in Fig. 17. T_i is the inflection point. The dashed line corresponds to the extrapolation of the function $\lambda^{-2}(T)$ from the region to the right of point T_i to the region to the left of this point.

of Ref. [52] believe that the manifestation of this feature in the theoretical curves $\lambda^{-2}(T)$ should be considered indirect confirmation of the spin-polaron nature of Fermi quasiparticles in copper-based superconductors.

In Ref. [52], it is shown that the modification of the spin-polaron spectrum E_k (74), with a correction due to considering the magnetic field, in the superconducting phase occurs additively,

$$E_k = \delta\epsilon_{1k} + \sqrt{\epsilon_{1k}^2 + \Delta_k^2}\,, \tag{82}$$

where $\delta\epsilon_{1k}$ is the linear in α_x correction to the normal-phase polaron spectrum ϵ_{1k}; the gap function Δ_k^2 in this case is expressed in terms of the only component Δ_{5k} of the order parameter,

$$\Delta_k^2 = \frac{|\Delta_{5k}|^2}{K_k^2}\,. \tag{83}$$

The simplicity of Δ_k^2 in this case is due to the fact that Ref. [52] did not take into account the contributions from the Coulomb interaction $\hat{U}_p$ and $\hat{V}_{pp}$.

To conclude this section, we note that, in spite of the three-band character of the model, the spectrum of Fermi excitations of spin polarons in the superconducting phase E_k is expressed solely through the normal phase lower band spectrum ϵ_{1k}. At small α_x, the Bogoliubov quasiparticle spectrum is renormalized in the same additive way as in the usual theory of London penetration depth [307, 309]. At the same time, the quasimomentum dependence of the normal phase spectrum ϵ_{1k} (and, therefore, its field-induced correction $\delta\epsilon_{1k}$) considerably differs from that in the simplest case of quadratic dispersion and is determined by the structure of the CuO_2 plane and strong spin-fermion interactions.

7. Conclusions

The presented review of theoretical papers on the development of the spin-fermion model for describing the electronic properties of hole-doped cuprates in the normal state and the mechanism of superconducting pairing within the spin-polaron concept allows the following statements.

(1) The mathematically rigorous procedure of considering strong correlations in the electronic system of copper and oxygen ions of the CuO_2 plane described by the Emery Hamiltonian leads to the spin-fermion model of cuprates. In this model, the subsystem of spins localized on copper ions nonlocally interacts with the subsystem of collective holes. The characteristic energy of coupling between the localized spins and collective holes is so large (~ 5 eV) that it substantially changes the nature of Fermi quasiparticles and induces a specific mechanism of superconducting pairing.

(2) The strong spin-fermion interaction gives rise to the formation of nonlocal spin polarons. This fact determines the nature of the Fermi quasiparticles in the spin-fermion model of cuprates and allows describing the set of experimental data on the cuprate properties both in the normal and in the superconducting state in the framework of a unified concept using a single fitting parameter of the model — the integral of direct hopping between oxygen ions t. Note that, to adequately reproduce the mentioned experimental data, the value of this parameter should be chosen equal to $t = 0.1$ eV, which considerably differs from the frequently used value $t_{pp} = 0.65$ eV.

(3) Physical characteristics of the normal phase of cuprates are reflected by the statistical properties of an ensemble of nonlocal spin polarons. In particular, the Fermi surface modification extracted from experimental data in cuprate compounds doped with holes is reproduced at a quantitative level.

(4) For the interval of hole doping values corresponding to a superconducting area in the phase diagram of cuprates, the spin-polaron ensemble exhibits Cooper instability with high values of critical temperature. In this case, the superconducting order parameter is characterized by $d_{x^2-y^2}$-wave symmetry. The effective Cooper pairing potential is proportional to the integral of exchange interaction between the nearest spins of copper ions. The physical reason for this effect is that at strong spin-fermion coupling the location of two spin polarons at nearest-neighbor sites leads to the exchange energy gain, as compared to the exchange energy of spatially remote spin polarons. This feature manifests itself as the mutual attraction of spin polarons and determines the mechanism of superconducting pairing in the ensemble of spin-polaron quasiparticles.

(5) In an ensemble of spin polarons, only the superconducting phase with $d_{x^2-y^2}$-wave symmetry of the order parameter can be implemented. The s-wave superconducting phase does not satisfy the system of integral self-consistence equations for any really acceptable levels of hole doping. This corresponds to the experimental data on the observed symmetry of the order parameter and serves as an additional argument in favor of the spin-polaron concept. Note that in other approaches the superconducting phase with an s-wave type of pairing not only could be implemented but also provided higher critical temperatures.

(6) The superconducting phase of the spin-polaron ensemble is not suppressed by introducing the Coulomb interaction of holes localized on the nearest-neighbor oxygen ions. This removes the long-standing problem of neutralizing the effect of Coulomb repulsion of holes on the implementation of Cooper instability. In this connection, note that, in traditional approaches based on the Hubbard model and its

effective low-energy versions, the superconducting phase was suppressed upon including into consideration the Coulomb repulsion of holes localized at the nearest-neighbor lattice sites. The urgency of the problem was exacerbated by the impossibility of using the effective Coulomb parameter, renormalized towards lower values at the expense of the screening effect at distances of a few angstroms.

The neutralization of the negative effect of the intersite Coulomb repulsion of neighboring holes on the superconducting $d_{x^2-y^2}$-wave pairing occurs under the influence of two factors. The first is due to taking into account the real crystallographic structure of the CuO_2 plane. In this case, the Coulomb repulsion of fermions in the sublattice of oxygen ions is described by the Fourier transform of the intersite Coulomb interaction $V_q = 4V_1 \cos(q_x/2) \cos(q_y/2)$. The second factor is associated with strong spin-charge coupling. As a result, the spin-polaron quasiparticles effectively move over the square lattice. For the superconducting state arising in such an ensemble, the Coulomb repulsion between non-renormalized holes with the Fourier transform V_q will transform into the interaction between spin polarons. Since the coefficient of expansion of V_q in square lattice invariants is zero, the effective interaction between spin-polaron quasiparticles also becomes zero. Therefore, the parameter V_1 does not enter the equations for the superconducting order parameter with $d_{x^2-y^2}$-wave symmetry and does not affect the critical temperature.

It is worth noting that the different contribution of the Coulomb interaction to the conditions of implementing the superconducting phase with different symmetries of the order parameter manifested itself earlier, e.g., in the Kohn–Luttinger superconductivity theory [75, 76]. In Refs [313–315], it is found that the intersite Coulomb interactions in lattice models usually contribute only to definite channels of pairing and do not affect other channels. At the same time, polarization contributions have components in all the channels and, as a rule, more than one of them 'plays' in favor of attraction. In such a situation, it turns out that the intersite interaction either does not affect the main components of the effective interaction leading to pairing or suppresses the major components but does not affect the minor ones [313–315].

(7) The Hubbard repulsion U_p and Coulomb interactions V_2 of holes located on next-nearest-neighbor oxygen ions affect the formation of the superconducting phase with d-wave symmetry of the order parameter, leading to an increase in the critical transition temperature. However, this temperature remains within the values which are observed experimentally. In this case, the superconducting gap is formed under the influence of three components of the order parameter.

(8) The possibility of applying the spin-polaron concept to the study of the system response to an external electromagnetic perturbation is demonstrated. Using the specific features of the spectrum of spin-polaron quasiparticles made it possible to explain fine peculiarities in the temperature and concentration dependences of the London penetration depth. The obtained dependences are in good agreement with the experimental data on cuprate superconductors.

Let us briefly dwell on the important areas of further application of the spin-polaron concept. One of them is the construction of an effective single-orbital model [316], operating in the truncated Hilbert space and, in contrast to the Hubbard and $t-J$ models, correctly taking into account both the specific features of the CuO_2 plane crystallographic structure and the strong spin-fermion coupling that determines the formation of spin-polaron quasiparticles. The creation of such a model seems necessary, since the analysis of low-temperature properties of cuprate superconductors within the spin-fermion model and even its simplified version, the so-called $\varphi-d$ model [273, 293], is still rather cumbersome. In particular, proceeding to such an effective model would allow reducing the rank of the self-consistent system of integral equations for the superconducting phase.

Another interesting area to further use the spin-polaron concept in is the investigation of conditions for the appearance of spectral intensity modulation at the Fermi contour [317], as well as the pseudogap state [6] in underdoped cuprate superconductors. This state manifests itself in experiments on nuclear magnetic resonance and inelastic neutron scattering, as well as in ARPES experiments [4], demonstrating strong anisotropic changes to the spectral density of charge carriers in a wide range of temperatures in normal and superconducting phases of cuprates [318]. The nature of the pseudogap state is still an open question; however, one of most frequently discussed scenarios for the occurrence of this state is related to the model of strong scattering of charge carriers by short-range AFM spin fluctuations [318–320]. This scattering leads to a substantial non-Fermi-liquid restructuring of the electronic spectrum in certain regions of the quasimomentum space near the Fermi surface in the vicinity of 'hot' points or near Fermi surface flat areas [321–323].

Moreover, it seems relevant to study kinetic, thermodynamic, and galvanomagnetic characteristics of cuprate superconductors, in which the charge carriers are spin polaron quasiparticles [324–329] formed upon taking into account the real crystallographic features of the CuO_2 plane.

The authors' study was supported by the Russian Foundation for Basic Research (RFBR) within project nos. 18-02-00837, 19-02-00509, and 20-32-70059, and partly by the Government of Krasnoyarsk Region and the Krasnoyarsk Region Science and Technology Support Fund within project no. 18-42-240014 "Single-orbital effective model of an ensemble of spin-polaron quasiparticles in the problem of describing the intermediate state and pseudogap behavior of cuprate superconductors." The review was carried out with support from the RFBR within the Expansion competition (project no. 19-12-50116).

References

1. Damascelli A, Hussain Z, Shen Z-X *Rev. Mod. Phys.* **75** 473 (2003)
2. Fischer Ø et al. *Rev. Mod. Phys.* **79** 353 (2007)
3. Fournier D et al. *Nat. Phys.* **6** 905 (2010)
4. Timusk T, Statt B *Rep. Prog. Phys.* **62** 61 (1999)
5. Chakravarty S et al. *Phys. Rev. B* **63** 094503 (2001)
6. Sadovskii M V *Phys. Usp.* **44** 515 (2001); *Usp. Fiz. Nauk* **171** 539 (2001)
7. Lee P A et al. *Rev. Mod. Phys.* **78** 17 (2006)
8. Yang K-Y, Rice T M, Zhang F-C *Phys. Rev. B* **73** 174501 (2006)
9. Hussey N E *Adv. Phys.* **51** 1685 (2002)
10. Riggs S C et al. *Nat. Phys.* **7** 332 (2011)
11. Chang J et al. *Nat. Phys.* **8** 871 (2012)
12. Mamsurova L G et al. *JETP Lett.* **105** 241 (2017); *Pis'ma Zh. Eksp. Teor. Fiz.* **105** 223 (2017)
13. Mamsurova L G et al. *JETP Lett.* **106** 378 (2017); *Pis'ma Zh. Eksp. Teor. Fiz.* **106** 351 (2017)
14. Gabovich A M et al. *Supercond. Sci. Technol.* **14** R1 (2001)
15. Forgan E M et al. *Nat. Commun.* **6** 10064 (2015)
16. Shen K M et al. *Science* **307** 901 (2005)

17. Vojta M *Adv. Phys.* **58** 699 (2009)
18. Berg E et al. *New J. Phys.* **11** 115004 (2009)
19. Plakida N *High-Temperature Cuprate Superconductors: Experiment, Theory, and Applications* (Dordrecht: Springer, 2010)
20. Keimer B et al. *Nature* **518** 179 (2015)
21. Zhang F C, Rice T M *Phys. Rev. B* **37** 3759(R) (1988)
22. Emery V J *Phys. Rev. Lett.* **58** 2794 (1987)
23. Anderson P W *Science* **235** 1196 (1987)
24. Barabanov A F, Maksimov L A, Uimin G V *JETP Lett.* **47** 622 (1988); *Pis'ma Zh. Eksp. Teor. Fiz.* **47** 532 (1988)
25. Barabanov A F, Maksimov L A, Uimin G V *Sov. Phys. JETP* **69** 371 (1989); *Zh. Eksp. Teor. Fiz.* **96** 665 (1989)
26. Prelovšek P *Phys. Lett. A* **126** 287 (1988)
27. Zaanen J, Oleś A M *Phys. Rev. B* **37** 9423 (1988)
28. Stechel E B, Jennison D R *Phys. Rev. B* **38** 4632 (1988)
29. Emery V J, Reiter G *Phys. Rev. B* **38** 4547 (1988)
30. Matsukawa H, Fukuyama H *J. Phys. Soc. Jpn.* **58** 2845 (1989)
31. Kuzian R O et al. *Phys. Rev. B* **58** 6194 (1998)
32. Barabanov A F, Maksimov L A, Mikheyenkov A V *AIP Conf. Proc.* **527** 1 (2000)
33. Barabanov A F, Mikheenkov A V, Belemuk A M *JETP Lett.* **75** 107 (2002); *Pis'ma Zh. Eksp. Teor. Fiz.* **75** 118 (2002)
34. Maksimov L A, Barabanov A F, Kuzian R O *Phys. Lett. A* **232** 286 (1997)
35. Maksimov L A, Hayn R, Barabanov A F *Phys. Lett. A* **238** 288 (1998)
36. Barabanov A F et al. *JETP Lett.* **68** 412 (1998); *Pis'ma Zh. Eksp. Teor. Fiz.* **68** 386 (1998)
37. Barabanov A F et al. *Phys. Lett. A* **265** 221 (2000)
38. Kampf A P, Schrieffer J R *Phys. Rev. B* **42** 7967 (1990)
39. Barabanov A F et al. *J. Exp. Theor. Phys.* **92** 677 (2001); *Zh. Eksp. Teor. Fiz.* **119** 777 (2001)
40. Dzebisashvili D M, Val'kov V V, Barabanov A F *JETP Lett.* **98** 528 (2013); *Pis'ma Zh. Eksp. Teor. Fiz.* **98** 596 (2013)
41. Val'kov V V, Korovushkin M M, Barabanov A F *JETP Lett.* **88** 370 (2008); *Pis'ma Zh. Eksp. Teor. Fiz.* **88** 426 (2008)
42. Val'kov V V, Dzebisashvili D M, Barabanov A F *Phys. Lett. A* **379** 421 (2015)
43. Val'kov V V et al. *JETP Lett.* **103** 385 (2016); *Pis'ma Zh. Eksp. Teor. Fiz.* **103** 433 (2016)
44. Val'kov V V et al. *J. Exp. Theor. Phys.* **125** 810 (2017); *Zh. Eksp. Teor. Fiz.* **152** 957 (2017)
45. Piekars P, Konior J, Jefferson J H *Phys. Rev. B* **59** 14697 (1999)
46. Makarov I A et al. *Phys. Rev. B* **92** 155143 (2015)
47. Shneyder E I et al. *J. Exp. Theor. Phys.* **126** 683 (2018); *Zh. Eksp. Teor. Fiz.* **153** 820 (2018)
48. Myasnikova A E, Zhileeva E A, Moseykin D V *J. Phys. Condens. Matter* **30** 125601 (2018)
49. Myasnikova A E et al. *J. Phys. Condens. Matter* **31** 235602 (2019)
50. Eliashberg G M *Sov. Phys. JETP* **11** 696 (1960); *Zh. Eksp. Teor. Fiz.* **38** 966 (1960)
51. Sadovskii M V *J. Exp. Theor. Phys.* **128** 455 (2019); *Zh. Eksp. Teor. Fiz.* **155** 527 (2019)
52. Dzebisashvili D M, Komarov K K *Eur. Phys. J. B* **91** 278 (2018)
53. Bardeen J, Cooper L N, Schrieffer J R *Phys. Rev.* **108** 1175 (1957)
54. Little W A *Phys. Rev.* **134** A1416 (1964)
55. Ginzburg V L *Phys. Lett.* **13** 101 (1964)
56. Bednorz J G, Müller K A *Z. Phys. B* **64** 189 (1986)
57. Wu M K et al. *Phys. Rev. Lett.* **58** 908 (1987)
58. Schilling A et al. *Nature* **363** 56 (1993)
59. Chu C W et al. *Nature* **365** 323 (1993)
60. Hubbard J C *Proc. R. Soc. Lond. A* **276** 238 (1963)
61. Ovchinnikov S G *Phys. Usp.* **40** 993 (1997); *Usp. Fiz. Nauk* **167** 1043 (1997)
62. Ovchinnikov S G, Val'kov V V *Hubbard Operators in the Theory of Strongly Correlated Electrons* (London: Imperial College Press, 2004); Translated from Russian: Val'kov V V, Ovchinnikov S G *Kvazichastitsy v Sil'no Korrelirovannykh Sistemakh* (Novosibirsk: Izd. SO RAN, 2001)
63. Izyumov Yu A *Phys. Usp.* **40** 445 (1997); *Usp. Fiz. Nauk* **167** 465 (1997)
64. Loktev V M *Low Temp. Phys.* **22** 1 (1996); *Fiz. Nizk. Temp.* **22** 3 (1996)
65. Mott N F *Metal–Insulator Transitions* (London: Taylor and Francis, 1990); Translated into Russian: *Perekhody Metall–Izolyator* (Moscow: Nauka, 1979)
66. Khomskii D I *Phys. Met. Metallogr.* **29** 31 (1970); *Fiz. Met. Metalloved.* **29** 31 (1970)
67. Izyumov Yu A *Sov. Phys. Usp.* **34** 935 (1991); *Usp. Fiz. Nauk* **161** (11) 1 (1991)
68. Baranov M A, Kagan M Yu *Z. Phys. B* **86** 237 (1992)
69. Kohn W, Luttinger J M *Phys. Rev. Lett.* **15** 524 (1965)
70. Fay D, Layzer A *Phys. Rev. Lett.* **20** 187 (1968)
71. Kagan M Yu, Chubukov A V *JETP Lett.* **47** 614 (1988); *Pis'ma Zh. Eksp. Teor. Fiz.* **47** 525 (1988)
72. Baranov M A, Chubukov A V, Kagan M Yu *Int. J. Mod. Phys. B* **6** 2471 (1992)
73. Alexandrov A S, Kabanov V V *Phys. Rev. Lett.* **106** 136403 (2011)
74. Maiti S, Chubukov A V *AIP Conf. Proc.* **1550** 3 (2013)
75. Kagan M Yu, Mitskan V A, Korovushkin M M *Phys. Usp.* **58** 733 (2015); *Usp. Fiz. Nauk* **185** 785 (2015)
76. Kagan M Yu *JETP Lett.* **103** 728 (2016); *Pis'ma Zh. Eksp. Teor. Fiz.* **103** 822 (2016)
77. Scalapino D J, Loh E (Jr.), Hirsch J E *Phys. Rev. B* **34** 8190(R) (1986)
78. Scalapino D J, Loh E (Jr.), Hirsch J E *Phys. Rev. B* **35** 6694 (1987)
79. Kozlov A N *Sverkhprovodimost' Fiz. Khim. Tekh.* **2** 64 (1989)
80. Zanchi D, Schulz H J *Phys. Rev. B* **54** 9509 (1996)
81. Hlubina R *Phys. Rev. B* **59** 9600 (1999)
82. Raghu S, Kivelson S A, Scalapino D J *Phys. Rev. B* **81** 224505 (2010)
83. Rømer A T et al. *Phys. Rev. Res.* **2** 013108 (2020)
84. Astretsov G V, Rohringer G, Rubtsov A N *Phys. Rev. B* **101** 075109 (2020)
85. Zaitsev R O, Ivanov V A *Sov. Phys. Solid State* **29** 475 (1987); *Fiz. Tverd. Tela* **29** 2554 (1987)
86. Hubbard J C *Proc. R. Soc. Lond. A* **285** 542 (1965)
87. Shubin S, Vonsowsky S *Proc. R. Soc. Lond. A* **145** 159 (1934)
88. Shubin S, Vonsowsky S *Phys. Z. Sowjetunion* **7** 292 (1935)
89. Shubin S, Vonsowsky S *Phys. Z. Sowjetunion* **10** 348 (1936)
90. Zaitsev R O, Ivanov V A, Mikhailova Yu V *Fiz. Met. Metalloved.* **65** 1032 (1988)
91. Zaitsev R O, Ivanov V A, Mikhailova Yu V *Fiz. Met. Metalloved.* **68** 1108 (1989)
92. Zaitsev R O *J. Exp. Theor. Phys.* **98** 780 (2004); *Zh. Eksp. Teor. Fiz.* **125** 891 (2004)
93. Izyumov Yu A, Skryabin Yu N *Statistical Mechanics of Magnetically Ordered Systems* (Berlin: Springer, 1988); Translated from Russian: *Statisticheskaya Mekhanika Magnitouporyadochennykh Sistem* (Moscow: Nauka, 1987)
94. Izyumov Yu A, Katsnel'son M I, Skryabin Yu N *Magnetizm Kollektivizirovannykh Elektronov* (Magnetism of Collectivized Electrons) (Moscow: Nauka, 1994)
95. Izyumov Yu A, Chashchin N I, Alekseev D S *Teoriya Sil'no Korrelirovannykh Sistem. Metod Proizvodyashchego Funktsionala* (Theory of Strongly Correlated Systems. Generating Functional Method) (Moscow–Izhevsk: RKhD, 2006)
96. Izyumov Yu A *Phys. Usp.* **38** 385 (1995); *Usp. Fiz. Nauk* **165** 403 (1995)
97. Georges A et al. *Rev. Mod. Phys.* **68** 13 (1996)
98. Tasaki H *J. Phys. Condens. Matter* **10** 4353 (1998)
99. Bulut N *Adv. Phys.* **51** 1587 (2002)
100. Mattheiss L F *Phys. Rev. Lett.* **58** 1028 (1987)
101. Jorgensen J D et al. *Phys. Rev. Lett.* **58** 1024 (1987)
102. Yu J, Freeman A J, Xu J-H *Phys. Rev. Lett.* **58** 1035 (1987)
103. Siegrist T et al. *Phys. Rev. B* **35** 7137 (1987)
104. Fulde P *Electron Correlations in Molecules and Solids* (Springer Series in Solid-State Sciences, Vol. 100) (Berlin: Springer-Verlag, 1991)
105. Varma C M, Schmitt-Rink S, Abrahams E *Solid State Commun.* **62** 681 (1987)
106. Nücker N et al. *Z. Phys. B* **67** 9 (1987)

107. Hybertsen M S, Schlüter M, Christensen N E *Phys. Rev. B* **39** 9028 (1989)
108. Eskes H, Tjeng L H, Sawatzky G A *Phys. Rev. B* **41** 288 (1990)
109. McMahan A K, Annett J F, Martin R M *Phys. Rev. B* **42** 6268 (1990)
110. Ogata M, Fukuyama H *Rep. Prog. Phys.* **71** 036501 (2008)
111. Dopf G, Muramatsu A, Hanke W *Phys. Rev. B* **41** 9264 (1990)
112. Dopf G, Muramatsu A, Hanke W *Phys. Rev. Lett.* **68** 353 (1992)
113. Imada M *J. Phys. Soc. Jpn.* **57** 3128 (1988)
114. Elesin V F et al. *Sov. Phys. JETP* **72** 133 (1991); *Zh. Eksp. Teor. Fiz.* **99** 237 (1991)
115. Lin H Q, Hirsch J E, Scalapino D J *Phys. Rev. B* **37** 7359 (1988)
116. Hirsch J E et al. *Phys. Rev. Lett.* **60** 1668 (1988)
117. Jones D H, Monaghan S *J. Phys. Condens. Matter* **1** 1843 (1989)
118. Ogata M, Shiba H *J. Phys. Soc. Jpn.* **57** 3074 (1988)
119. Schmidt H J, Kuramoto Y *Phys. Rev. B* **42** 2562 (1990)
120. Hirsch J E et al. *Phys. Rev. B* **39** 243 (1989)
121. Fujimori A *Phys. Rev. B* **39** 793(R) (1989)
122. Annett J F et al. *Phys. Rev. B* **40** 2620(R) (1989)
123. Grant J B, McMahan A K *Phys. Rev. Lett.* **66** 488 (1991)
124. Nücker N et al. *Phys. Rev. B* **39** 6619 (1989)
125. Romberg H et al. *Phys. Rev. B* **41** 2609(R) (1990)
126. Pompa M et al. *Physica C* **184** 102 (1991)
127. Chen C T et al. *Phys. Rev. Lett.* **68** 2543 (1992)
128. Dagotto E *Rev. Mod. Phys.* **66** 763 (1994)
129. Gaididei Yu B, Loktev V M *Phys. Status Solidi B* **147** 307 (1988)
130. Weber W *Z. Phys. B* **70** 323 (1988)
131. Kamimura H, Matsuno S, Saito R *Solid State Commun.* **67** 363 (1988)
132. Müller K A *Z. Phys. B* **80** 193 (1990)
133. Nickel J H, Morris D E, Ager J W (III) *Phys. Rev. Lett.* **70** 81 (1993)
134. De Leeuw D M et al. *Physica C* **166** 133 (1990)
135. Di Castro C, Feiner L F, Grilli M *Phys. Rev. Lett.* **66** 3209 (1991)
136. Bulaevskii L N, Nagaev E L, Khomskii D I *Sov. Phys. JETP* **27** 836 (1968); *Zh. Eksp. Teor. Fiz.* **54** 1562 (1968)
137. Chao K A, Spalek J, Oleś A M *J. Phys. C* **10** L271 (1977)
138. Hirsch J E *Phys. Lett. A* **136** 153 (1989)
139. Yushankhai V Yu, Vujicic G M, Zakula R B *Phys. Lett. A* **151** 254 (1990)
140. Val'kov V V et al. *JETP Lett.* **75** 378 (2002); *Pis'ma Zh. Eksp. Teor. Fiz.* **75** 450 (2002)
141. Val'kov V V et al. *Mod. Phys. Lett. B* **17** 441 (2003)
142. Val'kov V V, Dzebisashvili D M *J. Exp. Theor. Phys.* **100** 608 (2005); *Zh. Eksp. Teor. Fiz.* **127** 686 (2005)
143. Korshunov M M, Ovchinnikov S G, Sherman A V *JETP Lett.* **80** 39 (2004); *Pis'ma Zh. Eksp. Teor. Fiz.* **80** 45 (2004)
144. Val'kov V V, Golovnya A A *J. Exp. Theor. Phys.* **107** 996 (2008); *Zh. Eksp. Teor. Fiz.* **134** 1167 (2008)
145. Spalek J, Oleś A M, Chao K A *Phys. Status Solidi B* **108** 329 (1981)
146. Zhang F C *Phys. Rev. Lett.* **90** 207002 (2003)
147. Abram M et al. *Phys. Rev. B* **88** 094502 (2013)
148. Spalek J, Zegrodnik M, Kaczmarczyk J *Phys. Rev. B* **95** 024506 (2017)
149. Jefferson J H, Eskes H, Feiner L F *Phys. Rev. B* **45** 7959 (1992)
150. Lovtsov S V, Yushankhai V Yu *Physica C* **179** 159 (1991)
151. Schüttler H-B, Fedro A J *Phys. Rev. B* **45** 7588(R) (1992)
152. Belinicher V I, Chernyshev A L *Phys. Rev. B* **47** 390 (1993)
153. Belinicher V I, Chernyshev A L *Phys. Rev. B* **49** 9746 (1994)
154. Belinicher V I, Chernyshev A L, Shubin V A *Phys. Rev. B* **53** 335 (1996)
155. Feiner L F, Jefferson J H, Raimondi R *Phys. Rev. B* **53** 8751 (1996)
156. Raimondi R, Jefferson J H, Feiner L F *Phys. Rev. B* **53** 8774 (1996)
157. Gavrichkov V A et al. *J. Exp. Theor. Phys.* **91** 369 (2000); *Zh. Eksp. Teor. Fiz.* **118** 422 (2000)
158. Gavrichkov V, Borisov A, Ovchinnikov S G *Phys. Rev. B* **64** 235124 (2001)
159. Ramšak A, Prelovšek P *Phys. Rev. B* **40** 2239 (1989)
160. Ramšak A, Prelovšek P *Phys. Rev. B* **42** 10415 (1990)
161. Vonsovsky S V *Sov. Phys. JETP* **10** 468 (1946); *Zh. Eksp. Teor. Fiz.* **16** 981 (1946)
162. Izyumov Yu A, Kassan-ogly F A, Skryabin Yu N *Polevye Metody v Teorii Ferromagnetizma* (Field Methods in the Theory of Ferromagnetism) (Moscow: Nauka, 1974)
163. Izyumov Yu A, Skryabin Yu N *Bazovye Modeli v Teorii Ferromagnetizma* (Base Models in the Theory of Ferromagnetism) (Ekaterinburg: UrO RAN, 2002)
164. Klee S, Muramatsu A *Nucl. Phys. B* **473** 539 (1996)
165. Chakravarty S, Halperin B I, Nelson D R *Phys. Rev. Lett.* **60** 1057 (1988)
166. Chakravarty S, Halperin B I, Nelson D R *Phys. Rev. B* **39** 2344 (1989)
167. Hasenfratz P, Leutwyler H *Nucl. Phys. B* **343** 241 (1990)
168. Hasenfratz P, Niedermayer F *Phys. Lett. B* **268** 231 (1991)
169. Hasenfratz P, Niedermayer F *Z. Phys. B* **92** 91 (1993)
170. Ding H-Q, Makivić M S *Phys. Rev. Lett.* **64** 1449 (1990)
171. Aligia A A, Simon M E, Batista C D *Phys. Rev. B* **49** 13061 (1994)
172. Kondo J *Prog. Theor. Phys.* **32** 37 (1964)
173. Val'kov V V, Dzebisashvili D M, Barabanov A F *Theor. Math. Phys.* **191** 752 (2017); *Teor. Matem. Fiz.* **191** 319 (2017)
174. Emery V J, Reiter G *Phys. Rev. B* **38** 11938 (1988)
175. Zhang F C, Rice T M *Phys. Rev. B* **41** 7243 (1990)
176. Emery V J, Reiter G *Phys. Rev. B* **41** 7247 (1990)
177. Eskes H, Sawatzky G A, Feiner L F *Physica C* **160** 424 (1989)
178. Littlewood P B et al. *Phys. Rev. B* **39** 12371 (1989)
179. Schrieffer J R, Wolff P A *Phys. Rev.* **149** 491 (1966)
180. Bogoliubov N N *Lectures on Quantum Statistics* (London: Macdonald, 1968); Translated from Russian: *Lektsii po Kvantovoi Statistike* (Kiev: Naukova Dumka, 1949)
181. Tyablikov S V *Methods in the Quantum Theory of Magnetism* (New York: Plenum Press, 1967); Translated from Russian: *Metody Kvantovoi Teorii Magnetizma* (Moscow: Nauka, 1965)
182. Starykh O A, Bonfim O F A, Reiter G F *Phys. Rev. B* **52** 12534 (1995)
183. Monthoux P, Balatsky A V, Pines D *Phys. Rev. Lett.* **67** 63448 (1991)
184. Monthoux P, Pines D *Phys. Rev. Lett.* **69** 961 (1992)
185. Monthoux P, Pines D *Phys. Rev. B* **47** 6069 (1993)
186. Izyumov Yu A *Phys. Usp.* **42** 215 (1999); *Usp. Fiz. Nauk* **169** 225 (1999)
187. Chubukov A V, Pines D, Stojković B P *J. Phys. Condens. Matter* **8** 10017 (1996)
188. Abanov Ar, Chubukov A V *Phys. Rev. Lett.* **83** 1652 (1999)
189. Abanov Ar, Chubukov A V *Phys. Rev. Lett.* **84** 5608 (2000)
190. Abanov Ar, Chubukov A V, Finkel'stein A M *Europhys. Lett.* **54** 488 (2001)
191. Abanov Ar, Chubukov A V, Schmalian J *Adv. Phys.* **52** 119 (2003)
192. Abanov Ar, Chubukov A V *Phys. Rev. Lett.* **93** 255702 (2004)
193. Bang Y *New J. Phys.* **14** 043030 (2012)
194. Wang Y, Chubukov A V *Phys. Rev. B* **91** 195113 (2015)
195. Tsvelik A M *Phys. Rev. B* **95** 201112(R) (2017)
196. Classen L, Robinson N J, Tsvelik A M *Phys. Rev. B* **99** 115110 (2019)
197. Barabanov A F et al. *J. Exp. Theor. Phys.* **83** 819 (1996); *Zh. Eksp. Teor. Fiz.* **110** 1480 (1996)
198. Barabanov A F, Kuzian R O, Maksimov L A *Phys. Rev. B* **55** 4015 (1997)
199. Lau B, Berciu M, Sawatzky G A *Phys. Rev. Lett.* **106** 036401 (2011)
200. Schrieffer J R *J. Low Temp. Phys.* **99** 397 (1995)
201. Moraghebi M et al. *Phys. Rev. B* **63** 214513 (2001)
202. Moraghebi M, Yunoki S, Moreo A *Phys. Rev. Lett.* **88** 187001 (2002)
203. Moraghebi M, Yunoki S, Moreo A *Phys. Rev. B* **66** 214522 (2002)
204. Eremin I, Manske D *Low Temp. Phys.* **32** 519 (2006)
205. Silva Neto M B *Phys. Rev. B* **76** 033103 (2007)
206. Digor D F, Moskalenko V A *Theor. Math. Phys.* **130** 271 (2002); *Teor. Matem. Fiz.* **130** 320 (2002)
207. Borisenko S V et al. *Phys. Rev. Lett.* **84** 4453 (2000)
208. Yoshida T et al. *Phys. Rev. Lett.* **91** 027001 (2003)
209. Zhou X J et al. *Phys. Rev. Lett.* **92** 187001 (2004)
210. Yoshida T et al. *J. Phys. Condens. Matter* **19** 125209 (2007)
211. Wells B O et al. *Phys. Rev. Lett.* **74** 964 (1995)

212. Marshall D S et al. *Phys. Rev. Lett.* **76** 4841 (1996)
213. Ronning F et al. *Phys. Rev. B* **67** 035113 (2003)
214. Shen K M et al. *Phys. Rev. Lett.* **93** 267002 (2004)
215. Shen K M et al. *Phys. Rev. B* **75** 075115 (2007)
216. Tobin J G et al. *Phys. Rev. B* **45** 5563 (1992)
217. Abrikosov A A, Campuzano J C, Gofron K *Physica C* **214** 73 (1993)
218. Gofron K et al. *Phys. Rev. Lett.* **73** 3302 (1994)
219. Dessau D S et al. *Phys. Rev. Lett.* **71** 2781 (1993)
220. King D M et al. *Phys. Rev. Lett.* **73** 3298 (1994)
221. Aebi P et al. *Phys. Rev. Lett.* **72** 2757 (1994)
222. Loeser A G et al. *Science* **273** 325 (1996)
223. Ding H et al. *Nature* **382** 51 (1996)
224. Ding H et al. *Phys. Rev. Lett.* **78** 2628 (1997)
225. Morinari T *J. Phys. Soc. Jpn.* **88** 104707 (2019)
226. Berciu M *Phys. Rev. Lett.* **97** 036402 (2006)
227. Val'kov V V, Golovnya A A, Korovushkin M M *JETP Lett.* **94** 197 (2011); *Pis'ma Zh. Eksp. Teor. Fiz.* **94** 215 (2011)
228. Plakida N M, Oudovenko V S *J. Exp. Theor. Phys.* **119** 554 (2014); *Zh. Eksp. Teor. Fiz.* **146** 631 (2014)
229. Seibold G, Sigmund E, Hizhnyakov V *Phys. Rev. B* **48** 7537 (1993)
230. Seibold G, Sigmund E, Hizhnyakov V *Phys. Rev. B* **57** 6937 (1998)
231. Yamase H *Phys. Rev. B* **75** 014514 (2007)
232. Seibold G *Phys. Rev. B* **77** 235109 (2008)
233. Gan J Y et al. *Phys. Rev. B* **78** 094504 (2008)
234. Grusdt F et al. *Phys. Rev. B* **99** 224422 (2019)
235. Kane C L, Lee P A, Read N *Phys. Rev. B* **39** 6880 (1989)
236. Kane C L et al. *Phys. Rev. B* **41** 2653(R) (1990)
237. Martinez G, Horsch P *Phys. Rev. B* **44** 317 (1991)
238. Khaliullin G, Horsch P *Phys. Rev. B* **47** 462 (1993)
239. Ramsak A, Horsch P *Phys. Rev. B* **57** 4308 (1998)
240. Schmitt-Rink S, Varma C M, Ruckenstein A E *Phys. Rev. Lett.* **60** 2793 (1988)
241. Richard J L, Yushankhai V Yu *Phys. Rev. B* **47** 1103 (1993)
242. Feng S, Su Z B, Yu L *Phys. Rev. B* **49** 2368 (1994)
243. Pepino R T, Ferraz A, Kochetov E *Phys. Rev. B* **77** 035130 (2008)
244. Klosinski A et al. *Phys. Rev. B* **101** 035115 (2020)
245. Nagaev E L *Physics of Magnetic Semiconductors* (Moscow: Mir Publ., 1983); Translated from Russian: *Fizika Magnitnykh Poluprovodnikov* (Moscow: Nauka, 1979)
246. de Gennes P-G *Phys. Rev.* **118** 141 (1960)
247. Lyons K B et al. *Phys. Rev. Lett.* **60** 732 (1988)
248. Lyons K B et al. *Phys. Rev. B* **37** 2353 (1988)
249. Sugai S, Shamoto S, Sato M *Phys. Rev. B* **38** 6436 (1988)
250. Blumberg G et al. *Phys. Rev. B* **53** R11930 (1996)
251. Blumberg G et al. *Science* **278** 1427 (1997)
252. Bourges P et al. *Phys. Rev. Lett.* **79** 4906 (1997)
253. Inui M, Doniach S, Gabay M *Phys. Rev. B* **38** 6631 (1988)
254. Annet J F et al. *Phys. Rev. B* **40** 2620 (1989)
255. Kondo J, Yamaji K *Prog. Theor. Phys.* **47** 807 (1972)
256. Shimahara H, Takada S *J. Phys. Soc. Jpn.* **60** 2394 (1991)
257. Barabanov A F, Berezovsky V M *J. Exp. Theor. Phys.* **79** 627 (1994); *Zh. Eksp. Teor. Fiz.* **106** 1156 (1994)
258. Zwanzig R *Phys. Rev.* **124** 983 (1961)
259. Mori H *Prog. Theor. Phys.* **33** 423 (1965)
260. Roth L M *Phys. Rev. Lett.* **20** 1431 (1968)
261. Plakida N M et al. *J. Exp. Theor. Phys.* **97** 331 (2003); *Zh. Eksp. Teor. Fiz.* **124** 367 (2003)
262. Vladimirov A A, Ihle D, Plakida N M *Theor. Math. Phys.* **152** 1331 (2007); *Teor. Matem. Fiz.* **152** 538 (2007)
263. Barabanov A F et al. *JETP Lett.* **66** 182 (1997); *Pis'ma Zh. Eksp. Teor. Fiz.* **66** 173 (1997)
264. Sherman A *Phys. Rev. B* **73** 155105 (2006)
265. Sherman A *Eur. Phys. J. B* **92** 55 (2019)
266. Sherman A *Phys. Scripta* **94** 055802 (2019)
267. Sherman A *Eur. Phys. J. B* **93** 168 (2020)
268. Val'kov V V et al. *J. Low Temp. Phys.* **197** 34 (2019)
269. Mermin N D, Wagner H *Phys. Rev. Lett.* **17** 1133 (1966)
270. Barabanov A F, Mikheenkov A V, Shvartsberg A V *Theor. Math. Phys.* **168** 1192 (2011); *Teor. Matem. Fiz.* **168** 389 (2011)
271. Marshall W *Proc. R. Soc. Lond. A* **232** 48 (1955)
272. Izyumov Y A, Medvedev M V *Sov. Phys. JETP* **32** 302 (1971); *Zh. Eksp. Teor. Fiz.* **59** 553 (1971)
273. Val'kov V V, Dzebisashvili D M, Barabanov A F *J. Supercond. Nov. Magn.* **29** 1049 (2016)
274. Keimer B et al. *Phys. Rev. B* **46** 14034 (1992)
275. Barzykin V, Pines D *Phys. Rev. B* **52** 13585 (1995)
276. Barabanov A F, Maksimov L A, Mikheenkov A V *JETP Lett.* **74** 328 (2001); *Pis'ma Zh. Eksp. Teor. Fiz.* **74** 362 (2001)
277. Val'kov V, Korovushkin M *J. Phys. Soc. Jpn.* **80** 014703 (2011)
278. Val'kov V V, Korovushkin M M *J. Exp. Theor. Phys.* **112** 108 (2011); *Zh. Eksp. Teor. Fiz.* **139** 126 (2011)
279. Wollman D A et al. *Phys. Rev. Lett.* **71** 2134 (1993)
280. Van Harlingen D J *Rev. Mod. Phys.* **67** 515 (1995)
281. Scalapino D J *Phys. Rep.* **250** 329 (1995)
282. Tsuei C C, Kirtley J R *Rev. Mod. Phys.* **72** 969 (2000)
283. Plakida N M, Oudovenko V S *Eur. Phys. J. B* **86** 115 (2013)
284. Plakida N M *Physica C* **531** 39 (2016)
285. Plakida N M *Physica C* **549** 69 (2018)
286. Zaitsev R O "Issledovanie perekhoda metall–dielektrik" ("Investigation of metal–dielectric junction"), Preprint No. IAE-3927/1 (Moscow: Institute of Atomic Energy, Academy of Sciences of the USSR, 1984)
287. Fröhlich H *Phys. Rev.* **79** 845 (1950)
288. Tolmachev V V *Dokl. Akad. Nauk SSSR* **140** 563 (1961)
289. Val'kov V V et al. *J. Low Temp. Phys.* **191** 408 (2018)
290. Fischer M H, Kim E-A *Phys. Rev. B* **84** 144502 (2011)
291. Val'kov V V et al. *J. Magn. Magn. Mat.* **440** 123 (2017)
292. Zubarev D N *Sov. Phys. Usp.* **3** 320 (1960); *Usp. Fiz. Nauk* **81** 71 (1960)
293. Val'kov V V, Dzebisashvili D M, Barabanov A F *J. Low Temp. Phys.* **181** 134 (2015)
294. Val'kov V V, Korovushkin M M, Barabanov A F *J. Low Temp. Phys.* **196** 242 (2019)
295. Val'kov V V et al. *J. Exp. Theor. Phys.* **128** 885 (2019); *Zh. Eksp. Teor. Fiz.* **155** 1045 (2019)
296. Eremin M V, Malakhov M A *JETP Lett.* **105** 710 (2017); *Pis'ma Zh. Eksp. Teor. Fiz.* **105** 680 (2017)
297. Eremin M V, Kochergin D S, Malakhov M A *JETP Lett.* **108** 796 (2018); *Pis'ma Zh. Eksp. Teor. Fiz.* **108** 810 (2018)
298. Carbotte J P et al. *Phys. Rev. B* **81** 014522 (2010)
299. Eremin M V, Sunyaev D A *JETP Lett.* **103** 190 (2016); *Pis'ma Zh. Eksp. Teor. Fiz.* **103** 209 (2016)
300. Hardy W N et al. *Phys. Rev. Lett.* **70** 3999 (1993)
301. Khasanov R et al. *Phys. Rev. Lett.* **98** 057007 (2007)
302. Wojek B M et al. *Phys. Rev. B* **84** 144521 (2011)
303. Sonier J E et al. *Phys. Rev. Lett.* **83** 4156 (1999)
304. Khasanov R et al. *Phys. Rev. Lett.* **99** 237601 (2007)
305. Anukool W et al. *Phys. Rev. B* **80** 024516 (2009)
306. Eremin M V, Larionov I A, Lyubin I E *J. Phys. Condens. Matter* **22** 185704 (2010)
307. Schrieffer J R *Theory of Superconductivity* (New York: W.A. Benjamin, 1964); Translated into Russian: *Teoriya Sverkhprovodimosti* (Moscow: Nauka, 1970)
308. Sadovskii M V *Diagrammatika. Lektsii po Izbrannym Zadacham Teorii Kondensirovannogo Sostoyaniya* (Diagrammatics. Lecture on Selected Problems of Condensed Matter Physics) (Izhevsk: RKhD, 2010)
309. Tinkham M *Introduction to Superconductivity* (New York: McGraw-Hill, 1996); Translated into Russian: *Vvedenie v Sverkhprovodimost'* (Moscow: Atomizdat, 1980)
310. Bozovic I et al. *Nature* **536** 309 (2016)
311. Panagopoulos C et al. *Phys. Rev. B* **60** 14617 (1999)
312. Lemberger T R et al. *Phys. Rev. B* **82** 214513 (2010)
313. Raghu S et al. *Phys. Rev. B* **85** 024516 (2012)
314. Kagan M Yu et al. *JETP Lett.* **97** 226 (2013); *Pis'ma Zh. Eksp. Teor. Fiz.* **97** 253 (2013)
315. Kagan M Yu et al. *J. Exp. Theor. Phys.* **117** 728 (2013); *Zh. Eksp. Teor. Fiz.* **144** 837 (2013)
316. Val'kov V V et al. *Low Temp. Phys.* **44** 130 (2018); *Fiz. Nizk. Temp.* **44** 173 (2018)

317. Barabanov A F, Belemuk A M *JETP Lett*. **87** 628 (2004); *Pis'ma Zh. Eksp. Teor. Fiz*. **87** 725 (2008)
318. Kuchinskii E Z, Sadovskii M V *J. Exp. Theor. Phys*. **90** 535 (2000); *Zh. Eksp. Teor. Fiz*. **117** 613 (2000)
319. Kuchinskii E Z, Sadovskii M V *J. Exp. Theor. Phys*. **92** 480 (2001); *Zh. Eksp. Teor. Fiz*. **119** 553 (2001)
320. Kuchinskii E Z, Sadovskii M V *J. Exp. Theor. Phys*. **94** 654 (2002); *Zh. Eksp. Teor. Fiz*. **121** 758 (2002)
321. Sadovskii M V et al. *Phys. Rev. B* **72** 155105 (2005)
322. Kuchinskii E Z, Nekrasov I A, Sadovskii M V *Phys. Rev. B* **75** 115102 (2007)
323. Kuchinskii E Z, Nekrasov I A, Sadovskii M V *Phys. Usp*. **55** 325 (2012); *Usp. Fiz. Nauk* **182** 345 (2012)
324. Belemuk A M, Barabanov A F, Maksimov L A *JETP Lett*. **79** 160 (2004); *Pis'ma Zh. Eksp. Teor. Fiz*. **79** 195 (2004)
325. Belemuk A M, Barabanov A F, Maksimov L A *J. Exp. Theor. Phys*. **102** 431 (2006); *Zh. Eksp. Teor. Fiz*. **129** 493 (2006)
326. Belemuk A M, Barabanov A F, Maksimov L A *JETP Lett*. **86** 321 (2007); *Pis'ma Zh. Eksp. Teor. Fiz*. **86** 374 (2007)
327. Belemuk A M, Barabanov A F *JETP Lett*. **82** 731 (2005); *Pis'ma Zh. Eksp. Teor. Fiz*. **82** 827 (2005)
328. Larionov I A, Barabanov A F *JETP Lett*. **100** 712 (2014); *Pis'ma Zh. Eksp. Teor. Fiz*. **100** 811 (2014)
329. Barabanov A F et al. *Phys. Usp*. **58** 446 (2015); *Usp. Fiz. Nauk* **185** 479 (2015)